UNIVERSITY OF CALIFORNIA SAN DIEGO

A "Structure-Misfunction" Screen Unveils Diverse Quality-Control Responses to Minimally Misfolded Cytosolic Proteins

A dissertation submitted in partial satisfaction of the
requirements for the degree Doctor of Philosophy

in

Biology

by

Matthew Paul Flagg

Committee in Charge:

Professor Randolph Hampton, Chair
Professor Eric Bennett
Professor Partho Ghosh
Professor Maho Niwa
Professor Lorraine Pillus

2020

The dissertation of Matthew Paul Flagg is approved, and it is acceptable in quality and form for publication on microfilm and electronically:

Chair

University of California San Diego
2020

DEDICATION

This dissertation is dedicated to Burke Lynch, guide, mentor, friend.

TABLE OF CONTENTS

LIST OF FIGURES

LIST OF TABLES

ACKNOWLEDGEMENTS

Thank you, Hampton lab members. I am particularly grateful for Randy's extraordinary creativity and his willingness to take risks. His open office door meant my ideas—good or bad, considered or vague—always had an audience. I'm thankful for Maggie Wangeline's friendship and incisive thinking. Maggie can punch holes in most models, and I eventually stopped taking her criticism personally. Nidhi Vashistha has my thanks for her troubleshooting prowess, her ready availability by text, and her general support as a lab member and friend. Sonya Neal was an inspiration from day one, and the biochemistry she did for chapter III made submission possible. Sarah Holland also made critical contributions to chapter III. I look forward to working with her in the future as she earns a well-deserved Ph.D. Della Syau, Andy Kao, Yousif Slaiwa, Breanna "BL" Lam, and Darren Lam were all exemplary undergrad researchers. Each has my thanks for their hard work and for teaching me how to teach.

Eammon, Julie, Kyle, Will, Jacy, and Leo were critical to survival. Deirdre, Eric, Jana, Jessi, Mike, Maggie, Thomas, Phillip, and Julia made Austin a second home. My parents and family were always available for FaceTime—and support when my car died. And my dogson, Crosby, and my wife, Francesca, are everything, even when they're a thousand miles away.

Chapter II, in full, is a reproduction of the material as it appears in Yeast 2019. Flagg, Matthew P.; Kao, Andy; Randy, Hampton Y., John Wiley & Sons Ltd, 2019. The dissertation author was the primary investigator and first author of this paper, and permission from all other authors has been obtained.

Chapter III, in full, has been submitted for publication of the material as it may appear in Molecular Biology of the Cell, 2020, Matthew P. Flagg, Margaret A. Wangeline, Sarah R. Holland, Sascha H. Duttke, Christopher Benner, Sonya Neal, Randolph Y. Hampton, American Society for

Cell Biology, 2020. The dissertation author was the primary investigator and first author of this paper, and permission from all other authors has been obtained.

Chapter IV, in full, is currently being prepared for submission to ELife. Matthew P. Flagg, Breanna Lam, Yousif I. Slaiwa, Andy Kao, Darren K. Lam, Randolph Y. Hampton. The dissertation author was the primary investigator and first author of this paper, and permission from all other authors has been obtained.

VITA

2011	Bachelor of Science and Bachelor of Arts, Boston College
2011-2013	Research Technician, Massachusetts General Hospital
2020	Doctor of Philosophy, University of California San Diego

PUBLICATIONS

Flagg, M. P., Kao, A., & Hampton, R. Y. (2019). Integrating after CEN Excision (ICE) Plasmids: Combining the ease of yeast recombination cloning with the stability of genomic integration. *Yeast*, *36*(10), 593–605

ABSTRACT OF THE DISSERTATON

A “Structure-Misfunction” Screen Unveils Diverse Quality-Control Responses to Minimally Misfolded Cytosolic Proteins

by

Matthew Paul Flagg

Doctor of Philosophy in Biology

University of California San Diego, 2020

Professor Randolph Hampton, Chair

As a part of protein quality control (PQC), the ubiquitin-proteosome system (UPS) ubiquitinates and degrades aberrant proteins. In this role, the UPS must identify damaged, orphaned, and misfolded species amidst a proteome-worth of normal, folded proteins. This exquisite specificity is achieved by PQC E3 ligases, each of which recognizes a broad range of PQC substrates.

Alongside efforts to understand how PQC ligases effect selectivity, there has been sustained interest in PQC substrates and their distinguishing structural characteristics. Perhaps the best studied substrates are disease causative mutants, such as the most common cause of cystic fibrosis, CFTRΔF508. Numerous high-throughput screens have also aimed to identify “degrons,” discrete amino-acid sequences that elicit degradation. Despite these efforts, isolating and characterizing PQC substrates remains an exigent mode of inquiry in the field.

Here, we present insights gained from PQC substrates both new and old. An initial study underlines the benefits of integrating transgenes onto yeast chromosomes: Stable integration of GFP-tagged proteins allows rapid and reliable quantitation of protein steady-state levels, a crucial indicator of substrate (in)stability. A second study demonstrates the value of one model, misfolded substrate, Sec61-2-GFP. Sec61-2-GFP allowed us to monitor each step of inner-nuclear-membrane-associated degradation (INMAD), from ubiquitination to retrotranslocation of the full-length protein. Sec61-2-GFP was also lethal in the combined absence of ERAD and INMAD, further evincing the elucidative power of appropriate model substrates. These studies and others justify the "Structure-Misfunction" screen, a platform to isolate minimally misfolded versions of cytosolic proteins. Tellingly, the screen seems to have uncovered a novel PQC pathway in the *Saccharomyces cerevisiae* cytosol.

Structure-Misfunction analysis also provided insight into misfolding itself. Our studies show that different destabilizing point mutations within one domain can lead to entirely distinct PQC outcomes. These data suggest that minimal misfolding can cause "local" as opposed to "global" unfolding *in vivo*. The screen also identified mutants of chorismate mutase that can be stabilized by the allosteric effector tryptophan, a striking example of chemical chaperoning. Thus, the screen is a simple genetic approach to uncovering novel features of cell and structural biology.

CHAPTER I

Introduction

An Overview of Protein Quality Control

In a living cell, environmental stresses and biological errors routinely challenge protein folding. Thus, even under ideal conditions, proteins regularly misfold or become otherwise structurally aberrant. Having failed to achieve or maintain their folded state, proteins are thought to expose structural elements that are normally buried or at binding interfaces. These exposed structural elements promote protein-protein aggregation, leading misfolded proteins to interfere with or disable normal biological functions (Kim, Y. E., et al., 2016; Olzscha, H., et al., 2011). Accordingly, misfolded proteins are implicated in a growing list of human diseases (Klaips, C. L., et al., 2018; Ross, C. A., and Poirier, M. A., 2004), and genetic mutations that promote misfolding, such as those that lower translation fidelity, can have devastating neurological consequences (Lee, J. W., et al., 2006; Vo, M. N., et al. 2018).

Misfolded and otherwise aberrant proteins must therefore be recognized and addressed by the cell, a task that falls to an enormous network collectively known as protein quality control (PQC) (Jayaraj, G. G., et al., 2020). Broadly speaking, PQC relies on two strategies: 1) facilitating protein folding and refolding and 2) effecting protein degradation.

To mediate protein folding and refolding, PQC employs a range of molecular chaperones. Chaperones interact with nascent polypeptides at the ribosome (Preissler, S., and Deuerling, E., 2012; Willmund, F., et. al. 2013), with fully translated proteins upon misfolding and/or aggregation (Glover, J. R., and Lindquist, S., 1998; Haslbeck, M., & Vierling, E., 2015; Malinovska, L., et al., 2012; Nakatsukasa, K., et al. 2008; Nillegoda, N. B., et al. 2015), and with a host of other proteins throughout their normal lifespan (Neal, S., et al., 2017; Pobre, K. F. R., et al., 2019; Schmidt, O.,

2010). In humans, the chaperone network consists of roughly 88 chaperones and 244 co-chaperones (auxiliary proteins that facilitate chaperone function), and together, chaperones and cochaperones account for ~8-10% of the total protein mass in a human cell, a reflection of their omnipresence in cell biology (Brehme, M., et al., 2014; Finka, A., and Goloubinoff, P., 2013; Nagaraj N., et al., 2011).

To effect the degradation of misfolded proteins, PQC employs the ubiquitin-proteasome system (UPS) and the autophagy-lysosomal pathway (ALP) (Dikic, I., 2017). Like all UPS pathways, the PQC arm of the UPS is mediated by a cascade of enzymes, E1, E2, and E3. An E1 ubiquitin-activating enzyme and an E2 ubiquitin-conjugating enzyme first activate the small protein ubiquitin and prepare it for covalent attachment to misfolded-protein substrates (Finley, D., 2012). E3 ligases then recognize substrates and broker their ubiquitination (Zheng, N., and Shabek, N., 2017). Finally, ubiquitin chains act as a signal for substrate transport to (Richly, H., et al., 2005) and proteolysis by the 26S proteasome (Finley, D., 2009; Lander, G. C., et al., 2012; Shi, Y., Chen, et al. 2016). The PQC arm of the ALP effects bulk protein degradation via double-membrane vesicles, known as autophagosomes (Galluzzi, L., et al., 2017). Autophagosomes can be targeted to aggregated, ubiquitinated proteins (Arndt, V., et al., 2010) or can non-specifically engulf cytosolic material (Lamb, C. A., et al. 2013). Alternatively, individual misfolded proteins can be delivered directly to the lysosome (Dice, J. F.; 2007). Notably, the UPS and ALP are coordinated in a number of ways. For instance, proteasome inhibition leads to corresponding upregulation of autophagy (Rideout, H. J., et al. 2004; Suraweera, A., et al. 2012). In this way, the UPS and ALP comprise a broad and dynamic degradation network.

Superficially, the chaperone-mediated and degradative modes of PQC may seem to be in opposition, but chaperones are required components of most degradative pathways. In some cases, this connection facilitates protein triage, wherein chaperones mediate successive attempts at folding after which they present recalcitrant substrates to the UPS for degradation. The best described triage

system is that of the *Saccharomyces cerevisiae* ER lumen, which mediates either proper folding and post-translational modification or ubiquitination by the ER-localized E3 ligase Hrd1 (Sun, Z., & Brodsky, J. L., 2019; Xu, C., and Ng, D. T. W., 2015). In other cases, the exact nature of triage is less well defined, but chaperones are nonetheless required for substrate ubiquitination. The ER-bound PQC ligase Doa10 (Maurer, M. J., et al., 2016; Nakatsukasa, K., et al., 2008) and the cytosolic PQC E3 ligases CHIP and Ubr1 cannot ubiquitinate soluble substrates in the absence of chaperone activity (Heck, J. W. et al., 2010; Kundrat, L., and Regan, L., 2010; Murata, S. et al., 2001; Singh, A., et al., 2020). Several branches of the ALP are similarly chaperone dependent (Arndt, V., et al., 2010; Dice, J. F. 2007). Because of the connections between chaperones, the ALP, and the UPS, PQC represents a vast, interconnected network with built in decision points and compensatory mechanisms. The PQC network can also be rapidly modified by transcriptional stress responses, as reviewed elsewhere (Hetz, C., & Papa, F. R., 2018; Richter, K., Haslbeck, M., & Buchner, J., 2010).

Complex Proteomes Produce a Myriad of Misfolded Proteins

The PQC network's size, complexity, and flexibility reflect the challenges of monitoring a biochemically and structurally diverse proteome (Harper, J. W., and Bennett, E. J.; 2016; Wolff, S., 2014). A functional human proteome consists of roughly 10,000 different proteins (Huttlin, E. L., et al., 2015; Nagaraj, N., et al., 2011), ranging from soluble monomers to transmembrane subunits of multimeric complexes (Bai, L., et al., 2018; Wirth, C., et al., 2016); from <100 amino-acid short open reading frames (Couso, J. P., and Patraquim, P., 2017) to comparatively enormous, adaptable molecular machines such as dynein (Reck-Peterson, S. L., et al., 2018). While many proteins have well-defined structures, a subset is intrinsically disordered, allowing them to achieve numerous confirmations and to interact with many binding partners (Wright, P. E., & Dyson, H. J., 2015). The structure of individual proteins can also be altered by post-translational modifications, of which there are nearly 300 different kinds (Prabakaran, S., et al., 2012), and structure varies from one splicing

isoform to another (Pan, Q., et al., 2008). Envision this diversity applied to the several billion proteins in a cell (Wiśniewski, J. R., et al., 2014), and the incredible biochemical complexity of a proteome begins to come into focus. The PQC network must monitor all this in a crowded cellular milieu.

Into this already complex context, environmental stresses and routine biological errors introduce a range of structural insults that give rise to a range of misfolded and otherwise aberrant species. There are thought to be as many as 35 different kinds of oxidative damage that can be visited on a protein (Madian, A. G., and Regnier, F. E., 2010). Genomic mutations, transcriptional errors, and translational errors can lead to point mutations, expanded CAG tracts, truncations, mislocalization, and ribosomal stalling, all of which challenge PQC (Farzin Khosrow-Khavar, et al., 2012; Heck, J. W. et al., 2010; Hessa, T., et al., 2011; Joazeiro, C. A. P., 2019; Park, S. H., et al., 2013). The non-native species that arise because of these errors and structural insults are likely to be highly heterogenous, even in the restricted case of different point mutants of a single gene. There is mounting evidence, along with data presented in chapter four, that structural insults can produce "local" misfolding rather than "global" unfolding; rather than widespread unfolding and loss of tertiary structure, a small portion of a protein can misfold while the majority of the protein's structure is unperturbed (Abildgaard, A. B., et al., 2019; Nielsen, S. V., 2017). As a result, even a single domain of a soluble monomeric protein can misfold in more than one way and thereby unveil biochemically distinct lesions. The myriad of aberrant species that can arise from a single protein can, in turn, exist in a number of aggregated conformations, ranging from oligomers to large inclusions (Kim, Y. E., et al., 2016). These can pose strikingly different challenges for PQC and the cell (Bäuerlein, F. J. B., et al, 2017). In the midst of an already heterogenous proteome, misfolded and otherwise aberrant proteins unveil an additional multi-leveled structural landscape, further necessitating a broad PQC network.

Though this aberrant structural landscape includes species that are permanently unfolded and must be degraded by the UPS, it also includes subtly misfolded proteins that retain function but are nonetheless degraded. This dissertation focuses on the ability of UPS-mediated degradative PQC to detect and eliminate this latter category of minimally misfolding.

The "Broad Specificity" of PQC E3 Ligases

As mentioned above, the PQC arm of the UPS employs E3 ligases that recognize abnormal proteins and facilitate their ubiquitination. Decades of research in *S. cerevisiae* has identified and characterized PQC ligases in most subcellular contexts. The ER transmembrane ligases Hrd1 and Doa10 mediate ER-associated degradation (ERAD; Needham, P. G., et al., 2019). Hrd1 monitors the ER membrane and lumen, and it can target ER transmembrane proteins as well as soluble ER luminal ones (Bordallo, J., et al., 1998; Carvalho, P., et al., 2006; Hampton, R. Y., et al., 1996). Doa10 monitors the ER and the ER-contiguous inner-nuclear membrane (Deng, M., and Hochstrasser, M., 2006), and it can target transmembrane proteins with membranal and cytosolic lesions as well as soluble cytosolic and nucleoplasmic proteins (Boban, M., et al., 2014; Habeck, G., et al., 2015; Maurer, M. J., et al., 2016; Swanson, R., et al., 2001). The soluble ligase San1 resides in and monitors the nucleus (Gardner, R. G., et al., 2005) but also recognizes cytosolic proteins that are transported to the nucleus for degradation (Heck, J. W. et al., 2010). Ubr1 and Ltn1 are both soluble and cytosolic. Ubr1 recognizes cytosolic substrates and mediates the N-end-rule pathway (Eisele, F., and Wolf, D. H., 2008; Heck, J. W. et al., 2010; Varshavsky, 2011) and Ltn1 is recruited to stalled ribosomes to facilitate the ubiquitination of nascent polypeptides (Bengtson, M., and Joazeiro, C., 2010). Finally, the Asi complex resides in the inner-nuclear membrane and can recognize both soluble and transmembrane proteins (Foresti, O., et al., 2014; Khmelinskii, A., et al., 2014; Omnus, D. J., and Ljungdahl, P. O., 2014). Other than San1 and the Asi complex, each of these ligases is conserved in mammals. Unsurprisingly, mammals also have an expanded collection of PQC ligases

commensurate with their larger and more complex proteomes. These include the cytosolic ligase CHIP (Murata, S. et al., 2001), the nuclear ligases URHF-2 and RNF4 (Guo, L., Giasson, et al., 2014; Iwata, A., et al., 2009), the atypical cytosolic E2-E3 UBE20 (Yanagitani, K., et al., 2017), the ERAD ligase gp78 (Fang, S., et al, 2001), and as many as a dozen other ligases that seem to mediate ERAD (Claessen, J. H. L., et al., 2012).

Discovery and characterization of PQC ligases is an ongoing topic of research in yeast and mammalian models. In chapter four we present data that indicate an uncharacterized PQC ligase in the yeast cytosol. Similar observations indicate an additional ligase in the yeast nucleus (Fredrickson, E. K., et al., 2013). In the case of mammalian systems, CRISPR screens promise to accelerate ligase identification and characterization (Leto, D. E., and Kopito, R. R., 2019). PQC E3 ligases nonetheless represent a remarkably small fraction of the ~600 E3s in humans and the 80 E3s in yeast (Li, W., et al., 2008). A surprisingly small group of PQC ligases monitor the proteome and identify the enormous range of abnormal proteins that arise from it.

To achieve that feat, PQC ligases must possess several critical and interrelated features. Clearly, they must each be able to recognize a broad range of abnormal proteins with potentially diverse structural lesions. Yet, they must also ignore a proteome-worth of normally folded proteins: promiscuous degradation could cause disadvantageous or even pathogenic decreases in a protein abundance. Combined, these criteria demand an exquisite specificity for misfolded proteins and incredible sensitivity to even minor structural lesions. A large body of research demonstrates that PQC ligase possess these almost paradoxical features, which we collectively refer to as “broad specificity.”

In support of their broad specificity, canonical yeast PQC ligases have each been demonstrated to recognize an incredibly wide range of substrates. This has been most

comprehensively demonstrated by several high-throughput screens. For instance, a yeast two-hybrid approach was used to screen a yeast cDNA library for interactions with the E3 ligase San1. This analysis identified 22 truncations and 5 peptides from cDNAs translated in the reverse orientation (Rosenbaum, J. C., 2011). In another highly refined approach, researchers screen for PQC "degrons," minimal amino-acid sequences that elicit degradation. A library of short amino-acid sequences is fused to a cytosolic reporter protein, and reporter levels are used as a readout of degradation. In two recent studies, elegant variations of this method identified ~170 Doa10 substrates collectively (Geffen, Y., et al., 2016; Maurer, M. J., et al., 2016). Of these, 16 sequences were derived from native yeast proteins (Geffen, Y., et al., 2016). Though lower in throughput, the methods presented in chapter four were similarly effective in generating substrates derived from native proteins. The structure-misfunction screen ultimately yielded roughly 40 point mutants of full-length yeast proteins that are recognized by the UPS. These data (as well as the studies discussed below) make it clear that individual ligases can recognize an extraordinarily broad collection of abnormal proteins.

On the other hand, proteomic and direct biochemical studies suggest that PQC ligases ignore the majority of the proteome. A recent analysis of protein turnover in *S. cerevisiae* found that 86% of protein have a half-life of longer than five hours, a rate at which protein abundance is largely determined by dilution due to cell division rather than active degradation (Christiano, R., et al., 2014). In that analysis, the median half-life of ~4,000 *S. cerevisiae* proteins was eight hours. In two similar analyses, the median half-life of ~8000 HeLa-cell proteins was ~20hrs (Boisvert, F. M., et al., 2012), and the median half-life of ~5000 murine proteins was 48 hours (Schwanhüusser, B., et al., 2011). These timeframes are similar to mammalian-cell doubling times, which again suggests passive protein turnover. The ability of PQC ligases to ignore normal proteins has also been demonstrated more directly by several studies. For instance, the E3 ligase Hrd1 can be crosslinked to both the folded ER protein Hmg1 and the conditionally misfolded ER protein Hmg2, but the ligase only

brokers the ubiquitination of the latter (Gardner R.G., et al., 2001). Similarly, Ubr1 ignores the stably folded protein Gnd1, but a truncated version of Gnd1, stGND1, is recognized by the ligase, ubiquitinated, and rapidly degraded (Heck, J. W. et al., 2010). In chapter three, we show that wild-type Sec61 is stable, whereas the point mutant Sec61-2 is rapidly degraded. The ability of PQC E3 ligases to recognize a broad range of substrates does not come at the cost of degrading normal proteins.

Remarkably, this exquisite specificity for misfolded proteins is accompanied by incredible sensitivity for minor structural lesions. This is perhaps most impressively demonstrated by point mutants. Indeed, data presented in chapter three demonstrate the ability of PQC E3 ligases to recognize a broad array of point mutants that retain their native function and can be stabilized *in vivo* by the chemical chaperone glycerol; PQC E3 ligases possess the ability to differentiate between a structurally stable protein and even minimally misfolded point mutants. In sum, a small number of PQC ligases seem to possess the broad specificity necessary to monitor an entire proteome.

Broad Specificity Enables the Degradation of Diverse PQC Substrates

The broad specificity of individual ligases, in turn, allows UPS-mediated PQC to recognize and degrade the array of misfolded and otherwise aberrant proteins that arise even under ideal conditions. This has been demonstrated by a large and growing collection of model substrates that can be divided, for convenience sake, into three classes: proteins that fail to reach their native context, proteins with amino-acid substitutions or premature stop codons, and proteins that undergo a version of regulated degradation that co-opts PQC machinery. A broader survey might also include ribosomal quality control, the various mRNA transcripts that elicit co-translational quality control, and the potential errors of co-translational protein folding. However, these topics have been reviewed elsewhere (Joazeiro, C. A. P., 2019), and the considerable array of post-translational targets warrant a focused review.

Proteins that become mislocalized or do not assemble into their multimeric complexes, often referred to as "orphans," comprise a first, large class of PQC substrates (Hegde, R. S., and Zavodszky, E. 2019; Juszkiewicz, S., and Hegde, R. S., 2018). One source of orphans are proteins that fail to be co-translationally translocated into the ER. Upon emerging in the cytoplasm, these are captured by the Bag6 complex and ubiquitinated by the E3 ligase RNF126 (Hessa, T., et al., 2011; Rodrigo-Brenni, M. C., et al., 2014). A second class of orphans escape their appropriate subcellular compartment. For instance, proteins that mislocalize to the inner-nuclear membrane are recognized and degraded by the Asi complex in yeast (Khmelinskii, A., et al., 2014; Natarajan, N., et al., 2020; Smoyer, C. J., et al., 2019). Even upon proper localization, a substantial fraction of the proteome must assemble into multimeric complexes with strict stoichiometries. Excess subunits are another class of orphans. For instance, orphaned ribosomal subunits are recognized by the E3 ligase Tom1 in yeast and by both HUWE1 and UBE20 in mammals (Sung, M. K., et al., 2016; Yanagitani, K., et al., 2017). Similarly, the E3 ligases Ubr1 and Not4 can recognize orphaned subunits in the yeast cytosol (Scazzari, M., et al., 2015; Shemorry, A., et al., 2013) and Hrd1 can recognize orphaned subunits in the mammalian ER (Tyler, R. E., et al., 2012). In line with these observations, proteomic analysis suggests that newly synthesized copies of many proteins are targets of the UPS. In one analysis, out of 3,605 proteins assayed, 331 were degraded by the proteasome shortly after synthesis but became stable later in their lifetime. 70% of these were part of heteromeric structures, suggesting that a fraction of newly synthesized copies is orphaned and degraded while the remaining fraction become stably incorporated into a multimeric complex (McShane, E., et al., 2016). Individual proteins and proteomics suggest that normal biology generates an array of orphans, all of which seem to be efficiently recognized by PQC E3 ligases.

PQC ligases also recognize a second class of aberrant proteins that arise due to amino-acid substitutions and premature stop codons. For instance, it has been demonstrated that both San1 and

Ubr1 have a broad ability to recognize truncated proteins (Fredrickson, E. K., et al., 2011; Heck, J. W. et al., 2010; Rosenbaum, J. C., et al., 2011) and temperature-sensitive (TS) alleles (Farzin Khosrow-Khavar, et al., 2012; Fredrickson, E. K., et al., 2011; Gardner, R. G., et al., 2005). Likewise, the ERAD ligases Hrd1 and Doa10 recognize TS alleles and point mutants of ER-membranal proteins (Biederer, T., et al., 1996; Plemper, R. K., et al., 1998; Ravid, T., et al., 2006), as does the Asi complex (Foresti, O., et al., 2014). These model substrates closely resemble the more than 50 human disease alleles that elicit ERAD, thereby lowering protein concentrations to pathogenic levels (Guerriero, C. J., and Brodsky, J. L., 2012).

Indeed, destabilizing amino-acid substitutions that elicit PQC degradation underlie a broad swath of human disease alleles (Stein, A., et al., 2019). In a recent study, a site-saturation mutagenesis library of the tumor suppressor PTEN was assayed for PTEN protein abundance *in vivo*. A strong correlation was found between potentially tumorigenic decreases in abundance and amino-acid substitutions that lower thermodynamic stability (Matreyek, K. A., et al., 2018). Related studies of the mismatch repair proteins MSH2 and MLH1 produced similar findings: When a range of destabilizing mutations were chosen and studied *in vivo*, the majority of disease-causative mutations elicited degradation by the UPS (Abildgaard, A. B., et al., 2019; Nielsen, S. V., et al., 2017). Our own analyses in chapter four represent an orthogonal approach to these studies. We find that the UPS has a broad ability to recognize amino-acid substitutions that disrupt hydrophobic pockets or remove electrostatic interactions. As was observed with MSH2 variants, these tend to cluster within a protein's tertiary structure. Overall, these data suggest the possibility of identifying destabilizing, disease-causative mutations amongst variants of uncertain significance (VUS), and they underline the ability of UPS to recognize numerous structural lesions, including relatively minor structural perturbations.

Along with genetic mutations, destabilizing point mutations can also arise from translational errors. While these destabilized species have long evaded detection and quantitation, recent studies have begun to isolate and explore the global pool of translational errors in bacteria (Garofalo, R., et al., 2019; Mordret, E., et al., 2019). In these studies, amino-acid substitutions could be detected at a frequency as high as 1 in 1000 amino acids, though error frequency varied considerably by position. These observations agree with previous estimates and imply that 5 to 15% of proteins bear a mutation cause by mistranslation (Drummond, D.A., & Wilke, C. O., 2009). It should be noted, however, that several factors mitigate the burden that mistranslations pose for PQC. For instance, error rates are significantly lower at conserved and structurally critical residues (Mordret, E., et al., 2019). Nevertheless, elaborate and semi-redundant PQC systems are surely conceivable if even 1% of a billion proteins bear a translational error, and it will be intriguing to investigate the translational errors that accumulate upon proteasome inhibition in yeast and mammals. It is also worth noting that the above-described studies could not detect premature stop codons because of methodological limitations, leaving the burden of truncations on PCQ largely untested. The wide-ranging ability of PQC ligases to recognize such species suggests they routinely challenge the cell.

A final class of substrate displays quality-control determinants as a part of regulated degradation. A canonical example is the yeast protein Hmg2 (Gardner, R. G., & Hampton, R. Y., 1999; Hampton, R. Y., & Rine, J., 1994). Most targets of regulated degradation, such as proteins that mediate the cell cycle, possess defined “degrons” that allow context-specific degradation and regulation of protein steady state levels (Boisvert, F. M., 2012; Christiano, R., et al., 2014; Schwanhüusser, B., et al., 2011, Skaar, J. R., et al., 2013). Like such proteins, Hmg2 levels are mediated by a cellular signal: a downstream product of the isoprenoid pathway, GGPP, binds to Hmg2 and causes its rapid degradation by the HRD pathway (Garza, R. M., 2009; Wangeline, M.A., & Hampton, R.Y., 2018). However, unlike canonical targets of regulated degradation, Hmg2 does

not seem to unveil a defined degron upon GGPP binding (Gardner, R. G., & Hampton, R. Y., 1999). Studies from our lab demonstrate that, at nanomolar concentrations, GGPP elicits a conformational loosening of the Hmg2 structure that mimics misfolding (Shearer and Hampton, 2004; Shearer & Hampton 2005; Wangeline, M.A., & Hampton, R.Y., 2018; Wangeline, M.A., & Hampton, R.Y., 2020). The high potency of GGPP, the ineffectiveness of other molecules that resemble GGPP, and the ability of Hmg2 to form multimers all suggest a mechanism of allosteric misfolding that we have named "mallostery." Tellingly, GGPP-mediated mallostery can be antagonized, *in vivo* and *in vitro*, by the presence of the chemical chaperones, which promote protein folding (Shearer et. al., 2004; Wangeline and Hampton, 2018). This mode of quality-control-mediated regulated degradation may be a general feature of the regulation of sterol-synthetic pathways (Wangeline et. al., 2017).

Outlook: What to PQC E3s Recognize as Misfoldedness?

Despite the well-documented classes of PQC substrate, the numerous examples of each, and the substantial evidence for the broad specificity of PQC E3 ligases, the structural and biochemical nature of most PQC "degrons" has remained elusive; defining such determinants and developing predicative frameworks for PQC recognition remain goals of the field.

The model that discrete degrons elicit PQC degradation is, in part, informed by studies wherein well-defined UPS determinants were isolated and shown to confer degradation upon reporter proteins. Perhaps the canonical example is that of the N-end rule and the elucidation of the amino-acid code that determines the rate of degradation governed by the pathway (Varshavsky, A., 2011). Another instance is the isolation of an amphipathic α helix within Matα2 repressor that confers Doa10-mediated degradation (Johnson, P. R., et. al, 1998; Swanson, R., et. al, 2001). Similarly, a 56 amino-acid-long portion of the Erg11 transmembrane domain is sufficient to confer Asi-complex-mediated degradation (Natarajan, N., et al., 2020) as is 45 amino-acid-long portion of the soluble protein Stp2 (Omnus, D.J, & Ljungdahl, P.O., 2014). Though many of these degrons are derived

from targets of regulated degradation, it seems likely that they inform PQC degradation as well: degron screens have isolated amphipathic α-helices from ordinarily stable proteins that are sufficient to elicit Doa10 recognition (Geffen, Y., et al., 2016).

Other studies suggest less discrete degrons and the possibility of PQC determinants that are spread across a protein's primary structure. For instance, a Doa10 degron within the normally stable protein Ndc10 required two distinct portions of a 55-amino-acid peptide (Furth, N., et al., 2011). Similarly, Hmg2 seems to possess quality-control determinants that are dispersed across the protein. These seem to display structural features that elicit PQC as opposed to specific amino-acid sequences (Gardner, R. G., & Hampton, R. Y., 1999; Wangeline, M.A., and Hampton, R.Y., 2018). Indeed, a number of studies have supported the notion of structural determinants, such as exposed hydrophobicity and disorder, as the underlying signal for quality-control degradation (Rosenbaum, J. C., et al., 2011; Frederickson, E.K., Rosenbaum, J. C., et al, 2011; Frederickson, E.K., et al., 2013). For a cross-section of substrates, PQC determinants may not be reducible to small amino-acid sequences that can confer heterologous degradation.

It seems likely that PQC relies upon both discrete and distributed signals to trigger ubiquitination. How these features are excluded from the proteome, the degree to which they are unveiled by a given point mutation, and whether such point mutations afford opportunities for therapeutic intervention are amongst the most exigent questions in the field. One significant shortcoming of our present knowledge is the comparative paucity of substrates that bear close resemblance to wild-type proteins; degron screens tend to isolate exogenous peptides, often derived from frameshifts (Geffen, Y., et al., 2013). Chapter four presents many full-length PQC substrates that can be interpreted using solved crystal structures. Perhaps a broad collection of such substrates, along with *in vitro* techniques such as hydrogen-deuterium exchange and computational software such as FoldX, can begin to elucidate the consequences of minor modes of misfolding. Perhaps the

insight gained from such studies will also allow clinicians to predict which variants of uncertain significance elicit PQC degradation, and correctors can be made to restore protein folding and function. In sum, if tremendous strides have been made in solving the protein-folding problem, these studies, and others like it, represent early efforts in discerning how cells solve the protein-misfolding problem.

References

Abildgaard, A. B., Stein, A., Nielsen, S. V., Schultz-Knudsen, K., Papaleo, E., Shrikhande, A., … Hartmann-Petersen, R. (2019). Computational and cellular studies reveal structural destabilization and degradation of mlh1 variants in lynch syndrome. ELife, 8.

Arndt, V., Dick, N., Tawo, R., Dreiseidler, M., Wenzel, D., Hesse, M., … Höhfeld, J. (2010). Chaperone-Assisted Selective Autophagy Is Essential for Muscle Maintenance. Current Biology, 20(2), 143–148.

Bai, L., Wang, T., Zhao, G., Kovach, A., & Li, H. (2018). The atomic structure of a eukaryotic oligosaccharyltransferase complex. Nature, 555(7696), 328–333.

Bäuerlein, F. J. B., Saha, I., Mishra, A., Kalemanov, M., Martínez-Sánchez, A., Klein, R., … Fernández-Busnadiego, R. (2017). In Situ Architecture and Cellular Interactions of PolyQ Inclusions. Cell, 171(1), 179-187.e10.

Bengtson, M. H., & Joazeiro, C. A. P. (2010). Role of a ribosome-associated E3 ubiquitin ligase in protein quality control. Nature, 467(7314), 470–473.

Biederer, T., Volkwein, C., & Sommer, T. (1996). Degradation of subunits of the Sec61p complex, an integral component of the ER membrane, by the ubiquitin-proteasome pathway. The EMBO Journal, 15(9), 2069–2076.

Boban, M., Pantazopoulou, M., Schick, A., Ljungdahl, P. O., & Foisner, R. (2014). A nuclear ubiquitin-proteasome pathway targets the inner nuclear membrane protein Asi2 for degradation. Journal of Cell Science, 127(16), 3603–3613.

Boisvert, F. M., Ahmad, Y., Gierliński, M., Charrière, F., Lamont, D., Scott, M., … Lamond, A. I. (2012). A quantitative spatial proteomics analysis of proteome turnover in human cells. Molecular and Cellular Proteomics, 11(3), 1–15.

Bordallo, J., Plemper, R. K., Finger, A., & Wolf, D. H. (1998). Der3p/Hrd1p is required for endoplasmic reticulum-associated degradation of misfolded lumenal and integral membrane proteins. Molecular Biology of the Cell, 9(1), 209–222.

Brehme, M., Voisine, C., Rolland, T., Wachi, S., Soper, J. H., Zhu, Y., … Morimoto, R. I. (2014). A chaperome subnetwork safeguards proteostasis in aging and neurodegenerative disease. Cell Reports, 9(3), 1135–1150.

Carvalho, P., Goder, V., & Rapoport, T. A. (2006). Distinct Ubiquitin-Ligase Complexes Define Convergent Pathways for the Degradation of ER Proteins. Cell, 126(2), 361–373.

Christiano, R., Nagaraj, N., Fröhlich, F., & Walther, T. C. (2014). Global Proteome Turnover Analyses of the Yeasts S.cerevisiae and S.pombe. Cell Reports, 9(5), 1959–1965.

Claessen, J. H. L., Kundrat, L., & Ploegh, H. L. (2012). Protein quality control in the ER: Balancing the ubiquitin checkbook. Trends in Cell Biology, 22(1), 22–32.

Couso, J. P., & Patraquim, P. (2017). Classification and function of small open reading frames. Nature Reviews Molecular Cell Biology, 18(9), 575–589.

Deng, M., & Hochstrasser, M. (2006). Spatially regulated ubiquitin ligation by an ER/nuclear membrane ligase. Nature, 443(7113), 827–831.

Dice, J. F. (2007). Chaperone-mediated autophagy. Autophagy, 3:4, 295-299.

Dikic, I. (2017). Proteasomal and Autophagic Degradation Systems. Annual Review of Biochemistry, 86(1), 193–224.

Drummond, D.A., & Wilke, C. O. (2009). The evolutionary consequences of erroneous protein synthesis. Nature Reviews Genetics, 10(10), 715–724.

Eisele, F., & Wolf, D. H. (2008). Degradation of misfolded protein in the cytoplasm is mediated by the ubiquitin ligase Ubr1. FEBS Letters, 582(30), 4143–4146.

Fang, S., Ferrone, M., Yang, C., Jensen, J. P., Tiwari, S., & Weissman, A. M. (2001). The tumor autocrine motility factor receptor, gp78, is a ubiquitin protein ligase implicated in degradation from the endoplasmic reticulum. Proceedings of the National Academy of Sciences of the United States of America, 98(25), 14422–14427.

Farzin Khosrow-Khavar, Fang, N. N., Ng, A. H. M., Winget, J. M., Comyn, S. A., & Mayor, T. (2012). The yeast ubr1 ubiquitin ligase participates in a prominent pathway that targets cytosolic thermosensitive mutants for degradation. G3: Genes, Genomes, Genetics, 2(5), 619–628.

Finka, A., & Goloubinoff, P. (2013). Proteomic data from human cell cultures refine mechanisms of chaperone-mediated protein homeostasis. Cell Stress and Chaperones, 18(5), 591–605.

Finley, D. (2009). Recognition and Processing of Ubiquitin-Protein Conjugates by the Proteasome. Annual Review of Biochemistry, 78(1), 477–513.

Finley, D., Ulrich, H. D., Sommer, T., & Kaiser, P. (2012). The ubiquitin-proteasome system of Saccharomyces cerevisiae. Genetics, 192(2), 319–360.

Foresti, O., Rodriguez-Vaello, V., Funaya, C., & Carvalho, P. (2014). Quality control of inner nuclear membrane proteins by the Asi complex. Science, 346(6210), 751–755.

Fredrickson, E. K., Gallagher, P. S., Candadai, S. V. C., & Gardner, R. G. (2013). Substrate recognition in nuclear protein quality control degradation is governed by exposed hydrophobicity that correlates with aggregation and insolubility. Journal of Biological Chemistry, 288(9), 6130–6139.

Fredrickson, E. K., Rosenbaum, J. C., Locke, M. N., Milac, T. I., & Gardner, R. G. (2011). Exposed hydrophobicity is a key determinant of nuclear quality control degradation. Molecular Biology of the Cell, 22(13), 2384–2395.

Furth, N., Gertman, O. O., Shiber, A., Alfassy, O. S., Cohen, I., Rosenberg, M. M., … Ravid, T. (2011). Exposure of bipartite hydrophobic signal triggers nuclear quality control of Ndc10 at the endoplasmic reticulum/nuclear envelope. Molecular Biology of the Cell, 22(24), 4726–4739.

Galluzzi, L., Baehrecke, E. H., Ballabio, A., Boya, P., Bravo-San Pedro, J. M., Cecconi, F., … Kroemer, G. (2017). Molecular definitions of autophagy and related processes. The EMBO Journal, 36(13), 1811–1836.

Gardner, R. G., & Hampton, R. Y. (1999). A 'distributed degron' allows regulated entry into the ER degradation pathway, 18(21), 5994–6004.

Gardner, R. G., Nelson, Z. W., & Gottschling, D. E. (2005). Degradation-mediated protein quality control in the nucleus. Cell, 120(6), 803–815.

Gardner, R. G., Shearer, A. G., Randolph, Y., & Hampton, R. Y. (2001). In Vivo Action of the HRD Ubiquitin Ligase Complex: Mechanisms of Endoplasmic Reticulum Quality Control and Sterol Regulation In Vivo Action of the HRD Ubiquitin Ligase Complex: Mechanisms of Endoplasmic Reticulum Quality Control and Sterol Regulation. Society, 21(13), 4276–4291.

Garofalo, R., Wohlgemuth, I., Pearson, M., Lenz, C., Urlaub, H., & Rodnina, M. V. (2019). Broad range of missense error frequencies in cellular proteins. Nucleic Acids Research, 47(6), 2932–2945.

Garza, R. M., Tran, P. N., & Hampton, R. Y. (2009). Geranylgeranyl pyrophosphate is a potent regulator of HRD-dependent 3-hydroxy-3-methylglutaryl-CoA reductase degradation in yeast. Journal of Biological Chemistry, 284(51), 35368–35380.

Geffen, Y., Appleboim, A., Gardner, R. G., Friedman, N., Sadeh, R., & Ravid, T. (2016). Mapping the Landscape of a Eukaryotic Degronome. Molecular Cell, 63(6), 1055–1065.

Glover, J. R., & Lindquist, S. (1998). Hsp104, Hsp70, and Hsp40: A novel chaperone system that rescues previously aggregated proteins. Cell, 94(1), 73–82.

Guerriero, C. J., & Brodsky, J. L. (2012). The delicate balance between secreted protein folding and endoplasmic reticulum-associated degradation in human physiology. Physiological Reviews, 92(2), 537–576.

Guo, L., Giasson, B. I., Glavis-Bloom, A., Brewer, M. D., Shorter, J., Gitler, A. D., & Yang, X. (2014). A cellular system that degrades misfolded proteins and protects against neurodegeneration. Molecular Cell, 55(1), 15–30.

Habeck, G., Ebner, F. A., Shimada-Kreft, H., & Kreft, S. G. (2015). The yeast ERAD-C ubiquitin ligase Doa10 recognizes an intramembrane degron. Journal of Cell Biology, 209(2), 261–273.

Hampton, R. Y., & Rine, J. (1994). Regulated degradation of HMG-CoA reductase, an integral membrane protein of the endoplasmic reticulum, in yeast. Journal of Cell Biology, 125(2), 299–312.

Hampton, R. Y., Gardner, R. G., & Rine, J. (1996). Role of 26S proteasome and HRD genes in the degradation of 3-hydroxy-3-methylglutaryl-CoA reductase, an integral endoplasmic reticulum membrane protein. Molecular Biology of the Cell, 7(12), 2029–2044.

Harper, J. W., & Bennett, E. J. (2016). Proteome complexity and the forces that drive proteome imbalance. Nature.

Haslbeck, M., & Vierling, E. (2015). A first line of stress defense: Small heat shock proteins and their function in protein homeostasis. Journal of Molecular Biology, 427(7), 1537–1548.

Heck, J. W., Cheung, S. K., & Hampton, R. Y. (2010). Cytoplasmic protein quality control degradation mediated by parallel actions of the E3 ubiquitin ligases Ubr1 and San1. Proceedings of the National Academy of Sciences, 107(3), 1106–1111.

Hegde, R. S., & Zavodszky, E. (2019). Recognition and degradation of mislocalized proteins in health and disease. Cold Spring Harbor Perspectives in Biology, 11(11), 1–18.

Hessa, T., Sharma, A., Mariappan, M., Eshleman, H. D., Gutierrez, E., & Hegde, R. S. (2011). Protein targeting and degradation are coupled for elimination of mislocalized proteins. Nature, 475(7356), 394–399.

Hetz, C., & Papa, F. R. (2018). The Unfolded Protein Response and Cell Fate Control. Molecular Cell, 69(2), 169–181.

Huttlin, E. L., Ting, L., Bruckner, R. J., Gebreab, F., Gygi, M. P., Szpyt, J., … Gygi, S. P. (2015). The BioPlex Network: A Systematic Exploration of the Human Interactome. Cell, 162(2), 425–440.

Iwata, A., Nagashima, Y., Matsumoto, L., Suzuki, T., Yamanaka, T., Date, H., … Tsuji, S. (2009). Intranuclear degradation of polyglutamine aggregates by the ubiquitin-proteasome system. Journal of Biological Chemistry, 284(15), 9796–9803.

Jayaraj, G. G., Hipp, M. S., & Ulrich Hartl, F. (2020). Functional modules of the proteostasis network. Cold Spring Harbor Perspectives in Biology, 12(1).

Joazeiro, C. A. P. (2019). Mechanisms and functions of ribosome-associated protein quality control. Nature Reviews Molecular Cell Biology, 20(6), 368–383.

Johnson, P. R., Swanson, R., Rakhilina, L., & Hochstrasser, M. (1998). Degradation signal masking by heterodimerization of MATα2 and MATa1 blocks their mutual destruction by the ubiquitin-proteasome pathway. Cell, 94(2), 217–227.

Juszkiewicz, S., & Hegde, R. S. (2018). Quality Control of Orphaned Proteins. Molecular Cell, 71(3), 443–457.

Khmelinskii, A., Blaszczak, E., Pantazopoulou, M., Fischer, B., Omnus, D. J., Dez, G. Le, … Knop, M. (2014). Protein quality control at the inner nuclear membrane. Nature, 516(7531), 410–413.

Kim, Y. E., Hosp, F., Frottin, F., Ge, H., Mann, M., Hayer-Hartl, M., & Hartl, F. U. (2016). Soluble Oligomers of PolyQ-Expanded Huntingtin Target a Multiplicity of Key Cellular Factors. Molecular Cell, 63(6), 951–964.

Klaips, C. L., Jayaraj, G. G., & Hartl, F. U. (2018). Pathways of cellular proteostasis in aging and disease. Journal of Cell Biology, 217(1), 51–63.

Kundrat, L., & Regan, L. (2010). Balance between folding and degradation for Hsp90-dependent client proteins: A key role for CHIP. Biochemistry, 49(35), 7428–7438.

Lamb, C. A., Yoshimori, T., & Tooze, S. A. (2013). The autophagosome: Origins unknown, biogenesis complex. Nature Reviews Molecular Cell Biology, 14(12), 759–774.

Lander, G. C., Estrin, E., Matyskiela, M. E., Bashore, C., Nogales, E., & Martin, A. (2012). Complete subunit architecture of the proteasome regulatory particle. Nature, 482(7384), 186–191.

Lee, J. W., Beebe, K., Nangle, L. A., Jang, J., Longo-Guess, C. M., Cook, S. A., … Ackerman, S. L. (2006). Editing-defective tRNA synthetase causes protein misfolding and neurodegeneration. Nature, 443(7107), 50–55.

Leto, D. E., & Kopito, R. R. (2019). Methods for genetic analysis of mammalian ER-associated degradation. Methods in Enzymology (1st ed., Vol. 619). Elsevier Inc.

Li, W., Bengtson, M. H., Ulbrich, A., Matsuda, A., Reddy, V. A., Orth, A., … Joazeiro, C. A. P. (2008). Genome-wide and functional annotation of human E3 ubiquitin ligases identifies MULAN, a mitochondrial E3 that regulates the organelle's dynamics and signaling. PLoS ONE, 3(1).

Madian, A. G., & Regnier, F. E. (2010). Proteomic identification of carbonylated proteins and their oxidation sites. Journal of Proteome Research, 9(8), 3766–3780.

Malinovska, L., Kroschwald, S., Munder, M. C., Richter, D., & Alberti, S. (2012). Molecular chaperones and stress-inducible protein-sorting factors coordinate the spatiotemporal distribution of protein aggregates. Molecular Biology of the Cell, 23(16), 3041–3056.

Manolio, T. A., Fowler, D. M., Starita, L. M., Haendel, M. A., MacArthur, D. G., Biesecker, L. G., … Bult, C. (2017). Bedside Back to Bench: Building Bridges between Basic and Clinical Genomic Research. Cell, 169(1), 6–12.

Matreyek, K. A., Starita, L. M., Stephany, J. J., Martin, B., Chiasson, M. A., Gray, V. E., … Fowler, D. M. (2018). Multiplex assessment of protein variant abundance by massively parallel sequencing. Nature Genetics, 50(6), 874–882.

Maurer, M. J., Spear, E. D., Yu, A. T., Lee, E. J., Shahzad, S., & Michaelis, S. (2016). Degradation signals for ubiquitin-proteasome dependent cytosolic protein quality control (CytoQC) in yeast. G3: Genes, Genomes, Genetics, 6(7), 1853–1866.

McShane, E., Sin, C., Zauber, H., Wells, J. N., Donnelly, N., Wang, X., … Selbach, M. (2016). Kinetic Analysis of Protein Stability Reveals Age-Dependent Degradation. Cell, 167(3), 803-815.e21. https://doi.org/10.1016/j.cell.2016.09.015

Mordret, E., Dahan, O., Asraf, O., Rak, R., Yehonadav, A., Barnabas, G. D., … Pilpel, Y. (2019). Systematic Detection of Amino Acid Substitutions in Proteomes Reveals Mechanistic Basis of Ribosome Errors and Selection for Translation Fidelity. Molecular Cell, 75(3), 427-441.e5.

Murata, S., Minami, Y., Minami, M., Chiba, T., & Tanaka, K. (2001). CHIP is a chaperone-dependent E3 ligase that ubiquitylates unfolded protein. EMBO Reports, 2(12), 1133–1138.

Nagaraj, N., Wisniewski, J. R., Geiger, T., Cox, J., Kircher, M., Kelso, J., … Mann, M. (2011). Deep proteome and transcriptome mapping of a human cancer cell line. Molecular Systems Biology, 7(548), 1–8.

Nakatsukasa, K., Huyer, G., Michaelis, S., & Brodsky, J. L. (2008). Dissecting the ER-Associated Degradation of a Misfolded Polytopic Membrane Protein. Cell, 132(1), 101–112.

Natarajan, N., Foresti, O., Wendrich, K., Stein, A., & Carvalho, P. (2020). Quality Control of Protein Complex Assembly by a Transmembrane Recognition Factor. Molecular Cell, 77(1), 108-119.e9.

Neal, S., Mak, R., Bennett, E. J., & Hampton, R. (2017). A Cdc48 "retrochaperone" function is required for the solubility of retrotranslocated, integral membrane Endoplasmic Reticulum-associated Degradation (ERAD-M) substrates. Journal of Biological Chemistry, 292(8), 3112–3128.

Needham, P. G., Guerriero, C. J., & Brodsky, J. L. (2019). Chaperoning endoplasmic reticulum-associated degradation (ERAD) and protein conformational diseases. Cold Spring Harbor Perspectives in Biology, 11(8).

Nielsen, S. V., Stein, A., Dinitzen, A. B., Papaleo, E., Tatham, M. H., Poulsen, E. G., … Hartmann-Petersen, R. (2017). Predicting the impact of Lynch syndrome-causing missense mutations from structural calculations. PLoS Genetics, 13(4), 1–26.

Nillegoda, N. B., Kirstein, J., Szlachcic, A., Berynskyy, M., Stank, A., Stengel, F., … Bukau, B. (2015). Crucial HSP70 co-chaperone complex unlocks metazoan protein disaggregation. Nature, 524(7564), 247–251.

Olzscha, H., Schermann, S. M., Woerner, A. C., Pinkert, S., Hecht, M. H., Tartaglia, G. G., … Vabulas, R. M. (2011). Amyloid-like aggregates sequester numerous metastable proteins with essential cellular functions. Cell, 144(1), 67–78.

Omnus, D. J., & Ljungdahl, P. O. (2014). Latency of transcription factor Stp1 depends on a modular regulatory motif that functions as cytoplasmic retention determinant and nuclear degron. Molecular Biology of the Cell, 25(23), 3823–3833.

Pan, Q., Shai, O., Lee, L. J., Frey, B. J., & Blencowe, B. J. (2008). Deep surveying of alternative splicing complexity in the human transcriptome by high-throughput sequencing. Nature Genetics, 40(12), 1413–1415.

Park, S. H., Kukushkin, Y., Gupta, R., Chen, T., Konagai, A., Hipp, M. S., … Hartl, F. U. (2013). PolyQ proteins interfere with nuclear degradation of cytosolic proteins by sequestering the Sis1p chaperone. Cell, 154(1), 134–145.

Plemper, R. K., Egner, R., Kuchler, K., & Wolf, D. H. (1998). Endoplasmic reticulum degradation of a mutated ATP-binding cassette transporter Pdr5 proceeds in a concerted action of Sec61 and the proteasome. Journal of Biological Chemistry, 273(49), 32848–32856.

Pobre, K. F. R., Poet, G. J., & Hendershot, L. M. (2019). The endoplasmic reticulum (ER) chaperone BiP is a master regulator of ER functions: Getting by with a little help from ERdj friends. Journal of Biological Chemistry, 294(6), 2098–2108.

Prabakaran, S., Lippens, G., Steen, H., & Gunawardena, J. (2012). Post-translational modification: Nature's escape from genetic imprisonment and the basis for dynamic information encoding. Wiley Interdisciplinary Reviews: Systems Biology and Medicine, 4(6), 565–583.

Preissler, S., & Deuerling, E. (2012). Ribosome-associated chaperones as key players in proteostasis. Trends in Biochemical Sciences, 37(7), 274–283. https://doi.org/10.1016/j.tibs.2012.03.002

Ravid, T., & Hochstrasser, M. (2008). Diversity of degradation signals in the ubiquitin-proteasome system. Nature Reviews Molecular Cell Biology, 9(9), 679–689.

Ravid, T., Kreft, S. G., & Hochstrasser, M. (2006). Membrane and soluble substrates of the Doa10 ubiquitin ligase are degraded by distinct pathways. EMBO Journal, 25(3), 533–543.

Reck-Peterson, S. L., Redwine, W. B., Vale, R. D., & Carter, A. P. (2018). The cytoplasmic dynein transport machinery and its many cargoes. Nature Reviews Molecular Cell Biology, 19(6), 382–398.

Richly, H., Rape, M., Braun, S., Rumpf, S., Hoege, C., & Jentsch, S. (2005). A series of ubiquitin binding factors connects CDC48/p97 to substrate multiubiquitylation and proteasomal targeting. Cell, 120(1), 73–84.

Richter, K., Haslbeck, M., & Buchner, J. (2010). The Heat Shock Response: Life on the Verge of Death. Molecular Cell, 40(2), 253–266.

Rideout, H. J., Lang-Rollin, I., & Stefanis, L. (2004). Involvement of macroautophagy in the dissolution of neuronal inclusions. International Journal of Biochemistry and Cell Biology, 36(12), 2551–2562.

Rodrigo-Brenni, M. C., Gutierrez, E., & Hegde, R. S. (2014). Cytosolic Quality Control of Mislocalized Proteins Requires RNF126 Recruitment to Bag6. Molecular Cell, 55(2), 227–237.

Rosenbaum, J. C., Fredrickson, E. K., Oeser, M. L., Garrett-Engele, C. M., Locke, M. N., Richardson, L. A., … Gardner, R. G. (2011). Disorder targets misorder in nuclear quality control degradation: A disordered ubiquitin ligase directly recognizes its misfolded substrates. Molecular Cell, 41(1), 93–106.

Ross, C. A., & Poirier, M. A. (2004). Protein aggregation and neurodegenerative disease. Nature Medicine, 10(7), S10.

Scazzari, M., Amm, I., & Wolf, D. H. (2015). Quality control of a cytoplasmic protein complex: Chaperone motors and the ubiquitin-proteasome system govern the fate of orphan fatty acid synthase subunit Fas2 of yeast. Journal of Biological Chemistry, 290(8), 4677–4687.

Schmidt, O., Pfanner, N., & Meisinger, C. (2010). Mitochondrial protein import: From proteomics to functional mechanisms. Nature Reviews Molecular Cell Biology, 11(9), 655–667.

Schwanhüusser, B., Busse, D., Li, N., Dittmar, G., Schuchhardt, J., Wolf, J., … Selbach, M. (2011). Global quantification of mammalian gene expression control. Nature, 473(7347), 337–342.

Shao, S., & Hegde, R. S. (2016). Target Selection during Protein Quality Control. Trends in Biochemical Sciences, 41(2), 124–137.

Shearer, A. G., & Hampton, R. Y. (2004). Structural control of endoplasmic reticulum-associated degradation. Effect of chemical chaperones on 3-hydroxy-3-methylglutaryl-CoA reductase. Journal of Biological Chemistry, 279(1), 188–196

Shearer, A. G., & Hampton, R. Y. (2005). Lipid-mediated, reversible misfolding of a sterol-sensing domain protein. EMBO Journal, 24(1), 149–159.

Shemorry, A., Hwang, C. S., & Varshavsky, A. (2013). Control of Protein Quality and Stoichiometries by N-Terminal Acetylation and the N-End Rule Pathway. Molecular Cell, 50(4), 540–551.

Shi, Y., Chen, X., Elsasser, S., Stocks, B. B., Tian, G., Lee, B. H., … Walters, K. J. (2016). Rpn1 provides adjacent receptor sites for substrate binding and deubiquitination by the proteasome. Science, 351(6275).

Singh, A., Vashistha, N., Heck, J., Tang, X., Wipf, P., Brodsky, J. L., & Hampton, R. Y. (2020). Direct involvement of Hsp70 ATP hydrolysis in Ubr1-dependent quality control. Molecular Biology of the Cell, 31, mbc.E20-08-0541.

Skaar, J. R., Pagan, J. K., & Pagano, M. (2013). Mechanisms and function of substrate recruitment by F-box proteins. Nature Reviews Molecular Cell Biology, 14(6), 369–381.

Smoyer, C. J., Smith, S. E., Gardner, J. M., McCroskey, S., Unruh, J. R., & Jaspersen, S. L. (2019). Distribution of proteins at the inner nuclear membrane is regulated by the asi1 E3 ligase in saccharomyces cerevisiae. Genetics, 211(4), 1269–1282.

Stein, A., Fowler, D. M., Hartmann-Petersen, R., & Lindorff-Larsen, K. (2019). Biophysical and Mechanistic Models for Disease-Causing Protein Variants. Trends in Biochemical Sciences, 44(7), 575–588.

Sun, Z., & Brodsky, J. L. (2019). Protein quality control in the secretory pathway. Journal of Cell Biology, 218(10), 3171–3187.

Sung, M. K., Porras-Yakushi, T. R., Reitsma, J. M., Huber, F. M., Sweredoski, M. J., Hoelz, A., … Deshaies, R. J. (2016). A conserved quality-control pathway that mediates degradation of unassembled ribosomal proteins. ELife, 5(AUGUST), 1–28.

Suraweera, A., Münch, C., Hanssum, A., & Bertolotti, A. (2012). Failure of amino acid homeostasis causes cell death following proteasome inhibition. Molecular Cell, 48(2), 242–253.

Swanson, R., Locher, M., & Hochstrasser, M. (2001). A conserved ubiquitin ligase of the nuclear envelope/endoplasmic reticulum that functions in both ER-associated and Mat2 repressor degradation. Genes & Development, 2(20), 2660–2674.

Tyler, R. E., Pearce, M. M. P., Shaler, T. A., Olzmann, J. A., Greenblatt, E. J., & Kopito, R. R. (2012). Unassembled CD147 is an endogenous endoplasmic reticulum-associated degradation substrate. Molecular Biology of the Cell, 23(24), 4668–4678.

Varshavsky, A. (2011). The N-end rule pathway and regulation by proteolysis. Protein Science, 20(8), 1298–1345.

Vo, M. N., Terrey, M., Lee, J. W., Roy, B., Moresco, J. J., Sun, L., … Ackerman, S. L. (2018). ANKRD16 prevents neuron loss caused by an editing-defective tRNA synthetase. Nature, 557(7706), 510–515.

Wangeline MA, Hampton RY. An autonomous, but INSIG-modulated, role for the Sterol Sensing Domain in mallostery-regulated ERAD of yeast HMG-CoA reductase. (2020) J Biol Chem. Epub ahead of print.

Wangeline, M. A., & Hampton, R. Y. (2018). "Mallostery"—ligand-dependent protein misfolding enables physiological regulation by ERAD. Journal of Biological Chemistry, 293(38), 14937–14950.

Wangeline, M. A., Vashistha, N., & Hampton, R. Y. (2017). Proteostatic Tactics in the Strategy of Sterol Regulation. Annual Review of Cell and Developmental Biology, 33(1), 467–489.

Willmund, F., Del Alamo, M., Pechmann, S., Chen, T., Albanèse, V., Dammer, E. B., … Frydman, J. (2013). The cotranslational function of ribosome-associated Hsp70 in eukaryotic protein homeostasis. Cell, 152(1–2), 196–209.

Wirth, C., Brandt, U., Hunte, C., & Zickermann, V. (2016). Structure and function of mitochondrial complex i. Biochimica et Biophysica Acta - Bioenergetics, 1857(7), 902–914.

Wiśniewski, J. R., Hein, M. Y., Cox, J., & Mann, M. (2014). A "proteomic ruler" for protein copy number and concentration estimation without spike-in standards. Molecular and Cellular Proteomics, 13(12), 3497–3506.

Wolff, S., Weissman, J. S., & Dillin, A. (2014, March 27). Differential scales of protein quality control. Cell, 157(1), 52-64.

Wright, P. E., & Dyson, H. J. (2015). Intrinsically disordered proteins in cellular signalling and regulation. Nature Reviews Molecular Cell Biology, 16(1), 18–29.

Xu, C., & Ng, D. T. W. (2015). Glycosylation-directed quality control of protein folding. Nature Reviews Molecular Cell Biology, 16(12), 742–752.

Yanagitani, K., Juszkiewicz, S., & Hegde, R. S. (2017). UBE2O is a quality control factor for orphans of multiprotein complexes. Science, 357(6350), 472–475.

Zheng, N., & Shabek, N. (2017). Ubiquitin Ligases: Structure, Function, and Regulation. Annual Review of Biochemistry, 86(1), 129–157.

CHAPTER II

Integrating after CEN Excision (ICE) Plasmids: Combining the Ease of Yeast Recombination Cloning with the Stability of Genomic Integration

Received: 23 January 2019 | Revised: 23 March 2019 | Accepted: 3 May 2019

DOI: 10.1002/yea.3400

RESEARCH ARTICLE

WILEY Yeast 2019

Integrating after CEN Excision (ICE) Plasmids: Combining the ease of yeast recombination cloning with the stability of genomic integration

Matthew P. Flagg | Andy Kao | Randolph Y. Hampton

Division of Biological Sciences, Section of Cell and Developmental Biology, University of California San Diego, La Jolla, California

Correspondence
Randolph Y. Hampton, Division of Biological Sciences, Section of Cell and Developmental Biology, University of California San Diego, 9500 Gilman Dr., La Jolla, CA 92093-0347.
Email: rhampton@ucsd.edu

Funding information
National Institutes of Health Cell Molecular Genetics (CMG), Grant/Award Number: 5T32GM007240-37; National Institutes of Health, Grant/Award Number: 5R37DK051996-18

Abstract

Yeast recombination cloning is a straightforward and powerful method for recombining a plasmid backbone with a specific DNA fragment. However, the utility of yeast recombination cloning is limited by the requirement for the backbone to contain an *CEN/ARS* element, which allows for the recombined plasmids to propagate. Although yeast *CEN/ARS* plasmids are often suitable for further studies, we demonstrate here that they can vary considerably in copy number from cell to cell and from colony to colony. Variation in plasmid copy number can pose an unacceptable and often unacknowledged source of phenotypic variation. If expression levels are critical to experimentation, then constructs generated with yeast recombination cloning must be subcloned into integrating plasmids, a step that often abrogates the utility of recombination cloning. Accordingly, we have designed a vector that can be used for yeast recombination cloning but can be converted into the integrating version of the resulting vector without an additional subcloning. We call these "ICE" vectors, for "Integrating after *CEN* Excision." The ICE series was created by introducing a "rare-cutter" *Not*I-flanked *CEN/ARS* element into the multiple cloning sites of the pRS series yeast integration plasmids. Upon recovery from yeast, the *CEN/ARS* is excised by *Not*I digest and subsequently religated without need for purification or transfer to new conditions. Excision by this approach takes ~3 hr, allowing this refinement in the same time frame as standard recombination cloning.

KEYWORDS

ARS/CEN, molecular cloning, plasmid copy number, plasmids, recombination, stable integration

1 | INTRODUCTION

Saccharomyces cerevisiae is well known for its ability to perform homologous recombination with transformed DNA fragments. Although this ability is most often leveraged to perform targeted knockouts and knock ins, homologous recombination also facilitates a versatile methodology known as yeast recombination cloning (YRC). In the simplest case, YRC allows users to recombine a linear DNA fragment and a desired vector backbone in vivo to directly create fully usable recombinant plasmids (Ma, Kunes, Schatz, & Botstein, 1987). This is achieved by a simple cotransformation of the two fragments, wherein homology between the fragment and vector backbone facilitate recombination. An *CEN/ARS* element on the backbone allows propagation of the novel, circularized plasmid, and a selectable marker on the backbone enables isolation of a yeast strain bearing the successfully constructed plasmid.

YRC is a cost-effective, flexible, and straightforward methodology. In most cases, it requires only PCR, restriction enzyme digest, and

[Correction added on 10 October 2019, after first online publication on 09 August 2019: Figure 2 has been corrected in this version]

traditional yeast transformation, but it offers the ability to reliably assemble as many as 25 overlapping PCR fragments and a vector backbone (Gibson et al., 2008; Ma et al., 1987; Oldenburg, Vo, Michaelis, & Paddon, 1997). YRC also allows for recombination to occur at any point of homology between two DNA fragments (rather than at DNA ends alone), can be facilitated by ssDNA linkers that bridge dsDNA fragments, and can be executed using ssDNA fragments alone (Gibson, 2009; Raymond, Sims, & Olson, 2002). Together, these features can facilitate the assembly of most imaginable constructs, allowing users to test an array of promoters, terminators, and fusions at low cost with minimal additional workflow.

In addition to its use as a highly modular tool for creating plasmids, YRC also provides a rapid means to create yeast strains that bear a novel construct of interest. After transforming a cut backbone and desired fragments into yeast, researchers can immediately use the resultant transformants to assay functionality, stability, and so forth of a novel mutant, fusion protein, or promoter-gene-terminator combination. In many cases, this feature of YRC has been successfully employed to create a screening platform. For instance, by transforming yeast with a randomly mutated gene of interest and a suitable cut backbone, researchers can rapidly obtain a library of yeast transformants, each bearing a unique mutation of the gene of interest (Muhlrad, Hunter, & Parker, 1992). Transformants can then be screened for desired phenotypes. In this way and others, YRC offers powerful lines of inquiry to yeast geneticists, including using this method to study genes from other organisms, such as the many human genes that retain function in yeast (Kachroo et al., 2015).

A caveat of YRC is that it requires cloning into a yeast *CEN* plasmid (YCp) so that recombinant plasmids can propagate. Although YCps are acceptable for many applications and can often facilitate screening schemes, in some instances, they pose significant drawbacks. *CEN/ARS* elements confer incomplete stability upon a plasmid, leading to heterogeneity in plasmid copy number, even within clonal populations (Chou, Patel, & Gartenberg, 2015; Gnügge, Liphardt, & Rudolf, 2016; Hieter, Mann, Snyder, & Davis, 1985; and below). Conversely, constructs integrated into the genome using yeast integrating plasmids (YIps) are thought to be more stable, ensuring less varied levels of gene expression between clones. Here, we have confirmed differences in the expression profiles of YCp and YIp constructs, directly demonstrating the considerable phenotypic variation that arises from YCp gain and loss. We present these data to clarify the risks of using YCp constructs and to help readers to decide if those risks are acceptable in the context of their experimental systems.

Traditionally, when YCps caused an unacceptable source of phenotypic varitation, a product generated by YRC had to be subcloned into a new, non-*CEN/ARS* vector. This was often the case in our lab because the variability of *CEN/ARS*-based expression is on the same order of magnitude as the regulatory phenomena that we study (Hampton, Gardner, & Rine, 1996). Thus, we rarely employed YRC because it almost always led to additional subcloning. To obviate this issue, we have designed a plasmid that allows for facile conversion of a YRC product into an integrating plasmid, allowing for Integrating after *CEN* Excision (ICE). ICE plasmids are a variant of pRS40x series plasmids wherein a CEN/ARS element has been introduced into the multiple-cloning site at the rare-cutting (GC^GGCCGC) *Not*I site (Sikorski & Hieter, 1989). The result is a *CEN/ARS* flanked by *Not*I sites in an otherwise identical plasmid. After production of the desired plasmid by YRC, the *CEN*/ARS sequence can be excised by *Not*I digestion followed by reclosing of the site. To streamline this protocol, we optimized a procedure in which a yeast miniprep can be subjected to *Not*I digest and, without a buffer change, can be subsequently religated and transformed into *Escherichia coli*. This simple procedure produces the cognate YIps without a *CEN/ARS* at an extremely high frequency. The recovered plasmids are identical to the integrating pRS40x series plasmids, because *Not*I digest and religation lead to a "scarless" reassembly. This allows the product to be compared with traditional pRS series empty vector controls.

To facilitate broad utility, we have created and deposited a large family of ICE vectors, including a set that addresses the difficulties of using integrating constructs in the increasingly popular BY4741 "null collection" background. Because the auxotrophies of BY4741 are produced by complete deletion of the HIS3, LEU2, MET17, or URA3 coding regions, these sites are not amenable to traditional integration-selection approaches using landing sites within the coding region to be complemented (Brachmann et al., 1998). Accordingly, we created 21 plasmids, each bearing a region that allows integration at a neutral site (ADE2, LYS2, and TRP1) in addition to a separate selectable marker (HIS3, LEU2, MET17, URA3, HphMx, KanMx, and NatMx). In this way, one can integrate up to three constructs into BY4741. This group includes both the BY4741-friendly ICE plasmid and its cognate *CEN*-excised YIp version.

2 | MATERIALS AND METHODS

2.1 | Yeast and bacteria growth and media

Standard *Saccharomyces cerevisiae* media was used as previously described (Hampton & Rine, 1994). Media included yeast extract-peptone-dextrose (YPD) and ammonia-based synthetic complete (SC) or minimal media (YNB) supplemented with 2% dextrose and amino acids required for growth. All yeast cultures were grown at 30°C. *E. coli* Top 10 cells were grown at 37°C in standard LB medium with added ampicillin as previously described (Gardner, Cronin, Leader, Rine, & Hampton, 1998).

2.2 | Flow cytometry

Cells were inoculated in selective YNB dropout medium and grown overnight to saturation. The following day, cultures were diluted to 0.1 OD 600 in fresh YNB dropout medium and grown into log phase. GFP readings were obtained using a BD Accuri C6 flow cytometer as previously described (Garza, Tran, & Hampton, 2009). Cytometry population statistics and histograms were obtained from BD Accuri and FlowJo software.

2.3 | Fluorescence scanning and measurement of colony fluorescence

To detect sectoring, RHY10932 and RHY10933 were thawed, streaked onto SC −Leu plates, and grown for 3 days. Plates were then scanned by a GM Amersham Typhoon at maximum resolution (10 μm).

2.4 | YCp *pCPY::LYS1* escaper and revertant experiments

RHY11209 was maintained on SC −LEU dropout plates to select for plasmid presence but not lysine protorophy. The strain was inoculated into YNB −LEU medium and grown overnight. The following day, 1 OD 600 of stationary phase cells was spread by beads onto SC −LYS plates. Cells were grown at 30°C, and colonies were counted at various time points. One escaper that gained the lysine prototrophy was isolated as RHY11214.

RHY11214 was then streaked to a YPD plate three consecutive times to allow for plasmid loss. A single colony was used to streak a new plate with each passage. A single colony was isolated from the third passage and renamed RHY11808.

To determine the mean fluorescence of RHY11214 and RHY11808, flow cytometry was performed as described above. Escaper *pCPY::LYS1-GFP* colonies were inoculated in YNB −LYS, and parental *pCPY::LYS1-GFP* were inoculated into YNB −LEU. A *pTDH3::LYS1-GFP* strain was also inoculated into YNB −LYS or −LEU as indicated.

2.5 | Strains used and plasmid construction

Yeast strains used in this study can be found in Table S1. All transformations were performed using the typical LiOAc method (Ito, Fukuda, Murata, & Kimura, 1983).

A list of all the plasmids created and used in this study can be found in Table S2. Homologous recombination in yeast (Ma et al., 1987; Oldenburg et al., 1997) and restriction-mediated cloning (Heck, Cheung, & Hampton, 2010) were carried out as described elsewhere.

pRH2935 (YCp *URA3 pTDH3::GFP::tPGK1*) was made using homologous recombination in yeast. PCR was performed using oRH4805, oRH4852, and pRH2695, generating a *pTDH3::GFP::tPGK1* fragment. pRS416 (YCp *URA3*) was opened using *Xho*I and *Bam*HI and was cotransformed with the *pTDH3::GFP::tPGK1* fragment. Recombinants were selected on SC −URA plates. Plasmids were recovered as described below and transformed into *E. coli*. The entire insert was confirmed by sequencing (Eton Biosciences).

pRH2896 was created using gDNA from RHY10527 (BY4741 *LYS1-GFP::tADH1 HIS3Mx6*) and oRH4915 and oRH4926. The resultant *LYS1-GFP* PCR product was then recombined in yeast with a YCp *LEU2* plasmid bearing a *TDH3* promoter, GFP, and an *ADH1* terminator derived from the GFP collection. Transformants were selected on SC −LEU plates, and plasmids were recovered. The entire insert was confirmed by sequencing.

pRH2913 (YCp *LEU2 pADH1::LYS1-GFP::tADH1*), pRH2914 (YCp *LEU2 pCPY::LYS1-GFP::tADH1*), and pRH2915 (YCp *LEU2 pCYC1::LYS1-GFP::tADH1*) were created by substituting different promoters into pRH2896 by homologous recombination in yeast. For pRH2913, the ADH1 promoter was amplified from pRH2815 using oRH4938 and oRH4939. For pRH2914, the CPY promoter was amplified from pRH1941 using oRH4946 and oRH4947. For pRH2915, the CYC1 promoter was amplified from BY4741 (RHY7447) gDNA using oRH4941 and oRH4940. Additional homology was then added to the oRH4940-oRH4941 fragment with oRH4942 and oRH4943. In all three cases, promoter fragments were cotransformed with *Ale*I-*Spe*I digested pRH2896. Successful recombinants were selected on SC −LEU and were recovered to *E. coli*. Sequencing confirmed the presence of the appropriate promoters.

To create an initial ICE plasmid (pRH2952), the *CEN/ARS* of pRS415 (YCp *LEU2*) was amplified with oRH4866 and 4867, which both contain *Not*I sites. The resultant amplicon and pRS406 (YIp *URA3*) were digested and ligated together. Directionality was confirmed by sequencing. pRH2947 (ICE *ADE2*), pRH2948 (ICE *HIS3*), pRH2949 (ICE *LEU2*), pRH2950 (ICE *MET17*), pRH2951 (ICE *TRP1*), and pRH2970 (ICE *LYS2*) were created by homologous recombination in yeast. pRH2952 was linearized using *Stu*I and *Nco*I. oRH4736 and oRH4872 were used to amplify *ADE2*, *HIS3*, *LEU2*, *MET17*, and *TRP1* from pRS402 (YIp *ADE2*), pRS403 (YIp *HIS3*), pRS405 (YIp *LEU2*), pRS411 (YIp *MET17*), and pRS404 (YIp *TRP1*), respectively. With the exception of *MET17*, cut backbone and nutritional marker fragments were transformed into RHY2863 and transformants were selected on the appropriate SC dropout plates. *MET17* and cut backbone were cotransformed into RHY7447 (BY4741) and transformants were selected on SC −MET plates. Plasmids were recovered from yeast and transformed into Top 10 *E. coli* as described below.

pRH2953 (ICE *ADE2 HIS3*), pRH2954 (ICE *ADE2 LEU2*), pRH2955 (ICE *ADE2 MET17*), and pRH2956 (ICE *ADE2 URA3*) were derived from pRH2947 (ICE *ADE2*). pRH2947 was linearized by partial digest using *Aat*II. For pRH2953, *HIS3* was amplified from pRS403 using oRH5045 and 5046. For pRH2954, *LEU2* was amplified from pRS405 using oRH4892 and 4893. For pRH2955, *MET17* was amplified from pRS411 using oRH5049 and 5050. For pRH2956, *URA3* was amplified from pRS406 using oRH4980 and 4981. With the exception of *MET17*, each fragment was cotransformed into RHY2863 with partially digested pRH2947. Transformants bearing both *ADE2* and the desired additional nutritional marker were selected on appropriate SC dropout plates (e.g., SC −ADE −HIS). *MET17* and linearized pRH2947 were cotransformed into RHY7447 (BY4741) and selected on SC −MET dropout plates. Plasmids were recovered and transformed into *E. coli*.

pRH2971 (ICE *LYS2 HIS3*), pRH2972 (ICE *LYS2 LEU2*), pRH2973 (ICE *LYS2 MET17*), and pRH2974 (ICE *LYS2 URA3*) were created with the same strategy as the ADE double marker ICE plasmids. pRH2970 (ICE *LYS2*) was linearized using *Aat*II. *HIS3*, *LEU2*, *MET17*, and *URA3* fragments were generated as described above. Except in the construction of pRH2973, linearized pRH2970 and a PCR fragment bearing the appropriate nutritional marker were cotransformed into RHY2863.

Transformants with both *LYS2* and the desired second nutritional marker were selected using appropriate SC dropout plates (e.g., SC –LYS –HIS3). pRH2973 was constructed by cotransforming linearize pRH2970 and *MET17* PCR fragment into RHY7477. Transformants were selected on SC –MET plates. Plasmids were recovered and transformed into *E. coli*.

pRH2957 (ICE *TRP1 HIS3*), pRH2958 (ICE *TRP1 LEU2*), pRH2959 (ICE *TRP1 MET17*), and pRH2960 (ICE *TRP1 URA3*) were created by introducing a *TRP1* fragment into pRH2948, pRH2949, pRH2950, and pRH2952, respectively. *TRP1* was amplified from pRS404 using oRH4868 and oRH4869. pRH2948, pRH2949, pRH2950, and pRH2952 were linearized by *Aat*II digest. With the exception of pRH2959 (ICE *MET17*), the *TRP1* fragment and linearized backbones were cotransformed into RHY2863. Desired recombinants, which contained *TRP1* and a second nutritional marker, were selected on appropriate SC dropout plates (e.g. SC –TRP –HIS). Linearized pRH2959 and *TRP1* fragment were transformed into RHY7447 and selected on SC –MET plates. Plasmids were recovered and transformed into *E. coli*.

Plasmids bearing *ADE2*, *TRP1*, and *LYS2* plus a dominant drug resistance cassette (*HphMx*, *KanMx*, or *NatMx*) were also created by homologous recombination. *HphMx*, *KanMx*, and *NatMx* were amplified from pAG32, pUG6, and pRH1838 (respectively) using oRH5055 and oRH5056. pRH2947, pRH2951, and pRH2970 were linearized using *Aat*II. Linearized backbones and drug resistance fragments were cotransformed into RHY2863. Successful recombinants were selected by drug resistance and were subsequently tested for growth on appropriate SC dropout plates. Plasmids were recovered and transformed into *E. coli*.

A YIp version of all plasmids bearing two selectable makers was acquired using *CEN* excision and ligation, as described below.

All plasmid maps were created using SnapGene software (from GSLBiotech; available at snapgene.com).

2.6 | Plasmid recovery from yeast

Transformants were inoculated into 3-ml YPD and grown overnight. The following day, 1 ml of YPD was added to stationary phase cultures, which were then allowed to grow for an hour at 30°. The entire culture was then pelleted in a 2-ml microcentrifuge tube and resuspended in 250 µl of resuspension buffer from a Promega Wizard Plus SV Miniprep kit (catalogue number A1460). Resuspended cells were lysed with zirconia beads for 5 min in a multivortexer set to maximum speed. Lysed cells and supernatant were then collected by nesting the microcentrifuge tube into a 15-ml conical tube, piercing the 2-ml microcentrifuge tube with a needle, and spinning the nested tubes at 2000 RPM (720 RCF) for 2 min. Lysed cells and cell lysate were then thoroughly resuspended, and the remainder of the miniprep was carried out according to the manufacturer's protocol. When DNA was eluted in 40 µl of dH_2O, we routinely recovered between 30 and 100 ng/µl samples with a 260/280 in the 1.8 to 2.0 range and a 260/230 in the 0.7 to 1.2 range. Although these readings should be understood to reflect significant gDNA contamination, they nonetheless provide a simple benchmark for a high-quality yeast mini prep.

2.7 | *CEN* excision by *Not*I digest and ligation

A standard restriction enzyme digest was used to excise the *CEN/ARS* element from ICE plasmids. Digests were assembled in PCR tubes; 20 µl of yeast miniprep and 10 units of *Not*I-HF (0.5 µl) were added to a 50-µl reaction buffered by 1X CutSmart. Reaction mixtures were digested for 90 min at 37° in a thermocycler, followed by 20 min at 65°C to inactivate *Not*I. Notably, use of a thermocycle is helpful but not requisite for reproducibility and reliability.

The resultant digestion was then split into a ligation reaction and a control lacking T4 ligase. No purification is necessary at this step because T4 ligase is compatible with NEB CutSmart buffered solution supplemented with ATP. Therefore, 18 µl of digest was combined with 1 µl of 20-mM ATP (as specified by NEB) and either 1 µl of T4 DNA ligase or dH_2O. Ligation proceeded for 10 min at room temperature (20°C) and was then heat inactivated at 65°C; 10 µl of each reaction were then transformed into *E. coli* Top 10 cells using standard techniques. A 10- to 50-fold increase in transformants was routinely observed between ligase and no ligase control. Successful *CEN* excision was confirmed by *Not*I diagnostic digest. Successful excision resulted in plasmid linearization without the production of a ~550 bp *CEN/ARS* fragment.

2.8 | YIp linearization prior to transformation and single integrant selection

Prior to transformation, all YIps were linearized by restriction enzyme digest. Briefly, we chose a unique cutter with a recognition site within the yeast nutritional marker to be used for integration. Plasmids were digested for 30 min at 37°C, linearization was visualized on an agarose gel, and transformation proceeded as described above.

Successful transformants were checked for the presence of a single copy of the plasmid by screening four or more candidates by flow cytometry. Single integrants were identified as those strains expressing the lowest consensus mean fluorescence. Multiple integrants were identified as those strains expressing GFP at discrete integers above the single-integrant mean fluorescence.

3 | RESULTS

3.1 | YCp gain and loss leads to variable expression between cells and colonies

To directly compare the behaviour and stability of stable integrants to otherwise identical *CEN/ARS* plasmids, we created a cognate pair of YIp and YCp plasmids from the pRS series, each with a *pTDH3::GFP::tPGK1* expression cassette. It has been demonstrated elsewhere that fluorescence levels and plasmid copy number are highly correlated (Lian, Jin, & Zhao, 2016). Thus, these constructs allowed scoring of

plasmid number based on live-cell or whole-colony fluorescence. After transformation into yeast, we identified a strain bearing a single integrant of the YIp construct and confirmed that strains bearing a YCp produced relatively similar fluorescence levels (data not shown). As previously observed (Chou et al., 2015; Gnügge et al., 2016; Jensen et al., 2014), strains bearing YIp or YCp constructs produce dissimilar histograms of GFP expression when assayed by flow cytometry (Figure 1a). Even in plasmid-selecting medium, a proportion of cells transformed with a YCp (blue histogram) appear to lose the plasmid and are optically dark (peak to the far left). Those cells that retain the YCp create a broad histogram of GFP expression in comparison to YIp-bearing cells (red histogram). By contrast, there was no appearance of "dark" cells expressing the cognate YIp, and the histogram of that strain was considerably narrower: the coefficient of variation (variance divided by the mean) is much higher in the YCp populations (132%) than in the YIp populations (56%).

We confirmed that variance associated with the YCp optical plasmid was due to variance in copy number from cell to cell (Hieter, Mann, Snyder, & Davis, 1985). To do so, we grew both YIp and YCp strains on agar plates and imaged colonies with a florescence scanner. In accordance with previous publications, the YCp construct produced colonies with sectored GFP intensities (Figure 1b) whereas the YIp construct produced uniformly fluorescent colonies with no apparent sectoring (Figure 1c). The mechanism of YCp loss and gain that accounts for sectoring has undergone particularly detailed analysis elsewhere (Gnügge et al., 2016). Using time-lapse fluorescence microscopy, it has been shown that YCp loss in one of two dividing cells is almost always accompanied by the gain of a plasmid in the other cell. Thus, sectoring and both high-copy-number and low-copy-number cells can be explained predominantly by plasmid segregation errors.

Despite cell-to-cell variation, it remained possible that YCp constructs provide reproducible mean expression levels from colony

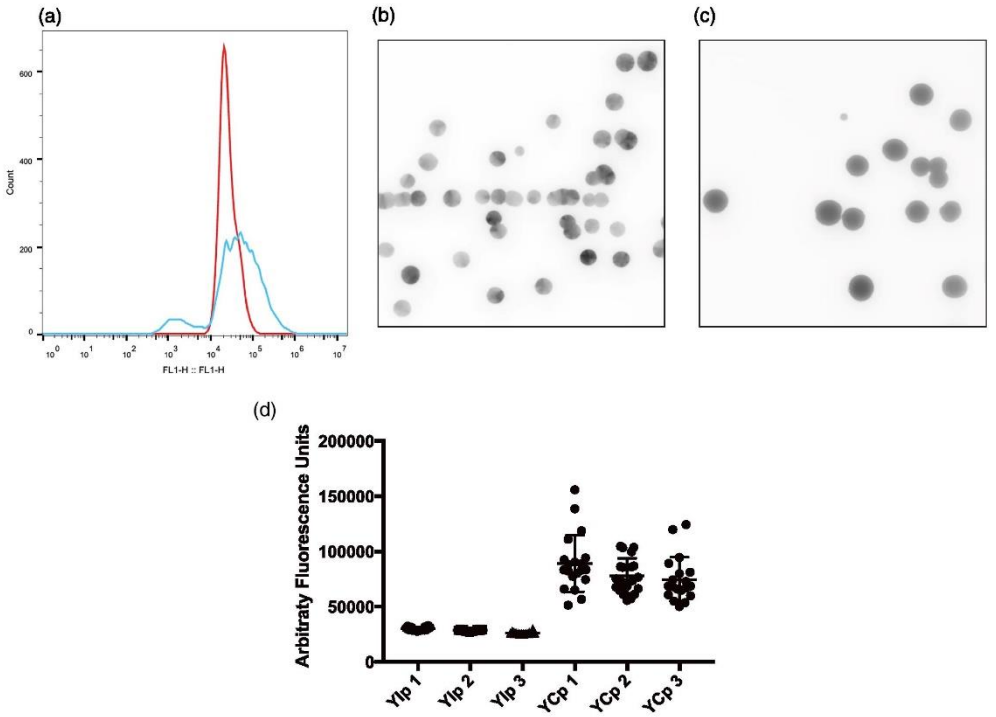

FIGURE 1 The consequences of variation in yeast *CEN* plasmid (YCp) copy number. (a) Log-phase cultures of yeast strains bearing GFP on a yeast integrating plasmid (YIp; red histogram) or YCp (blue histogram) were subjected to flow cyometry; each histogram represents 10,000 cells. (b) Colonies of a strain expressing GFP from a YCp were scanned for fluorescence at high resolution, (c) as was a strain expressing GFP from a YIp. Greyscale images of GFP signal are shown. (d) Twenty colonies of a strain expressing GFP from a YIp (columns YIps 1–3) or from a YCp (columns YCps 1–3) were subjected to flow cytometry. Mean fluorescence of each colony is represented by a circle, and total mean fluorescence and standard deviation of all 20 cultures are represented with central horizontal line and error bars, respectively [Colour figure can be viewed at wileyonlinelibrary.com]

to colony. To examine this idea, we thawed frozen stocks of YIp and YCp strains (each made from a single colony culture), grew log-phase cultures derived from 20 separate colonies of each, and measured their mean fluorescence by flow cytometry (Figure 1d). The YIp strain showed consistent GFP expression from colony to colony (Figure 1d, YIps 1–3), whereas colonies of the YCp strain produced surprisingly variable mean fluorescence (Figure 1d, YCps 1–3). Taken together, these data indicate that YCps give rise to significant phenotypic variation at both the cell and colony level whereas YIps show consistency at all levels tested.

It is also worth noting that our YCp construct produced a mean fluorescence roughly three times that of the cognate YIp (Figure 1a,d). If a YIp represents a single copy of a construct, this suggests that the average cell contains roughly three copies of our YCp. This estimation is within the range of more thorough measurements of plasmid copy number performed by others, though plasmid copy number can vary depending on both the selectable marker and expression cassette (Fang et al., 2011; Gnügge et al., 2016; Karim, Curran, & Alper, 2013). In most cases, YCps should be understood to cause moderate overexpression in comparison with YIps.

3.2 | YCp copy number increases under positive selection

Having confirmed the variability of YCp copy number form cell to cell and from colony to colony, we sought to test if cells bearing high YCp copy numbers could be selected under the appropriate conditions. To do so, we made use of a lysine auxotrophy governed by *LYS1*. *LYS1* catalyses the final step of lysine biosynthesis, the oxidative deamination of saccharopine to yield L-lysine and αketoglutarate (Burk et al., 2007), and *lys1Δ* nulls cannot grow in the absence of lysine (Figure 2a).

We hypothesized that, under a weak promoter, *LYS1* expression would be insufficient to support prototrophy. Accordingly, we created a panel of YCps that carried the functional LYS1-GFP fusion (Figure 2a) under the control of four promoters of decreasing strength: *pTDH3*, *pADH1*, *pCPY*, and *pCYC1*. Flow cytometry confirmed that these constructs provided a range of LYS1-GFP expression (Figure 2b). All four constructs were transformed into a *lys1Δ* null background to test for their ability to support growth on medium lacking lysine. Whereas the stronger *TDH3* and *ADH1* promoters were capable of supporting growth, the weaker *CPY* promoter supported only sporadic growth, and the very weak *CYC1* promoter did not support growth at all (Figure 2c). We selected the *CPY* promoter for further study because it produced a strong GFP signal by flow cytometry (with a mean FL1-H roughly six-fold above autofluorescence) and only poorly supported lysine prototrophy. We hypothesized that this *pCPY::LYS1*-GFP YCp would allow growth in the *lys1Δ* null at sufficiently high copy number. We tested if dosage prototrophy could be obtained by selection.

In a similar case, it has been shown that 2-μm copy number can be manipulated using a KanMx cassette with a truncated promoter (Lian et al., 2016). Cells bearing high copy numbers of this KanMx YCp could be selected by increasing G418 dosage. We asked if selection could be imposed by demand for increased nutritional marker. We plated 1 OD 600 (~10^7 cells) of *lys1Δ* nulls bearing YCp *pCPY::LYS1-GFP* onto lysine dropout plates, and the strain rapidly produced escapers (Table 1). When isolated, these escapers retained the ability to grow on plates lacking lysine (Figure 2d). To determine if selection for lysine prototrophy led to increased plasmid copy number, we maintained selection for lysine prototrophy and subjected an escaper to flow cytometry (Figure 2e). Indeed, the mean fluorescence of the escaper strain exhibited a five-fold increase above the parental *pCPY* strain (Figure 2f). A strain with a YCp that supports lysine prototrophy (*pTDH3::LYS1-GFP*) was not subject to these effects and produced indistinguishable histograms (Figure S1A) and mean fluorescence (Figure S1B) after outgrowth in medium lacking leucine or lysine. Thus, under the appropriate conditions, cells bearing elevated YCp copy number can be selected, in some cases within the same timeframe that a mutant of interest would require for outgrowth.

To ensure that this increase in fluorescence was dependent on plasmid copy number alone, we set out to isolate a revertant from our escaper strain. It has been demonstrated that elevated plasmid copy numbers rapidly decline upon cell passaging (Wittrup, Bailey, Ratzkin, & Patel, 1990). Therefore, we streaked the escaper strain to YPD three times to allow plasmid loss and then tested the resultant strain for both the ability to grown on lysine dropout plates and for fluorescence levels. The putative revertant retained the ability to grow on leucine dropout plates (Figure 2d, −LEU) but was no longer prototrophic for lysine (Figure 2d, −LYS). Flow cytometry indicated that loss of prototrophy was due to lowered plasmid copy number. Indeed, the mean fluorescence of the revertant declined below that of the parental *pCPY* strain (Figure 2e,f). Thus, escapers gained lysine prototrophy through increased YCp copy number alone.

Taken together, these data suggest that YCps pose significant risks in any system in which plasmid copy number is subject to selection pressure. Plasmid copy number can rise rapidly in response to such pressures and diminish as quickly in their absence, potentially causing a strain to gain or lose a desirable phenotype.

3.3 | ICE plasmid construction

Given the significant advantages of YRC and the idiosyncrasies of YCps, we sought to design a yeast-recombination-cloning scheme that would allow facile production of the more desirable YIp version from the easily obtained YCp YRC product. We stipulated that using this strategy would (a) require as little additional molecular biology as possible, (b) produce a YIp efficiently and reproducibly, (c) impose as few constraints on cloning as possible, and (d) require few or no novel lab reagents.

With these features in mind, we chose to use the pRS40x series as a starting point for our plasmid collection (Brachmann et al., 1998; Sikorski & Hieter, 1989). We chose the pRS40x series because our lab has designed thousands of vectors based upon it. Those plasmids, in turn, have been transformed into thousands of yeast strains, including strains bearing empty pRS40x vectors for use as controls.

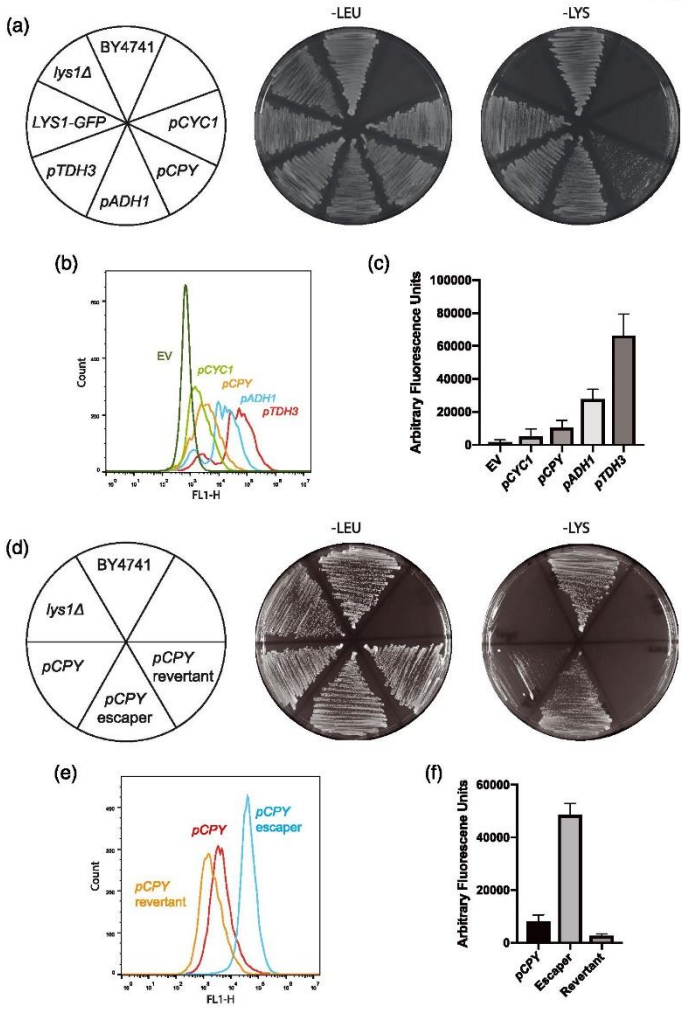

FIGURE 2 *CEN* plasmid copy number increases under positive selection. (a) Strains bearing WT *LYS1* (BY4741), *lys1Δ*, *LYS1* tagged with GFP at the endogenous locus (*LYS1-GFP*), and four strains bearing a yeast *CEN* plasmid (YCp) expressing *LYS1-GFP* from promoters of decreasing strength (*pTDH3*, *pADH1*, *pCPY*, and *pCYC1*) were streaked to plates permissive for growth (−LEU) or plates requiring lysine prototrophy (−LYS). (b) Liquid cultures of strain bearing an empty vector (EV) or *CEN* plasmids expressing *LYS1-GFP* from various promoters were subjected to flow cytometry; *pTDH3*, red histogram; *pADH1*, blue histogram; *pCPY*, yellow histogram; *pCYC1*, light-green histogram; EV, dark green histogram. (c) Strains bearing a YCp expressing *LYS1-GFP* on various promoters were subjected to flow cytometry and the mean fluorescence was recorded. *N* = 3. Bars represent the mean of three experiments. Error bars report standard deviation. (d) Strains bearing *pCPY::LYS1-GFP* were spread onto plates lacking lysine and a high-YCP-copy escaper was picked. The escaper was then streaked to YPD serially to allow for plasmid loss and the subsequent isolation of a revertant strain. Both the escaper and revertant were streaked to permissive plates (−LEU) and plates requiring lysine prototrophy (−LYS) in order to observe the maintenance or loss of lysine prototrophy. (e) Liquid cultures of parental *pCPY* (red histogram), escaper (blue histogram), and revertant strains (yellow histogram) were subjected to flow cytometry. Escapers were grown in YNB −LYS medium that maintained selection, whereas the parental and revertant strain were necessarily grown YNB −LEU medium that selected for the plasmid alone. (f) Liquid cultures of parental *pCPY*, escaper, and revertant strains were subjected to flow cytometry and the mean fluorescence was recorded. Escapers were grown in YNB −LYS medium that maintained selection, whereas the parental and revertant strain were grown YNB −LEU medium that selected for the plasmid alone. *N* = 3. Bars show the mean of three experiments. Error bars represent standard deviation [Colour figure can be viewed at wileyonlinelibrary.com]

TABLE 1 Escaper colony counts

Day	Colonies
2	2
3	533
4	1,021
5	2,369

Note. Strains expressing *LYS1-GFP* from the *CPY* promoter were grown to saturation overnight in selective medium; 1 OD 600 of each culture was then spread onto plates lacking lysine, and colonies were counted across a 5-day period. *N* = 3. The average of three experiments is reported.

Potential users of the ICE plasmids series should be aware, though, that a tremendous amount of effort has been put into updating and redesigning yeast shuttle vectors (Chee & Haase, 2012; Chou et al., 2015; Fang et al., 2011; Frazer & O'Keefe, 2007; Gnügge et al., 2016; Jensen et al., 2014; Lian et al., 2016). These include both updates to the pRS40x series, such as the removal of restriction sites from yeast selectable markers to increase the number of unique cutters in the multiple cloning site (MCS; Chee & Haase, 2012), as well as completely redesigned vector backbones (Gnügge et al., 2016). In our hands, however, an ICE plasmid based upon the pRS40x already provided a wealth of unique cut sites for YRC and promised to create YIps that could be readily added to our existing collection of plasmids.

We designed a *CEN/ARS* flanked by two copies of the same rare-cutting *Not*I restriction-enzyme site. In this format, the *CEN/ARS* can be used for YRC and can subsequently be excised by single-enzyme digestion. The remaining, desired YRC product can then be recircularized by intramolecular ligation to produce the integrating version.

*Not*I is an ideal restriction enzyme for this approach for a number of reasons. First, *Not*I is a rare cutter with an eight-base-pair recognition sequence (GC^GGCCGC). Second, New England Biolabs offers a "high-fidelity" (HF) version of the enzyme, minimizing the possibility of restriction-enzyme artefacts. Third, *Not*I-HF allows for the use of NEB's CutSmart buffer. CutSmart is compatible with T4 ligase upon

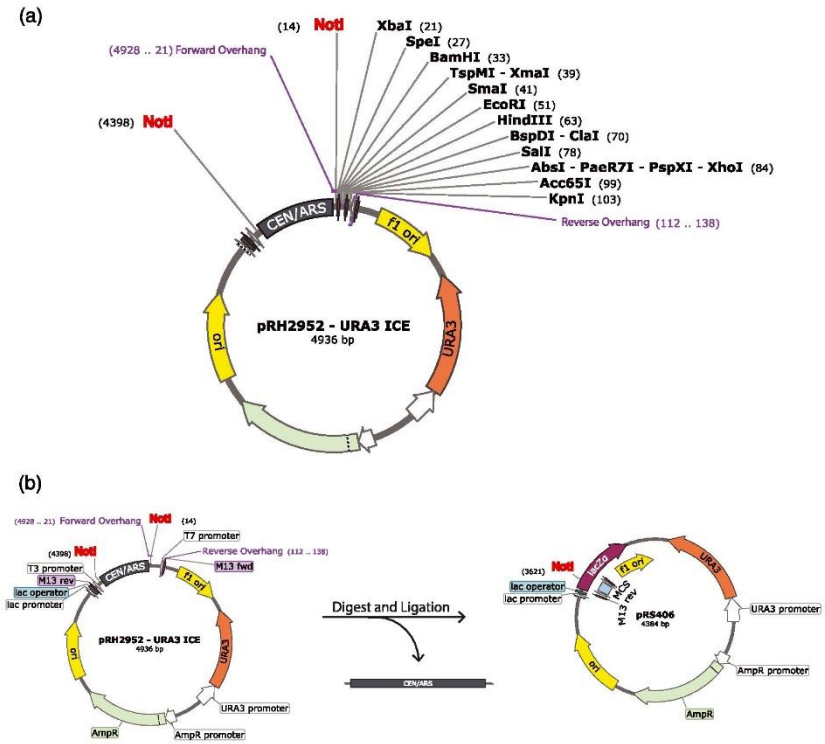

FIGURE 3 ICE plasmid schematics. (a) A URA3 ICE plasmid. Yeast recombination cloning can be achieved by adding two 27-base-pair-long sequences of homology (forward and reverse overhang) to primers and by digestion with any multiple-cloning-site restriction enzyme between those sequences (enzymes listed in black). (b) *Not*I digestion and religation leads to *CEN* excision and reconstitution of a plasmid identical to its pRS series counterpart. In the case of an empty vector, excision and religation remove the *CEN/ARS* (black) of the *URA3* ICE plasmid (left) and reconstitute pRS406 (right) [Colour figure can be viewed at wileyonlinelibrary.com]

the addition of ATP, which allowed us to design a simplified protocol. After *CEN* excision, *Not*I is inactivated by incubation at 65°C, and ligation can proceed without a buffer change.

Finally, *Not*I is a unique cutter in the MCS of all pRS40x series plasmids. This allowed us to create the desired *Not*I-flanked *CEN*/*ARS* element by simple insertion into the MCS, absent any changes to the pRS series backbone (Figure 3a). Accordingly, when the *CEN*/*ARS* is excised with *Not*I and reclosed, the resulting plasmid bears its original *Not*I site and no scars from the cloning strategy (Figure 3b). This allows direct comparison between vectors created using the method presented here and any pRS-based plasmids or empty vectors already extant in many labs.

Notably, this approach comes with the drawback of interrupting the lacZa of the pBluescript backbone, thereby precluding blue/white screening during cloning. In our hands, the loss of blue/white has not proven to be detrimental because we identify successful recombinants after yeast transformants are isolated. In some cases, successful recombinants can be identified by phenotypes (e.g., colony fluorescence). In the remaining cases, a diagnostic PCR can be performed that uses a yeast miniprep as template. Given the routine nature of these approaches, we concluded that achieving a "scarless" religation outweighed loss of blue/white screening.

Using YRC, we have created a panel of these ICE (Integrating after *CEN* Excision) plasmids, one for each of the commonly used pRS series plasmids (*ADE2*, *HIS3*, *LEU2*, *LYS2*, *MET17*, *TRP1*, and *URA3*). Each plasmid can be used for recombination using stereotyped, 27-base-pair-long overhangs on the forward (GTCCTAAGAAGCGCTAAGAGG GCGGCCGCT) and reverse (GCGCGCGTAATACGACTCACTATA GGG) primers of a desired PCR product, and by cutting the ICE plasmid at any restriction site between those overhangs (Figure 3a). All plasmids are available through AddGene.

3.4 | Plasmids with two selectable markers

Having created a basic set of ICE plasmids, we set out to test their reliability and to demonstrate their usefulness. In our lab, an unmet need was a set of standard YIps that allow for multiple integrations into the BY4741 background. Because the BY4741 auxotrophies are entire reading frame deletions, the strain is rarely amenable to integration using the standard auxotrophy complementing genes. This significantly limited the usefulness of a number of resources created in the BY4741 background, including the deletion, GFP, and DAmP collections (Breslow et al., 2008; Giaever et al., 2002; Huh et al., 2003).

To address this issue, we sought to create a series of YIps and corresponding ICE plasmids with two markers: an integration marker (*ADE2*, *LYS2*, and *TRP1*) to allow high-efficiency integration at the indicated genes, combined with a selection marker (*HIS3*, *LEU2*, *MET17*, *URA3*, *HphMx*, *KanMx*, and *NatMx*) that will complement the completely absent nutritional marker, or provide a novel drug resistance. In total, we created 42 plasmids, 21 YIps, and 21 corresponding ICE plasmids. These plasmids are also available through AddGene.

To construct these double-marker plasmids, we made use of our single-marker ICE plasmids and used YRC to add additional nutritional/drug markers as desired. Along with isolating the resultant ICE plasmid, we used the *CEN* excision protocol to create cognate YIps for use as empty vector controls. This allowed us to both expand our ICE plasmid collection and to test the reliability of our excision and religation protocol.

In short, YRC allowed for selection of recombinants that bore functional copies of the added selectable markers, ensuring fidelity in both amplification and recombination. Following recovery of the plasmids by bead beating and use of a Promega miniprep kit, *CEN* excision produced YIps consistently. Minipreps were subjected to *Not*I digest in a thermocycler at 37°C for 1.5 hr, followed by enzyme inactivation at 65°C for 20 min. Because T4 ligase is compatible with CutSmart buffer, digests were then ligated simply by adding ligase and supplemental ATP. As an example of excision and religation efficiency, we subjected two plasmids (Figure 4a,c) to *Not*I digestion followed by either mock-ligation control (no ligase) or a standard T4 ligation. Upon transformation, ligated plasmid produces significantly more colonies than mock-ligated plasmid (Table 2), suggesting both efficient cutting by *Not*I and efficient ligation by T4 ligase. Following *E. coli* isolation and plasmid minipreps, putative YIps were then subjected to a diagnostic digest to test for both *CEN* excision and fidelity in *Not*I cut-site reconstitution. In each case, we chose three restriction enzymes: one that cuts in TRP1 (Bsu36I), one that cuts in HphMx or NatMx (NdeI and SfoI, respectively), and *Not*I. In every case tested, the ICE plasmid parent produced a ~550 bp *CEN*/*ARS* fragment upon *Not*I digest (Figure 4b ICE parent, 4D ICE parent) whereas putative YIps were cut at a single reconstituted *Not*I restriction site (Figure 4b, 1–5, and 4d, 1–5), resulting in the expected backbone fragments but not the released *CEN*/*ARS* insert. Thus, the fold enrichment between ligated plasmid and an unligated control were a reliable indicator of complete *CEN* excision, and digestion and religation were efficient enough to require minimal if any screening of *E. coli* clones. Nonetheless, we always perform the *Not*I diagnostic digest demonstrated here to confirm *CEN* excision.

3.5 | ICE plasmids behave similarly to YCps

By creating each ICE plasmid with YRC, we were able to test that each ICE plasmid bore a functional *CEN*/*ARS*. However, it remained formally possible that placing a transgene beside a *CEN*/*ARS* would affect plasmid propagation, recombination, or transgene expression. To test this, we subcloned *pTDH3::GFP* from the YCp used in Figure 1 to an ICE plasmid. Transformation yielded successful recombinants, and the plasmid was recovered. We subjected both YCp and ICE-plasmid strains to flow cytometry to test for any changes to *GFP* expression. Both histograms of GFP expression (Figure 5a) and mean fluorescence intensity (Figure 5b) were comparable between strains. The *CEN*/*ARS* of ICE plasmids allows for successful recombination, plasmid propagation, and transgene expression.

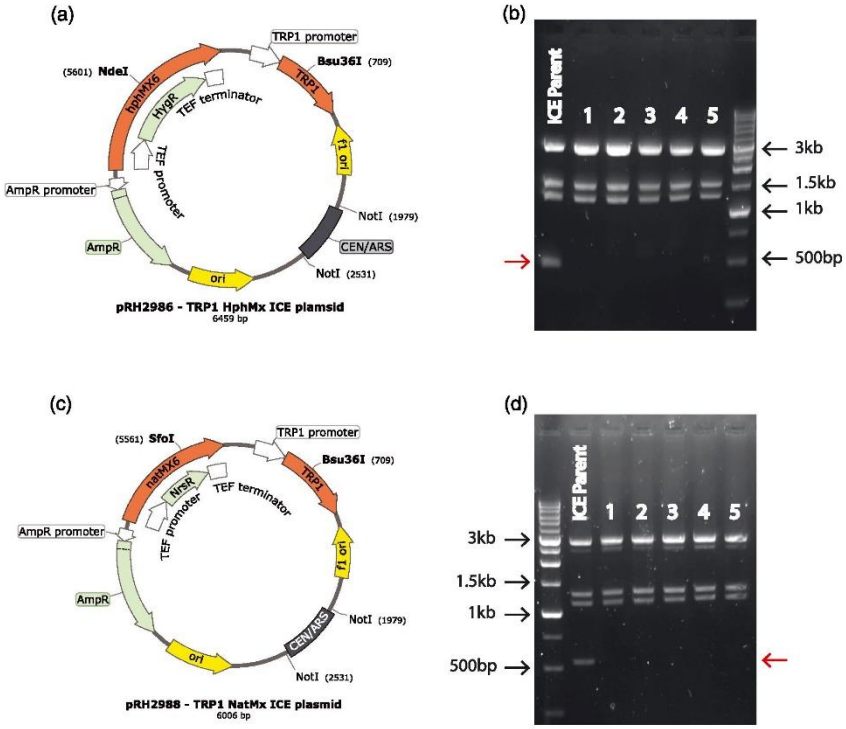

FIGURE 4 Same solution *Not*I digest and religation allows facile *CEN* excision. (a) *HphMx-TRP1* ICE and (c) *NatMx-TRP1* ICE plasmids that were recovered from yeast and subjected to *CEN* excision. (b) A parent *HphMx-TRP1* ICE plasmid (ICE parent) and five plasmids recovered from five independent *Escherichia coli* transformants bearing putative yeast integrating plasmids (YIps; Baudin et al., 1993; Brachmann et al., 1998; Breslow et al., 2008; Burk et al., 2007; Casini et al., 2013) were subjected to diagnostic digest with *Nde*I, *Bsu*36I, and *Not*I. Restriction-enzyme sites are marked in (a). Red arrow indicates expected mobility of liberated *CEN/ARS* fragment (d) Parent *NatMx-TRP1* ICE plasmid (ICE parent) and five putative YIps (Baudin et al., 1993; Brachmann et al., 1998; Breslow et al., 2008; Burk et al., 2007; Casini et al., 2013) were subjected to diagnostic digest using *Sfo*I, *Bsu*36I, and *Not*I. Restriction enzyme sites are notated in (c) [Colour figure can be viewed at wileyonlinelibrary.com]

4 | DISCUSSION

In general, cloning by recombination is becoming an increasingly popular method for gene manipulation, tagging, and mutagenesis. Especially when paired with custom synthesized dsDNAs, recombination offers the ability to construct most imaginable plasmids in a single step without ever relying on more traditional stepwise constructive bacterial cloning. Point mutations can be introduced in overhangs or ssDNA "bridges" to facilitate simple site-directed mutagenesis, and when desired, site-directed mutagenesis can be extended into saturation mutagenesis by designing an overhang with a randomized codon (often NNK, where N is any nucleotide and K is G or T).

Whereas Gibson Assembly can facilitate any of the above, YRC offers the significant advantage that yeast bearing recombined products can immediately be screened for phenotypes. Given the idiosyncrasies of creating novel fusion proteins, the ability to test a new construct in yeast immediately can save significant amounts of time and effort as a user investigates different gene orientations, linkers, and tags. The ability to directly screen a randomly mutagenized gene also remains a popular and powerful method.

TABLE 2 *Escherichia coli* colony counts

Plasmid	No ligase	Ligase	Fold increase
Trp NatMx	36	603	17
Trp HphMx	18	628	35

Note. A *TRP NatMx* and a *TRP HphMx* ICE plasmid were generated by YRC and recovered from yeast by minipreps. Yeast minipreps were digested using *Not*I and were subsequently mock ligated (No Ligase) or treated with T4 DNA ligase (Ligase). Mock ligated and ligated DNA were then transformed into *E. coli*, and *E. coli* colonies were counted the following day. The fold enrichment in colonies between mock ligation and ligase (fold increase) is reported as an estimation of *Not*I and ligase efficiency

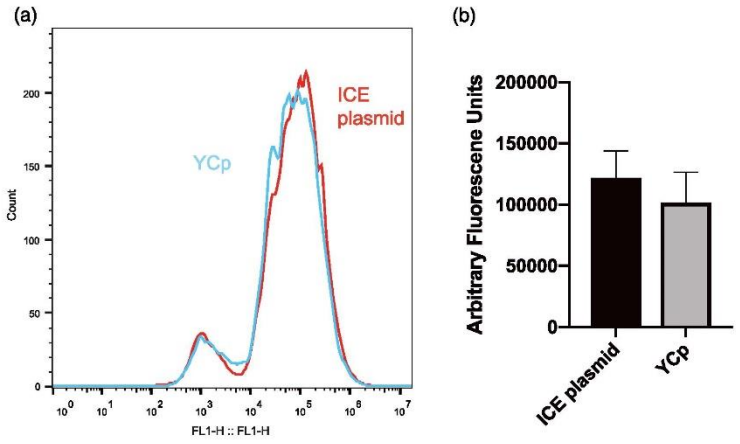

FIGURE 5 Comparison of original pRS yeast *CEN* plasmid (YCp) and ICE plasmids. (a) Strains bearing *pTDH3::GFP* on either a YCp (blue histogram) or an ICE plasmid (red histogram) were subjected to flow cytometry in liquid culture. (b) Mean fluorescence of ICE plasmid or YCp borne *pTDH3::GFP* were recorded by flow cytometry. *N* = 3. Error bars represent standard deviation [Colour figure can be viewed at wileyonlinelibrary.com]

When considering the choice to use YRC, it is useful to recall several drawbacks that might limit the utility of this powerful technique. For instance, repetitive sequences can lead to unintended recombination events and improper assembly of DNA fragments. This is particularly inconvenient for those assembling synthetic biological circuits and metabolic pathways, which often include several instances of a well-characterized promoter or terminator. A significant effort has been made to overcome this obstacle, and several workarounds have been described that employ computationally designed "linkers" (or unique nucleotide sequences). These sequences are appended to repetitive DNA fragments and provide homology that ensures the desired assembly (Casini et al., 2013; Ramon & Smith, 2011; Torella et al., 2014). This approach has been successfully employed in YRC (Casini et al., 2013). However, linkers leave behind "scars" that may be undesirable in certain instances. Those cases may preclude recombination and call for other cloning methods that allow for a "scarless" assembly, such as those that rely on type IIS restriction endonucleases (Casini, Storch, Baldwin, & Ellis, 2015).

YRC also suffers from several drawbacks that in vitro recombination does not. The most obvious and unavoidable drawback is the duration of YRC. Two days are required for yeast transformation, after which plasmids are recovered from yeast and transformed into *E. coli*. In vitro recombination, on the other hand, allows for direct transformation of recombined products into *E. coli*. Users should therefore consider in vitro recombination if they are uninterested in phenotyping yeast transformants or do not plan to make use of the other benefits of YRC listed above. A second drawback of YRC is the low yield obtained when recovering plasmids from yeast. Even with commercial kits, users should expect a yield of many orders of magnitude lower than an *E. coli* miniprep. It should be noted, though, that higher yield methods have been described (Singh & Weil, 2002) and that low-yield yeast minipreps still produce a DNA product that is competent for some molecular biology, such as PCR, digestion, and ligation.

Even with the above caveats in mind, YRC is remarkably useful when compared with many traditional recombinant strategies for constructing plasmids. Until recently, we had hesitated to use YRC because in our lines of inquiry YCps were undesirable. A critical phenotypic readout of the degradation pathways we study is the dynamic range between the expression of stable and degraded substrates, and this range is quantitatively similar to the variability of expression seen with YCps (Gardner et al., 1998). As shown above, this variability was easily observed and resulted in a wide range of expression levels depending on selection conditions. The requirement for a *CEN/ARS* to allow YRC meant that we only used YRC in the relatively infrequent cases in which a YCp was an acceptable end product.

ICE plasmids can be used to address this shortcoming, and they have helped us to diversify our repertoire of YIps. The workflow involved in going from the YCp product to the desired YIp is simple, reliable, and requires little additional handling. In fact, as a proof of concept, we used it in this work to create the panel of double-marker plasmids for use in BY4741.

One caveat of the ICE plasmid design is the requirement that a desired insert lack *Not*I sites. To address possible issues, a second generation of ICE plasmids could be created with a different rare cutter on either side of the *CEN/ARS*. Both *Asc*I (GG^CGCGCC) and *Fse*I (GGCCGG^CC) are good choices. However, neither enzyme is available in an HF version and neither is present in the pRS MCS. Digest could produce STAR activity, and the resulting plasmid would be not be identical to empty vectors commonly in use among yeast biologists.

While preparing this manuscript, we came across a similar methodology to the ICE strategy (Chou et al., 2015). It uses a novel plasmid (pXR) bearing a *CEN/ARS* flanked by LoxP sites. Recombinants are

transformed into an *E. coli* strain expressing Cre recombinase to remove a *CEN/ARS*, but Cre recombinase often produces *E. coli* bearing both recombined and unrecombined plasmid. The authors report that roughly 20% of *E. coli* colonies isolated bear pure, recombined plasmid. They suggest either screening 2–5 colonies or cutting the *CEN/ARS* with *Swa*I after plasmid retrieval from yeast. The latter results in only recombined plasmids, but it requires an ethanol precipitation before transformation into bacteria. By contrast, the *Not*I excision followed by common-buffer religation results in essentially 100% successful conversion, and there is no need for subcloning into the excising bacteria followed by miniprep and screening.

It is also important to note that Colman-Lerner *et al*. developed a family of plasmids that employs the same excision and religation strategy as ICE plasmids (Colman-Lerner et al., 2005; Gordon et al., 2007). These plasmids (pTC7) contain an *Aat*II-flanked (GACGT^C) *CEN/ARS*, which was introduced at the unique *Aat*II site of a backbone derived from pRS406 (*URA3* YIp). Notably, this design leaves the MCS of the pTC7 series intact, which may prove to be advantageous for some labs. However, the *Aat*II design choice also comes with the drawback of incompatibility with the ADE2 and LYS2 markers, which both contain an AatII recognition site.

Gnügge et al. (2016) also present a fully redesigned vector backbone, pRG, that could act as an alternative to ICE plasmids. In their *CEN* plasmid design, the MCS is flanked by both homology to the genome and rare-cutter *Asc*I cut sites. Cutting with *Asc*I liberates the MCS and yeast selectable marker from the *CEN/ARS* (as well as the bacterial sequences) and exposes the homology arms, which are capable of performing integration by double crossover. Thus, their plasmids are competent for both YRC and genomic integration, with the caveat that integration is less efficient than that of a pRS40x plasmid (Gnügge et al., 2016). Several pRG plasmids are also designed to solve the issue of integrating into the yeast deletion collection. The design of these plasmids includes homology arms that target upstream and downstream of the Δ0 loci, thereby allowing integration at those sites. Labs in a position to adopt a new series of empty vectors should carefully consider the pRG series. Those looking to continue using the pRS40x series may prefer to use ICE plasmids.

Finally, it is possible to simply perform PCR on a plasmid such that the primers contain overhangs with homology to the genome and the amplicon contains both an expression cassette and a selectable marker (Brachmann et al., 1998; Baudin, Ozier-kalogeropoulos, Denouel, Lacroute, & Cullin, 1993; Chee & Haase, 2012; Fang et al., 2011). This approach offers the ability to integrate constructs at neutral sites throughout the genome. However, in our hands and others', this approach leads to very low transformation efficiency compared with other methods of integration (Gnügge et al., 2016). We prefer the ease of obtaining a large yield of plasmid from a miniprep and performing a high-efficiency yeast transformation by linearizing the plasmid. This is especially true of plasmids that need to be introduced into numerous genetic backgrounds.

As with all cloning strategies, the methodology chosen will depend on the desired product and the existing infrastructure within a lab. The more options available, the better.

ACKNOWLEDGEMENTS

This work was supported in part by National Institutes of Health Grant 5R37DK051996-18 (to R. Y. H.). M. P. F. was supported in part by National Institutes of Health Cell Molecular Genetics (CMG) Training Grant 5T32GM007240-37. The authors would like to thank all members of the Hampton lab for their feedback and encouragement. In particular, we thank Lilia Ornelas for streamlining and disseminating YRC in our group, and Maggie Wangeline for suggesting the use of a rare cutter, the icing on the ICE plasmid approach.

ORCID

Matthew P. Flagg https://orcid.org/0000-0001-6449-2137

REFERENCES

Baudin, A., Ozier-kalogeropoulos, O., Denouel, A., Lacroute, F., & Cullin, C. (1993). A simple and efficient method for direct gene deletion in *Saccharomyces cerevisiae*. *Nucleic Acids Research*, *21*(14), 3329–3330. https://doi.org/10.1093/nar/21.14.3329

Brachmann, C. B., Davies, A., Cost, G. J., Caputo, E., Li, J., Hieter, P., & Boeke, J. D. (1998). Designer deletion strains derived from *Saccharomyces cerevisiae* S288C: A useful set of strains and plasmids for PCR-mediated gene disruption and other applications. *Yeast*, *14*(2), 115–132. https://doi.org/10.1002/(SICI)1097-0061(19980130)14:2<115::AID-YEA204>3.0.CO;2-2

Breslow, D. K., Cameron, D. M., Collins, S. R., Schuldiner, M., Stewart-Ornstein, J., Newman, H. W., … Weissman, J. S. (2008). A comprehensive strategy enabling high-resolution functional analysis of the yeast genome. *Nature Methods*, *5*(8), 711–718. https://doi.org/10.1038/nmeth.1234

Burk, D. L., Hwang, J., Kwok, E., Marrone, L., Goodfellow, V., Dmitrienko, G. I., & Berghuis, A. M. (2007). Structural studies of the final enzyme in the α-aminoadipate pathway-saccharopine dehydrogenase from *Saccharomyces cerevisiae*. *Journal of Molecular Biology*, *373*(3), 745–754. https://doi.org/10.1016/j.jmb.2007.08.044

Casini, A., MacDonald, J. T., De Jonghe, J., Christodoulou, G., Freemont, P. S., Baldwin, G. S., & Ellis, T. (2013). One-pot DNA construction for synthetic biology: The Modular Overlap-directed Assembly With Linkers (MODAL) strategy. *Nucleic Acids Research*, *42*(1), e7–e7.

Casini, A., Storch, M., Baldwin, G. S., & Ellis, T. (2015). Bricks and blueprints: Methods and standards for DNA assembly. *Nature Reviews Molecular Cell Biology*, *16*(9), 568–576. https://doi.org/10.1038/nrm4014

Chee, M. K., & Haase, S. B. (2012). New and redesigned pRS plasmid shuttle vectors for genetic manipulation of *Saccharomyces cerevisiae*. *G3 (Bethesda, Md.)*, *2*(5), 515–526. https://doi.org/10.1534/g3.111.001917

Chou, C. C., Patel, M. T., & Gartenberg, M. R. (2015). A series of conditional shuttle vectors for targeted genomic integration in budding yeast. *FEMS Yeast Research*, *15*(3), 1–9.

Colman-Lerner, A., Gordon, A., Serra, E., Chin, T., Resnekov, O., Endy, D., … Brent, R. (2005). Regulated cell-to-cell variation in a cell-fate decision system. *Nature*, *437*(7059), 699–706. https://doi.org/10.1038/nature03998

Fang, F., Salmon, K., Shen, M. W. Y., Aeling, K. A., Ito, E., Irwin, B., … Sandmeyer, S. (2011). A vector set for systematic metabolic engineering in *Saccharomyces cerevisiae*. *Yeast*, *28*(2), 123–136. https://doi.org/10.1002/yea.1824

Frazer, L. N., & O'Keefe, R. T. (2007). A new series of yeast shuttle vectors for the recovery and identification of multiple plasmids from

Saccharomyces cerevisiae. *Yeast*, *24*(9), 777–789. https://doi.org/10.1002/yea.1509

Gardner, R., Cronin, S., Leader, B., Rine, J., & Hampton, R. (1998). Sequence determinants for regulated degradation of yeast 3-hydroxy-3-methylglutaryl-CoA reductase, an integral endoplasmic reticulum membrane protein. *Molecular Biology of the Cell*, *9*(9), 2611–2626. https://doi.org/10.1091/mbc.9.9.2611

Garza, R. M., Tran, P. N., & Hampton, R. Y. (2009). Geranylgeranyl pyrophosphate is a potent regulator of HRD-dependent 3-hydroxy-3-methylglutaryl-CoA reductase degradation in yeast. *Journal of Biological Chemistry*, *284*(51), 35368–35380. https://doi.org/10.1074/jbc.M109.023994

Giaever, G., Chu, A. M., Ni, L., Connelly, C., Riles, L., Véronneau, S., … Johnston, M. (2002). Functional profiling of the *Saccharomyces cerevisiae* genome. *Nature*, *418*(6896), 387–391. https://doi.org/10.1038/nature00935

Gibson, D. G. (2009). Synthesis of DNA fragments in yeast by one-step assembly of overlapping oligonucleotides. *Nucleic Acids Research.*, *37*, 6984–6990. https://doi.org/10.1093/nar/gkp687

Gibson, D. G., Benders, G. A., Axelrod, K. C., Zaveri, J., Algire, M. A., Moodie, M., … Hutchison, C. A. (2008). One-step assembly in yeast of 25 overlapping DNA fragments to form a complete synthetic Mycoplasma genitalium genome. *Proceedings of the National Academy of Sciences*, *105*(51), 20404–20409. https://doi.org/10.1073/pnas.0811011106

Gnügge, R., Liphardt, T., & Rudolf, F. (2016). A shuttle vector series for precise genetic engineering of *Saccharomyces cerevisiae*. *Yeast*, *33*(3), 83–98. https://doi.org/10.1002/yea.3144

Gordon, A., Colman-Lerner, A., Chin, T. E., Benjamin, K. R., Yu, R. C., & Brent, R. (2007). Single-cell quantification of molecules and rates using open-source microscope-based cytometry. *Nature Methods*, *4*(2), 175–181. https://doi.org/10.1038/nmeth1008

Hampton, R. Y., Gardner, R. G., & Rine, J. (1996). Role of 26S proteasome and HRD genes in the degradation of 3-hydroxy-3-methylglutaryl-CoA reductase, an integral endoplasmic reticulum membrane protein. *Molecular Biology of the Cell*, *7*(12), 2029–2044. https://doi.org/10.1091/mbc.7.12.2029

Hampton, R. Y., & Rine, J. (1994). Regulated degradation of HMG-CoA reductase, an integral membrane protein of the endoplasmic reticulum, in yeast. *Journal of Cell Biology*, *125*(2), 299–312. https://doi.org/10.1083/jcb.125.2.299

Heck, J. W., Cheung, S. K., & Hampton, R. Y. (2010). Cytoplasmic protein quality control degradation mediated by parallel actions of the E3 ubiquitin ligases Ubr1 and San1. *Proceedings of the National Academy of Sciences*, *107*(3), 1106–1111. http://doi.org/10.1073/pnas.0910591107

Hieter, P., Mann, C., Snyder, M., & Davis, R. W. (1985). Mitotic stability of yeast chromosomes: A colony color assay that measures nondisjunction and chromosome loss. *Cell*, *40*(2), 381–392. https://doi.org/10.1016/0092-8674(85)90152-7

Huh, W. K., Falvo, J. V., Gerke, L. C., Carroll, A. S., Howson, R. W., Weissman, J. S., & O'Shea, E. K. (2003). Global analysis of protein localization in budding yeast. *Nature*, *425*(6959), 686–691. https://doi.org/10.1038/nature02026

Ito, H., Fukuda, Y., Murata, K., & Kimura, A. (1983). Transformation of intact yeast cells treated with alkali cations. *Journal of Bacteriology*, *153*(1), 163–168.

Jensen, N. B., Strucko, T., Kildegaard, K. R., David, F., Maury, J., Mortensen, U. H., … Borodina, I. (2014). EasyClone: Method for iterative chromosomal integration of multiple genes *Saccharomyces cerevisiae*. *FEMS Yeast Research*, *14*(2), 238–248. https://doi.org/10.1111/1567-1364.12118

Kachroo, A. H., Laurent, J. M., Yellman, C. M., Meyer, A. G., Wilke, C. O., & Marcotte, E. M. (2015). Systematic humanization of yeast genes reveals conserved functions and genetic modularity. *Science*, *348*(6237), 921–925. https://doi.org/10.1126/science.aaa0769

Karim, A. S., Curran, K. A., & Alper, H. S. (2013). Characterization of plasmid burden and copy number in *Saccharomyces cerevisiae* for optimization of metabolic engineering applications. *FEMS Yeast Research*, *13*(1), 107–116. https://doi.org/10.1111/1567-1364.12016

Lian, J., Jin, R., & Zhao, H. (2016). Construction of plasmids with tunable copy numbers in *Saccharomyces cerevisiae* and their applications in pathway optimization and multiplex genome integration. *Biotechnology and Bioengineering*, *113*(11), 2462–2473. https://doi.org/10.1002/bit.26004

Ma, H., Kunes, S., Schatz, P. J., & Botstein, D. (1987). Plasmid construction by homologous recombination in yeast. *Gene*, *58*(2–3), 201–216. https://doi.org/10.1016/0378-1119(87)90376-3

Muhlrad, D., Hunter, R., & Parker, R. (1992). A rapid method for localized mutagenesis of yeast genes. *Yeast*, *8*(2), 79–82. https://doi.org/10.1002/yea.320080202

Oldenburg, K. R., Vo, K. T., Michaelis, S., & Paddon, C. (1997). Recombination-mediated PCR-directed plasmid construction in vivo in yeast. *Nucleic Acids Research*, *25*(2), 451–452. https://doi.org/10.1093/nar/25.2.451

Ramon, A., & Smith, H. O. (2011). Single-step linker-based combinatorial assembly of promoter and gene cassettes for pathway engineering. *Biotechnology Letters*, *33*(3), 549–555. https://doi.org/10.1007/s10529-010-0455-x

Raymond, C. K., Sims, E. H., & Olson, M. V. (2002). Linker-mediated recombinational subcloning of large DNA fragments using yeast. *Genome Research*, *12*(1), 190–197. https://doi.org/10.1101/gr.205201

Sikorski, R. S., & Hieter, P. (1989). A system of shuttle vectors and yeast host strains designed for efficient manipulation of DNA in *Saccharomyces cerevisiae*. *Genetics*, *122*(1), 19–27.

Singh, M. V., & Weil, P. A. (2002). A method for plasmid purification directly from yeast. *Analytical Biochemistry*, *307*(1), 13–17. https://doi.org/10.1016/S0003-2697(02)00018-0

Torella, J. P., Boehm, C. R., Lienert, F., Chen, J.-H., Way, J. C., & Silver, P. A. (2014). Rapid construction of insulated genetic circuits via synthetic sequence-guided isothermal assembly. *Nucleic Acids Research*, *42*(1), 681–689. https://doi.org/10.1093/nar/gkt860

Wittrup, K. D., Bailey, J. E., Ratzkin, B., & Patel, A. (1990). Propagation of an amplifiable recombinant plasmid in *Saccharomyces cerevisiae*: Flow cytometry studies and segregated modeling. *Biotechnology and Bioengineering*, *35*(6), 565–577. https://doi.org/10.1002/bit.260350604

SUPPORTING INFORMATION

Additional supporting information may be found online in the Supporting Information section at the end of the article.

How to cite this article: Flagg MP, Kao A, Hampton RY. Integrating after CEN Excision (ICE) Plasmids: Combining the ease of yeast recombination cloning with the stability of genomic integration. *Yeast*. 2019;36:593–605. https://doi.org/10.1002/yea.3400

ACKNOWLEDGMENTS

Chapter II, in full, is a reproduction of the material as it appears in Yeast 2019. Flagg, Matthew P.; Kao, Andy; Randy, Hampton Y., John Wiley & Sons Ltd, 2019. The dissertation author was the primary investigator and first author of this paper, and permission from all other authors has been obtained.

Supplemental Figures

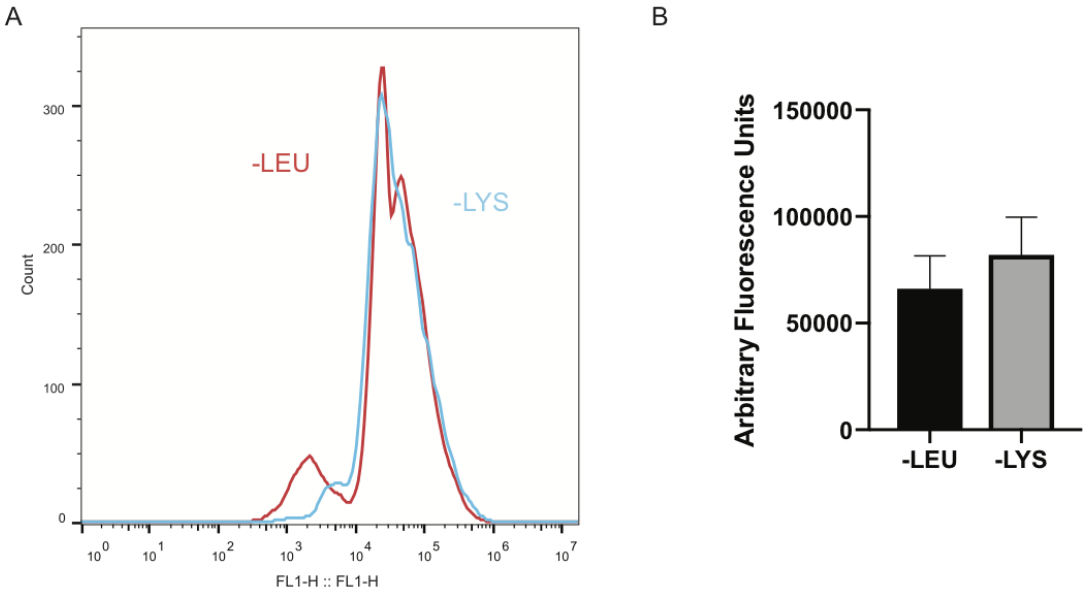

Figure 2.S1: A plasmid that supports lysine prototrophy is not subject to positive selection in medium lacking lysine. (A) Cells bearing a pTDH3::LYS1-GFP YCp were subjected to flow cytometry after outgrowth in medium lacking leucine (red histogram) or lysine (blue histogram). (B) Mean fluorescence after outgrowth in -LEU or -LYS medium was recorded using flow cytometry. N = 3. Bars show the mean of three experiments. Error bars represent standard deviation.

A

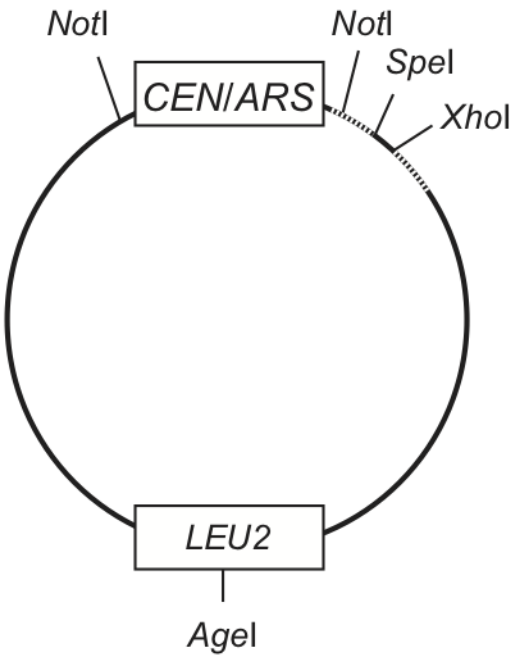

Figure 2.S2: Simplified schematic of a *LEU2* ICE plasmid. (A) The key features of an ICE plasmid include a CEN/ARS flanked by NotI sites, defined sequences (dashed line) upstream and downstream to the MCS (denoted by the unique cutter SpeI and XhoI) that can be added to an expression cassette by overhang primers, and a yeast selection cassette (LEU2) with a unique cut site (AgeI) that can be used for plasmid linearization and genomic integration.

Figure 2.S3: Graphical protocol of ICE plasmid workflow. (A) In preparation for YRC, an ICE plasmid is linearized by digestion. Any restriction enzyme with a unique cut site in the MCS is suitable. We recommend using two restriction enzymes, as this can lower the frequency of plasmid closure by non-homologous end joining. (B) To prepare an insert for recombination, amplify *Your Favorite Gene* (*YFG*) using PCR. Primers should include overhangs with homology to the ICE plasmid backbone. (C) PCR product and cut backbone are co-transformed into yeast to achieve recombination (dotted lines). We recommend between a 1:9 and 1:18 vector to insert ratio. It should also be noted that recombination often outcompetes non-homologous end joining, and that a lack of enrichment between a cut-vector-only control and a vector-plus-insert transformation should not always be interpreted as an unsuccessful attempt at cloning. (D) Isolated colonies are subjected to a yeast miniprep, and the new plasmid is recovered. At this stage, we recommend performing a diagnostic PCR with yeast miniprep to determine if cloning has been successful. Desired plasmids are then subjected to digestion by *Not*I, religation by T4 DNA ligase, and transformation into *Escherichia coli*. We suggest using a no-ligase control as an indicator of successful *CEN* excision and plasmid religation. A successful product of the ICE plasmid protocol has a single, reconstituted *Not*I site, which can be used in a diagnostic digest to demonstrate presence or absence of the ~500 bp *CEN*/*ARS* fragment. (E) The YIp generated by *CEN* excision is prepared for integration by plasmid linearization. Any restriction enzyme with a unique cut site in the yeast selectable marker is suitable (*E.g. Age*I). Upon transformation, the plasmid integrates at the homologous genomic locus by recombination and supports prototrophy or drug resistance. Notably, this method of plasmid integration can lead to tandem plasmid integration. Users should identify strains with a single plasmid integration by PCR, Western blot, or flow cytometry. Our preferred PCR strategy detects a novel junction between multiple plasmid integrations. This novel junction is produced where the plasmid is juxtaposed to an additional plasmid rather than the genome.

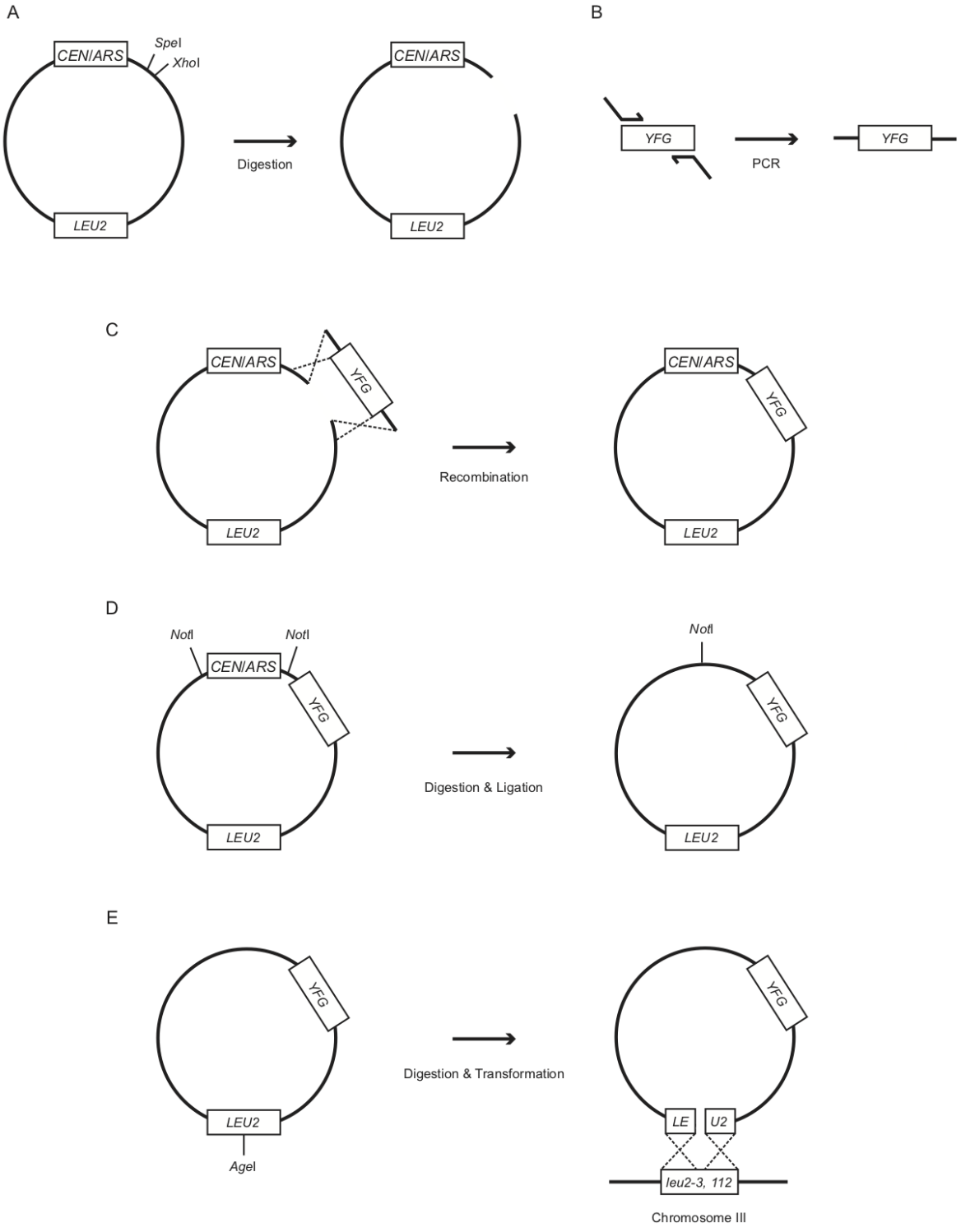
A
CEN/ARS
SpeI
XhoI
LEU2
Digestion
CEN/ARS
LEU2
B
YFG
PCR
YFG
C
CEN/ARS
YFG
LEU2
Recombination
CEN/ARS
YFG
LEU2
D
NotI
NotI
CEN/ARS
YFG
LEU2
Digestion & Ligation
NotI
YFG
LEU2
E
YFG
LEU2
AgeI
Digestion & Transformation
YFG
LE
U2
leu2-3, 112
Chromosome III

Supplemental Tables

Table 2.S1: Plasmids used in this study

Plasmid	AddGene alias	Gene	Reference
pRS317	N/A	YCp *LYS2*	Sikorski et. al., 1991
pRS402	N/A	YIp *ADE2*	Brachmann et. al., 1998
pRS403	N/A	YIp *HIS3*	Sikorski et. al., 1989
pRS404	N/A	YIp *TRP1*	Sikorski et. al., 1989
pRS405	N/A	YIp *LEU2*	Sikorski et. al., 1989
pRS406	N/A	YIp *URA3*	Sikorski et. al., 1989
pRS411	N/A	YIp *MET17*	Brachmann et. al., 1998
pRS415	N/A	YCp LEU2	Sikorski et. al., 1989
pUG6	N/A	*KanMx*	Güldener et. al., 1996
pAG32	N/A	*HphMx4*	Goldstein et. al., 1999
pRH1838	N/A	*NatMx*	This study
pRH1941	N/A	YCp *URA3 CPY*-GFP*	Medicherla et. al., 2004
pRH2815	N/A	YCp *LEU2 pADH1::FLAG-UBR1*	This study
pRH2695	N/A	YIp *URA3 pTDH3::GFP::tPGK1*	This study
pRH2935	N/A	YCp *URA3 pTDH3::GFP::tPGK1*	This study
pRH2896	N/A	YCp *LEU2 pTDH3::LYS1-GFP::tADH1*	This study
pRH2913	N/A	YCp *LEU2 pADH1::LYS1-GFP::tADH1*	This study
pRH2914	N/A	YCp *LEU2 pCPY::LYS1-GFP::tADH1*	This study
pRH2915	N/A	YCp *LEU2 pCYC1::LYS1-GFP::tADH1*	This study
pRH2947	pICE ADE2	ICE *ADE2*	This study
pRH2948	pICE HIS3	ICE *HIS3*	This study
pRH2949	pICE LEU2	ICE *LEU2*	This study
pRH2970	pICE LYS2	ICE *LYS2*	This study
pRH2950	pICE MET17	ICE *MET17*	This study
pRH2951	pICE TRP1	ICE *TRP1*	This study
pRH2952	pICE URA3	ICE *URA3*	This study
pRH2953	pICE ADE2-HIS3	ICE *ADE2 HIS3*	This study

Plasmid	AddGene alias	Gene	Reference
pRH2954	pICE ADE2-LEU2	ICE *ADE2 LEU2*	This study
pRH2955	pICE ADE2-MET17	ICE *ADE2 MET17*	This study
pRH2956	pICE ADE2-URA3	ICE *ADE2 URA3*	This study
pRH2971	pICE LYS2-HIS3	ICE *LYS2 HIS3*	This study
pRH2972	pICE LYS2-LEU2	ICE *LYS2 LEU2*	This study
pRH2973	pICE LYS2-MET17	ICE *LYS2 MET17*	This study
pRH2974	pICE LYS2-URA3	ICE *LYS2 URA3*	This study
pRH2957	pICE TRP1-HIS3	ICE *TRP1 HIS3*	This study
pRH2958	pICE TRP1-LEU2	ICE *TRP1 LEU2*	This study
pRH2959	pICE TRP1-MET17	ICE *TRP1 MET17*	This study
pRH2960	pICE TRP1-URA3	ICE *TRP1 URA3*	This study
PRH2980	pICE ADE2-HphMx	ICE *ADE2 HphMx*	This study
PRH2981	pICE ADE2-KanMx	ICE *ADE2 KanMx*	This study
PRH2982	pICE ADE2-NatMx	ICE *ADE2 NatMx*	This study
PRH2983	pICE LYS2-HphMx	ICE *LYS2 HphMx*	This study
PRH2984	pICE LYS2-KanMx	ICE *LYS2 KanMx*	This study
PRH2985	pICE LYS2-NatMx	ICE *LYS2 NatMx*	This study
PRH2986	pICE TRP1-HphMx	ICE *TRP1 HphMx*	This study
PRH2987	pICE TRP1-KanMx	ICE *TRP1 KanMx*	This study
PRH2988	pICE TRP1-NatMx	ICE *TRP1 NatMx*	This study
pRH3021	YIp ADE2-HIS3	YIp ADE2 HIS3	This study
pRH3022	YIp ADE2-LEU2	YIp ADE2 LEU2	This study
pRH3023	YIp ADE2-MET17	YIp ADE2 MET17	This study

Plasmid	AddGene alias	Gene	Reference
pRH3024	YIp ADE2-URA3	YIp ADE2 URA3	This study
pRH3017	YIp LYS2-HIS3	YIp LYS2 HIS3	This study
pRH3018	YIp LYS2-LEU2	YIp LYS2 LEU2	This study
pRH3019	YIp LYS2-MET17	YIp LYS2 MET17	This study
pRH3020	YIp LYS2-URA3	YIp LYS2 URA3	This study
pRH3025	YIp TRP1-HIS3	YIp TRP1 HIS3	This study
pRH3026	YIp TRP1-LEU2	YIp TRP1 LEU2	This study
pRH3027	YIp TRP1-MET17	YIp TRP1 MET17	This study
pRH3028	YIp TRP1-URA3	YIp TRP1 URA3	This study
pRH3029	YIp ADE2-HphMx	YIp ADE2 HphMx	This study
pRH3030	YIp ADE2-KanMx	YIp ADE2 KanMx	This study
pRH3031	YIp ADE2-NatMx	YIp ADE2 NatMx	This study
pRH3032	YIp LYS2-HphMx	YIp LYS2 HphMx	This study
pRH3033	YIp LYS2-KanMx	YIp LYS2 KanMx	This study
pRH3034	YIp LYS2-NatMx	YIp LYS2 NatMx	This study
pRH3035	YIp TRP1-HphMx	YIp TRP1 HphMx	This study
pRH3036	YIp TRP1-KanMx	YIp TRP1 KanMx	This study
pRH3037	YIp TRP1-NatMx	YIp TRP1 NatMx	This study
pRH3138	N/A	ICE *URA3 pTDH3::GFP::tPGK1*	This study

Table 2.S2: Yeast strains used in this study

Strain	Genotype	Reference
RHY2863	MATa *ade2-101 met2 lys2-801 his3Δ200 ura3-52 trp1Δ::hisG leu2Δ*	
RHY7447	BY4741	
RHY9697	RHY2863 pRH2935 (YIp *URA3 pTDH3::GFP::tPGK1*)	This study
RHY10932	RHY2863 pRH2935 (YCp *URA3 pTDH3::GFP::tPGK1*)	This study
RHY10527	BY4741 *LYS1-GFP::tADH1 HIS3MX6*	GFP collection
RHY10528	BY4741 *lys1Δ::KanMx*	Knockout collection
RHY11208	RHY10528 pRH2913 (YCp *LEU2 pTDH3::LYS1-GFP::tADH1*)	This study
RHY11209	RHY10528 pRH2914 (YCp *LUE2 pCPY::LYS1-GFP::tADH1*)	This study
RHY11210	RHY10528 pRH2915 (YCp *LUE2 pCYC1::LYS1-GFP::tADH1*)	This study
RHY11213	RHY10528 pRH2913 (YCp *LUE2 pADH1::LYS1-GFP::tADH1*)	This study
RHY11214	RHY10528 pRH2914 (YCp *LUE2 pCPY::LYS1-GFP::tADH1*)	This study
RHY11230	RHY10528 pRS415 (YCp *LEU2*)	This study
RHY11231	RHY10527 pRS415 (YCp *LEU2*)	This study
RHY11232	RHY7447 pRS415 (YCp *LEU2*)	This study
RHY11808	RHY10528 pRH2914 (YCp *LUE2 pCPY::LYS1-GFP::tADH1*)	This study
RHY11809	RHY2863 pRH3138 (ICE *URA3 pTDH3::GFP::tPGK1*)	This study

Table 2.S3: Oligonucleotides used in this study

Oligo	Sequence	Amplicon
oRH 4866	CTTTTTGCGGCCGCGCCACCTGGGTCCTTTTCAT	CEN/ARS
oRH 4867	CTTTTTGCGGCCGCCCTCTTAGCGCTTCTTAGGACGG ATCGCTTGC	CEN/ARS
oRH 4736	AACACTCAACCCTATCTCGG	*ADE2*, *HIS3*, *LEU2*, *MET17*, and *TRP1*
oRH 4872	TATCACGAGGCCCTTTCGTC	*ADE2*, *HIS3*, *LEU2*, *MET17*, and *TRP1*
oRH 5045	cctatttttataggttaatgtcatgatGCCTCGTTCAGAATGACACGT A	*HIS3*
oRH 5046	CATTTCCCCGAAAAGTGCCACCTGACGTCTAACACA GTCCTTTCCCGCAA	*HIS3*
oRH 4982	CATTTCCCCGAAAAGTGCCACCTGACGTCTCCTGTAC TTCCTTGTTCATGTGT	*LEU2*
oRH 4983	acgcctatttttataggttaatgtcatgatCTTTTTGTGTGGTGCCCTCC	*LEU2*
oRH 5049	cctatttttataggttaatgtcatgatAGCCATCCTCATGAAAACTGT	*MET17*
oRH 5050	CATTTCCCCGAAAAGTGCCACCTGACGTCTACAACT CATTACGCACACTCA	*MET17*
oRH 4980	acgcctatttttataggttaatgtcatgatGCACCATACCACAGCTTTTC	*URA3*
oRH 4981	CATTTCCCCGAAAAGTGCCACCTGACGTCTGAAGCT CTAATTTGTGAGTT	*URA3*
oRH 4868	gttccgcgcacatttccccgaaaagtgccacctgacgtcTGCACCATAAAC GACATTACT	*TRP1*
oRH 4869	GCCTCGTGATACGCCTATTTTTATAGGTTAATGTCAT GATTAGGCAAGTGCACAAACAAT	*TRP1*
oRH 5055	CATTTCCCCGAAAAGTGCCACCTGACGTCTTGTTTAG CTTGCCTCGTCCC	*HphMx, KanMx, NatMx*
oRH 5056	cctatttttataggttaatgtcatgatCTGGATGGCGGCGTTAGTAT	*HphMx, KanMx, NatMx*
oRH 4926	aattcgatatcaagcttatcgataccgtcgacctcgag AATGGCTGCCGTCACATTAC	*LYS1-GFP*
oRH 4915	accttcaccctctccactga	*LYS1-GFP*
oRH 4805	CCTCTTCGCTATTACGCCA	*pTDH3::GFP::tPGK1*
oRH 4852	TGTGTGGAATTGTGAGCGG	*pTDH3::GFP::tPGK1*
oRH 4938	GCGCGCAATTAACCCTCACTAAAGGGAACAAAAGCT GGAGATCCTTTTGTTGTTTCCGGG	*pADH1*
oRH 4939	atcgataagcttgatatcgaattCCTGCAGATCCGTCGAAAGTTGA TTGTATGCTTGGTATAGCTTGA	*pADH1*

Oligo	Sequence	Amplicon
oRH 4946	GCGCGCAATTAACCCTCACTAAAGGGAACAAAAGCTGGAGATTTCCGTATATGATGATAC	*pCPY*
oRH 4947	atcgataagcttgatatcgaattCCTGCAGATCCGTCGAGCGTATGTATACTTTAAGTTG	*pCPY*
oRH 4940	atttggcgagcgttggtt	*pCYC1*
oRH 4941	tagtgtgtgtatttgtgtttgcgtg	*pCYC1*
oRH 4942	GCAATTAACCCTCACTAAAGGGAACAAAAGCTGGAGACTAGTatttggcgagcgttggtt	*pCYC1*
oRH 4943	taagcttgatatcgaattCCTGCAGATCCGtCGAAtagtgtgtgtatttgtgtttgcgtg	*pCYC1*

CHAPTER III

Inner-Nuclear-Membrane-Associated Degradation Employs Dfm1-Independent Retrotranslocation and Alleviates Misfolded Transmembrane-Protein Toxicity

Abstract

Prior to their delivery to and degradation by the 26S proteasome, misfolded integral-membrane proteins of both the ER and inner-nuclear membrane must be extracted from lipid bilayers. It has become clear that this extraction process, known as retrotranslocation, requires not only quality-control E3 ubiquitin ligases but also dislocation factors that diminish the energetic cost of dislodging the transmembrane segments of a protein. Recently, we showed that retrotranslocation of all ER transmembrane proteins requires the Dfm1 rhomboid pseudoprotease. However, we did not investigate whether Dfm1 also mediated retrotranslocation of integral membrane degradation substrates in the inner-nuclear membrane (INM), which is contiguous with the ER but functionally separated from it by nucleoporins. Here we show that canonical retrotranslocation of such substrates occurs during INM-associated degradation (INMAD), but proceeds independently of Dfm1. Despite this independence, ERAD-M and INMAD pathways act in concert to ameliorate membrane-protein-associated proteotoxicity. We also show that this novel proteotoxic stress can elicit genetic suppression, demonstrating the cell's ability to remodel a poorly understood proteostatic network to tolerate a toxic burden of misfolded membrane proteins without functional INMAD or ERAD-M. This was in striking contrast to our previous observation of suppression of the *dfm1*Δ null, which leads to the resumption of ERAD-M through HRD-complex remodeling. Thus, we conclude that INM retrotranslocation proceeds through a novel private channel, which can be studied by virtue of its role in alleviating membrane-associated proteotoxicity.

Introduction

The ubiquitin proteasome system (UPS) monitors and degrades integral inner-nuclear-membrane (INM) proteins through a process known as inner-nuclear-membrane-associated degradation (INMAD) (Smoyer and Jaspersen, 2019). Discovered and characterized in *Saccharomyces cerevisiae*, INMAD employs the classic cascade of E1, E2, and E3 enzymes to recognize and polyubiquitinate integral INM-localized substrates (Deng and Hochstrasser, 2006; Omnus and Ljungdahl, 2014). Ubiquitination of substrates by INMAD-specific E3 ligases results in their subsequent degradation by nuclear-localized 26S proteasomes (Chen et al., 2011; Boban et al., 2014). In this way, INMAD facilitates both regulated degradation, wherein normal proteins are degraded to control their abundance, and degradative protein quality control, wherein misfolded and otherwise aberrant proteins are degraded to prevent proteotoxic stress (Foresti et al., 2014; Khmelinskii, Blaszczak et al., 2014).

The inner nuclear membrane is contiguous with the canonical endoplasmic reticulum (ER) but separated by the complex barrier of the nuclear pore. Thus, it is important and interesting to compare the relatively new INMAD to the conical pathways of endoplasmic-reticulum-associated degradation (ERAD) (Hampton and Garza, 2009a; Sun and Brodsky, 2019). ERAD governs both regulated and quality-control degradation of ER proteins, and the ERAD pathway employs dedicated E3 ligases that determine substrate selection. Specifically, the Hrd1 E3 ligase mediates the ubiquitination of membrane (ERAD-M) and luminal (ERAD-L) substrates (Plemper et al., 1998; Vashist and Ng, 2004) and the Doa10 E3 ligase primarily mediates the ubiquitination of cytosolic (ERAD-C) substrates (Carvalho et al., 2006; Swanson, et al., 2001). In all cases, substrates are retrotranslocated into the cytosol and transported to cytosolic 26S proteasome for degradation (Richly, et al., 2005).

Given the similar molecular challenges faced by INMAD and ERAD, it is unsurprising that these pathways employ some of the same UPS machinery. For instance, it has been shown that the hexameric AAA ATPase Cdc48 (known as p97 in mammals) is required for the retrotranslocation and degradation of all ER and INM substrates studied to date (Braun et al., 2002; Foresti et al., 2014; Ye et al., 2001). Similarly, a portion of ERAD and INMAD are governed by Doa10, which recognizes and ubiquitinates substrates in both subcellular compartments (Deng and Hochstrasser, 2006). Alternatively, some substrates access both the ER and INM and undergo degradation by the HRD (HMG-CoA Reductase Degradation) pathway when in the canonical ER and the INMAD pathway when in the nucleus (Foresti et al., 2014), the proportion of each probably determined by the stochastic partitioning between the two compartments.

These overlaps are made possible by two features of the inner nuclear membrane. First, the INM encloses and is in direct contact with the nucleoplasm, which is the same aqueous compartment as the cytosol (Figure 1A). Cdc48 and the 26S proteasome are permitted into nucleoplasm from the cytosol through nucleoporins and thereby gain access to INMAD substrates (Chen et al., 2011; Foresti et al., 2014; Gallagher et al., 2014). Second, the INM is continuous with the ER which allows a subset of proteins, such as Doa10, to diffuse freely between the two compartments (Deng and Hochstrasser, 2006; Foresti et al., 2014; Natarajan et al., 2020). It seems diffusion of membrane proteins is also gated by nucleoporins and that the size of a protein's cytosolic domain(s) is the major determinant of diffusion into the INM (Ohba et al., 2004; Smoyer et al., 2016).

While the INM structure allows significant overlap in the use of INMAD and ERAD machinery, the INM also possesses UPS components distinct from those employed in ERAD. The best characterized of these is the Asi E3 ligase complex. Originally identified as a component of nutrient-sensing pathways, the Asi complex is composed of two RING-H2 motif E3 ubiquitin ligases, Asi1 and Asi3, and an adaptor, Asi2 (Zargari, Boban et al., 2007). All three components are restricted

to the INM (Smoyer et al., 2016; Zargari, Boban et al., 2007). Like other INMAD and ERAD ligases, the Asi complex has been shown to promote regulated degradation of substrates such as Erg11 and quality-control degradation of misfolded substrates such as Sec61-2 (Foresti et al., 2014; Khmelinskii, Blaszczak et al., 2014; Natarajan, N. et al., 2020). However, the degree to which the Asi complex and INMAD rely upon known components of the UPS remains uncertain.

In particular, it is unclear how INMAD pathways perform the critical step of retrotranslocation. In the case of integral membrane substrates, retrotranslocation involves extraction of full-length, ubiquitinated proteins from the membrane, thereby facilitating transport to and degradation by the 26S proteasome (Garza et al., 2009a; Neal et al., 2018). As in ERAD, the Asi complex seems to rely on Cdc48 ATP hydrolysis to provide the free energy required for this process (Foresti et al., 2014). However, in all known cases, Cdc48 is not sufficient to promote retrotranslocation, and there is a growing consensus that retrotranslocation requires other factors that can facilitate the thermodynamically challenging extraction of membrane proteins from their stable locations within the ER/IN membrane (Baldridge and Rapoport, 2016; Natarajan, et al., 2020; Neal et al., 2018; Neal et al., 2020; Schmidt et al., 2020; Schoebel et al., 2017; Vasic et al., 2020; Wu et al., 2020). A recent study shows that the Asi complex itself can play this role in a purified system, at least for the subset of INMAD substrates that engage Asi2 (Natarajan, et al., 2020). In these instances, Asi2 performs an essential role in retrotranslocation by binding to substrates within the lipid bilayer. Upon Asi2-mediated interaction, clients can be retrotranslocated *in vitro* by a reconstituted INMAD pathway including ubiquitin, appropriate E2s, Asi1, Asi2, Asi3, and Cdc48. However, several substrates of the Asi complex, such as Sec61-2 (studied below), do not require Asi2 for degradation and instead rely solely upon As1 and Asi3. These Asi2-independent substrates suggest the presence of another route of retrotranslocation in the INM.

Recently, we identified a key ERAD-M retrotranslocation factor, the derlin Dfm1, a six-pass integral ER membrane protein. Dfm1 is a member of the rhomboid pseudoprotease family (Kandel and Neal, 2020) and bears a cytosolic SHP box that anchors Cdc48 to the ER membrane (Sato and Hampton, 2006; Stolz et al., 2010). We showed that Dfm1 is necessary for the retrotranslocation of a remarkably wide variety of integral ER membrane substrates, including HRD and DOA10 membrane substrates as well as Hrd1 itself (Neal et al., 2018). We also demonstrated that successful retrotranslocation requires both the SHP box and transmembrane domains. However, we did not directly investigate Dfm1 involvement in INMAD in those studies, and the question of Dfm1 involvement in Asi-complex retrotranslocation remained unaddressed. In this work we have addressed this question.

Here, we demonstrate that classical ERAD-M retrotranslocation of full-length multispanning INMAD substrates occurs, and that Dfm1 is not involved in this process. We show that the Hrd1-Asi client Sec61-2 is ubiquitinated by Hrd1 and the Asi complex *in vivo* and that the substrate is then successfully retrotranslocated from the INM *in vivo* in *dfm1Δ* null strains. To further confirm the Dfm1 independence of the Asi complex, we show that Erg11, like Sec61-2, is degraded in a *dfm1* null background. Finally, we show that the Doa10 client Asi2 (a protein localized exclusively in the INM) is successfully degraded in the absence of Dfm1. Based on these data, we conclude that one or more INM factors must substitute for Dfm1 in both Asi- and Doa10-mediated INMAD.

To better understand the proteostatic physiology of the interconnected ER and INM membranes, we also demonstrate a novel form of proteotoxicity mediated by the misfolded substrate Sec61-2. We show that a lethal proteotoxic stress is imposed by Sec61-2 in the absence of both INMAD and ERAD-M, suggesting a form of proteotoxicity specific to the contiguous ER-INM membrane. We also show that this lethal proteotoxic stress can select for the sequential duplication of chromosomes V and XIV. In cells that achieve this aneuploidy, Sec61-2 is tolerated when both

INMAD and ERAD-M are absent. Importantly, these changes do not restore degradation. These results demonstrate a novel form of ER-INM proteotoxic stress as well as a genetic pathway that allows the suppression of such stress. The detailed mechanism(s) by which a misfolded protein such as Sec61-2 interfere with cellular health present a promising direction for future studies, and the conditional lethality of Sec61-2 provides a novel means for the discovery of new INMAD/ERAD components.

Results

INMAD Substrates Were Degraded in the Absence of Dfm1

To determine whether Dfm1 plays a role in INMAD, we set out to investigate a functional, misfolded *sec61-2* allele of the essential protein Sec61 (Biederer et al., 1996). Previously, Sec61-2 has been demonstrated to be a target of both Asi-mediated INMAD and Hrd1-mediated ERAD-M (Foresti et al., 2014). These pathways function in parallel, and Sec61-2 degradation persists unless both pathways are disrupted.

To construct quantifiable *SEC61* and *sec61*-2 fusions, we capitalized on the *SEC61*-GFP strain from the yeast GFP collection. In previous studies, a *SEC61*-GFP strain was viable and produced the expected ER localization of Sec61, suggesting that the C-terminal GFP tag interfered with neither function nor localization of its essential fusion partner (Huh et al., 2003). We subcloned both *SEC61-GFP* and corresponding *sec61-2-GFP* into constructs bearing a *GAL1* inducible promoter. As expected, Sec61-GFP was stable when subjected to cycloheximide chase, whereas Sec61-2-GFP was rapidly degraded (Figure 1B). Notably, rapid degradation of Sec61-2-GFP was observable at 30° C and did not require shifting cells to 37° C, despite the supposition that elevated temperature is required for degradation of the original Sec61-2 protein (Biederer et al., 1996; Foresti et al., 2014). Like the parent mutant, Sec61-2-GFP still supported cell growth at the permissive

temperature and showed the expected temperature sensitivity: when we integrated *sec61-2*-GFP at the endogenous *SEC61* locus, the resultant strain was viable at 30° C and inviable at 37° C (Figure S1A). Moreover, our Sec61-2-GFP fusion had a half-life equivalent to untagged Sec61-2, as reported in other studies (Sato et al., 2009). Finally, Sec61-2-GFP degradation was fully proteasome dependent. Pre-treatment with the proteasome inhibitor MG132 led to complete stabilization of Sec61-2-GFP in a cycloheximide chase (Figure 1C).

We introduced *pGal1::sec61-2 CEN/ARS* plasmids into an ERAD-M-deficient *hrd1Δ* strain, an INMAD-deficient *asi1Δ* strain, and a *asi1Δhrd1Δ* strain lacking both pathways. When these strains were subjected to cycloheximide chase, *asi1Δ* and *hrd1Δ* strains showed only modest stabilization of Sec61-2-GFP. However, the *asi1Δhrd1Δ* double null strain was completely unable to degrade the substrate (Figure 1D). Consistent with previous studies on Sec61-2, the Sec61-2-GFP fusion was a substrate of both HRD and ASI pathways, and its degradation was mediated by the joint efforts of these routes (Foresti et al., 2014).

We next used the Sec61-2-GFP substrate to explore the requirements for INMAD retrotranslocation. We first confirmed the expected "universal" role of the AAA-ATPase Cdc48 in both pathways. Cycloheximide chase demonstrated that a strain with the retrotranslocation-deficient *cdc48-2* allele strongly stabilized Sec61-2-GFP degradation. Indeed, the degradation kinetics of a *cdc48-2* strain phenocopied those of the *asi1Δhrd1Δ* strain (Figure 1E). These findings are in accordance with previous studies (Foresti et al., 2014).

We next tested the role of the Dfm1 ERAD-M retrotranslocation factor in degradation of Sec61-2-GFP. We expected the ERAD-M pathway of Sec61-2 degradation to be ablated in a *dfm1Δ* strain because Dfm1 has been shown to mediate the retrotranslocation of all ERAD-M substrates studied to date. Indeed, our previous studies showed stabilization of Sec61-2 in a *dfm1Δ* strain (Neal et al., 2018). On the other hand, the Asi complex's contribution to Sec61-2 degradation has not been

systematically examined for Dfm1 involvement. We therefore used cycloheximide chase to make a preliminary inquiry into the role of Dfm1 in the INMAD component of Sec61-2 retrotranslocation. We expressed Sec61-2-GFP in *dfm1Δ*, *dfm1Δhrd1Δ*, and *asi1Δdfm1Δ* strains and assessed degradation in each. The results suggested that Dfm1 did not participate in the INMAD portion of Sec61-2-GFP degradation: both *dfm1Δ* and *dfm1Δhrd1Δ* were partially and identically deficient in their ability to degrade the Sec61-2-GFP, whereas the *asi1Δdfm1Δ* strain was fully incapable of degrading the substrate and was thus a phenocopy of the *asi1Δhrd1Δ* strain (Figure 2A). These results were recapitulated by flow cytometry, with which Sec61-2-GFP degradation can be quantitated by loss of fluorescence over time (Figure 2B). Dfm1 seemed to be restricted to the HRD component of Sec61-2 degradation; the Asi pathway did not seem to employ the widely used extraction factor.

To further test the idea that Dfm1 did not participate in Asi-complex-mediated degradation, we conducted cycloheximide chase experiments on Erg11. Erg11 is a single-pass transmembrane protein, and Erg11-3HA has been shown to be a specific substrate of only Asi-complex-mediated INMAD (Foresti et al., 2014; Natarajan et al., 2020). In contrast to Sec61-2-GFP degradation, which requires only Asi1 and Asi3, Erg11-3HA degradation requires Asi1, Asi2, and Asi3 (Foresti et al., 2014; Natarajan et al., 2020). We performed cycloheximide chase of Erg11-3HA and found that As12-Asi2-Asi3-dependent INMAD similarly did not require Dfm1 (Figure 2C). A *dfm1Δ* strain degraded Erg11-3HA with kinetics identical to a WT strain, whereas an *asi1Δ* strain was completely unable to degrade the Erg11 substrate. Thus, cycloheximide chase of Sec61-2-GFP and Erg11-3HA both strongly suggested the Dfm1 independence of Asi-complex-mediated INMAD.

We wondered whether Asi-dependent degradation was a unique case of Dfm1-independent INMAD or if Doa10-mediated INMAD was also Dfm1 independent. To test these possibilities, we used Asi2 itself as a model substrate (Boban et al., 2014). Asi2 is an integral membrane protein that localizes almost exclusively to the INM (Zargari, Boban et al., 2007), and undergoes degradation

mediated by Doa10 when its binding partners (Asi1 or Asi2) are absent. Asi2 thereby provided an opportunity to evaluate Doa10-mediated INMAD with little or no contribution from canonical Doa10-mediated ERAD-M, which is entirely Dfm1-dependent (Neal et al., 2018). We introduced HA-Asi2 into WT, *dfm1Δ*, and *doa10Δ* strains and performed cycloheximide chase. HA-Asi2 was rapidly degraded in each of these null mutants, and we were unable to observe increases in stability or steady-state levels of HA-Asi2 that have been observed in other *doa10Δ* strains (Boban et al., 2014; Figure 2D). We wondered if HA-Asi2 was substrate of both Asi-complex- and DOA-mediated INMAD, and if the loss of both pathways was required to observe HA-Asi2 stabilization. To test this possibility, we introduced the HA-Asi2 substrate into *asi1Δ*, *asi1Δdfm1Δ*, and *asi1Δdoa10Δ* strains. HA-Asi2 was strongly stabilized in the *asi1Δdoa10Δ* strain, indicating that HA-Asi2 was indeed a substrate of both INMAD pathways (Figure 2E). By contrast, HA-Asi2 underwent rapid degradation identical to that of the single asi1 null in an *asi1Δdfm1Δ* strain (Figure 2E). These data strongly suggested that, like the Asi complex, Doa10 promoted INMAD independently of Dfm1. Notably, recent *in vitro* studies suggest the possibility that purified Doa10 itself could serve as a retrotranslocon (Schmidt et al., 2020).

Dfm1 Was Not Required for INMAD Retrotranslocation

Having observed Dfm1-independent degradation of a variety of INMAD substrates, we set out to test if INMAD substrates still underwent the canonical mechanism of ubiquitination followed by Cdc48-dependent retrotranslocation of the full-length substrate. To do so, we focused again on Sec61-2-GFP as model substrate.

First, we performed *in vivo* ubiquitination assays on WT, *asi1Δ*, *hrd1Δ*, and *asi1Δhrd1Δ* strains. As suggested by our and others' cycloheximide chase experiments, Sec61-2-GFP was polyubiquitinated by both the Asi and HRD complexes (Figure 3). Proteasome inhibition with MG132 increased the degree of polyubiquitination by the Asi (*hrd1Δ*) or the HRD (*asi1Δ*) complex,

demonstrating that polyubiquitination was on pathway with proteasomal degradation in each pathway. The *in vivo* ubiquitination assay also showed that each complex can ubiquitinate Sec61-2-GFP independently: single nulls displayed diminished ubiquitination while the *asi1Δhrd1Δ* double null displayed none, even with added proteasome inhibitor.

We next directly tested for retrotranslocation of polyubiquitinated Sec61-2-GFP with an *in vivo* retrotranslocation assay developed in our Dfm1 studies (Garza et al., 2009a; Neal et al., 2018). Strains expressing Sec61-2-GFP were treated with proteasome inhibitor for an incubation period, then subjected to detergent-free lysis. Membrane and soluble fractions from these cells were isolated by ultracentrifugation, allowing the separation of soluble, retrotranslocated Sec61-2-GFP from membrane-bound Sec61-2-GFP. The soluble fraction was then subjected to immunoprecipitation (IP) using anti-GFP antibody, followed by immunoblotting (IB) with anti-ubiquitin and anti-GFP. In parallel, the pellet fraction, containing polyubiquitinated material that has not been retrotranslocated, was solubilized and subjected to identical IP/IB analysis. For each strain, total (T), pellet (P), and supernatant (S) fractions were compared, and volumes were used that allow direct comparison of % of total by visual inspection (see material and methods). Strains capable of retrotranslocation were expected to produce ubiquitin signal in both P and S fractions, whereas retrotranslocation-deficient strains were expected to retain all polyubiquitinated substrate in the membrane fractions (ER and INM), leading to ubiquitin signal only in the P fraction.

We first confirmed that the ERAD and INMAD pathways were each capable of retrotranslocating Sec61-2-GFP. We assayed for Sec61-2-GFP retrotranslocation in WT, *asi1Δ*, *hrd1Δ*, and *cdc48-2* backgrounds (Figure 4A). In the retrotranslocation-competent WT strain, a fraction of ubiquitinated Sec61-2-GFP was detected in the soluble fraction, demonstrating that Sec61-2-GFP undergoes retrotranslocation into the cytosol and/or nucleoplasm under standard conditions. Conversely, a strain bearing the retrotranslocation-deficient *cdc48-2* allele retained all

ubiquitinated Sec61-2-GFP in pellet fraction, showing no retrotranslocation of ubiquitinated material into the soluble fraction. Finally, *asi1Δ* and *hrd1Δ* strains indicated that retrotranslocation could occur through either the ERAD or INMAD pathway, respectively. In each null mutant, a fraction of polyubiquitinated material was still retrotranslocated into the soluble fraction through the remaining pathway.

A remarkable feature of ERAD-M retrotranslocation is extraction of full-length multispanning substrates from the ER membrane and into the soluble fraction (Garza et al., 2009a; Neal et al., 2018). Full-length retrotranslocation is observable by treating the soluble, polyubiquitinated, retrotranslocated material gathered in an *in vivo* retrotranslocation assay with the catalytic core of the deubiquitinase Usp2 (Ryu et al., 2006). Usp2 removes polyubiqutin chains from the substrate and thereby causes characteristic polyubiquitination laddering to collapse to the expected size of the full-length, retrotranslocated ERAD-M substrates (Garza et al., 2009a; Neal et al., 2018). We used this method to test if retrotranslocation by INMAD also involved the extraction of full-length substrate from the INM. WT, *asi1Δ*, and *hrd1Δ* strains expressing Sec61-2-GFP were subjected to the *in vivo* retrotranslocation protocol, and polyubiquitination of Sec61-2-GFP was detected before and after treatment with Usp2. In all cases, laddered, polyubiquitinated Sec61-2-GFP collapsed to a single band of the expected molecular weight, indicating that both ERAD and INMAD remove the full-length substrate from the ER and INM, respectively.

Having demonstrated the ability of the ERAD and INMAD pathways to perform classical retrotranslocation of Sec61-2-GFP, we used the *in vivo* retrotranslocation assay to elucidate Dfm1's role in retrotranslocation from the INM. WT, *dfm1Δ*, *dfm1Δhrd1Δ*, *dfm1Δasi1Δ* and *cdc48-2* strains expressing Sec61-2-GFP were tested. Retrotranslocation persisted in both the *dfm1Δ* and *dfm1Δhrd1Δ* backgrounds, suggesting that Dfm1 mediated retrotranslocation through the ER alone (Figure 4C). By contrast, the *dfm1Δasi1Δ* background could not perform retrotranslocation,

indicating that the loss of both pathways was necessary to ablate the retrotranslocation of the polyubiquitinated substrate. In agreement with our preliminary cycloheximide chase results, the *in vivo* ubiquitination and retrotranslocation assays confirmed that INMAD acts independently of Dfm1.

ERAD and INMAD Ameliorated a Lethal Proteotoxic Membrane Stress in Parallel

Despite the functional separation of INMAD and ERAD retrotranslocation suggested by these data, it now seems clear that these two degradative pathways comprise an interconnected proteostasis network. This is not limited to the quality-control and regulated degradation affected by each pathway in its respective compartment. For instance, the ASI complex seems to provide a means of clearing orphaned subunits from the ER: in the absence of their binding partners, these lone subunits freely diffuse into the INM where they are recognized and degraded (Natarajan, et al., 2020). Research into how INMAD and ERAD overlap, complement, and compensate for one another is in its infancy, but the physiological importance of the INMAD-ERAD network has been clearly demonstrated by the synthetic lethality of *asi1Δhrd1Δire1Δ* strains (Foresti et al., 2014; Khmelinskii, Blaszczak et al., 2014). We wondered if a membrane quality-control substrate recognized by both ERAD and INMAD would cause discernable cell stress or lethality in the absence of either or both pathways. To pursue this line of inquiry, we again turned to the model substrate Sec61-2-GFP.

To control the imposition of a membrane-protein induced toxic stress, we employed a powerful galactose-regulated promoter (*pGAL1*) to allow sudden expression of a test protein. The *GAL1* promoter is essentially inactive when cells are grown in glucose but is strongly and suddenly activated when glucose is replaced with galactose in the growth medium. In this way, levels of Sec61-2 or the WT Sec61-GFP could be strongly elevated in a controlled manner to test for growth stress. We introduced a *pGAL1::sec61-2-GFP* or *pGAL1::SEC61-GFP* constructs on low-copy plasmids into WT, *asi1Δ*, *hrd1Δ,* and *asi1Δhrd1Δ* in the BY4741 background. These strains were then serially

diluted onto either 2% dextrose or 2% galactose plates, and their growth was monitored over time. Under inducing conditions, WT and *asi1Δ* strains bearing *sec61-2-GFP* grew normally, while a *hrd1Δ* strain bearing *sec61-2-GFP* evinced mild slow growth (Figure 5A). In striking contrast, the *asi1Δhrd1Δ* strain was inviable upon *sec61-2-GFP* induction (Figure 5A). Cells identically expressing wild-type *SEC61-GFP*, on the other hand, were uniformly viable, suggesting that the lethality observed in our *sec61-2-GFP* experiments reflected a bona fide misfolded membrane-protein toxicity that is mitigated by ERAD and INMAD in parallel (Figure 5B).

To further explore the role of the Asi complex in alleviating this proteotoxic stress, we also tested the effect of Sec61-2 stress in the absence of Asi3 and Asi2. Elsewhere, Asi3 has been shown to be necessary for Sec61-2 degradation (Foresti et al., 2014). In our growth assay, Asi3 also proved necessary for alleviating Sec61-2 proteotoxicity: an *asi3Δhrd1Δ* strain recapitulated the *asi1Δhrd1Δ* lethality (Figure 5C). In contrast to Asi1 and Asi3, Asi2 is not required for Sec61-2 degradation (Foresti et al., 2014). However, this did not preclude a role for Asi2 in alleviating the observed Sec61-2 toxicity, especially considering the recent finding that Asi2 can interact directly with substrates through membrane residues (Natarajan, et al., 2020). Nevertheless, unlike the *asi1Δhrd1Δ* and *asi3Δhrd1Δ* double nulls, an *asi2Δhrd1Δ* strain phenocopied a *hrd1Δ* strain, showing some slow growth but not lethality upon induction on galactose. In line with its dispensability for degradation, we did not observe a role for Asi2 in mitigating Sec61-2 toxicity.

While an *asi1Δhrd1Δ* strain demonstrated the crucial role of Asi1 in this system, it did not allow us to assess whether the catalytic activity of Asi1 or an unknown property of its transmembrane domain were responsible for combatting proteotoxicity. We therefore set out to test a catalytically inactive RING-dead (Boban et al., 2006) Asi1 in our toxicity assay. We introduced either a Asi1-RD (C583S-C585S) or a WT ASI1 plasmid into *asi1Δ* and *asi1Δhrd1Δ* strains. While the WT gene fully complemented the null mutant (Figure 5E), the RING-dead version failed to rescue the phenotype

(Figure 5F). These observations suggest that Asi1-mediated ubiquitination is required to prevent cell death.

Sec61-2 Toxicity Could Be Suppressed by Aneuploidy

The above-described proteotoxicity represents one of only two well-documented membrane-associated quality-control toxicities. The other is caused by overexpressing ERAD-M substrates in a *dfm1Δ* null background, which prevents retrotranslocation and traps substrates in the ER (Neal et al., 2018; Neal et al., 2020). This latter stress not only causes a strong growth defect but also leads to rapid suppression by the duplication of chromosome XV (Neal et al., 2018). Remarkably, suppression of *dfm1Δ* alleviates proteotoxic stress by fully restoring retrotranslocation, and chromosome XV is duplicated for the sole purpose of increasing the gene dosage of *HRD1*. In a recent analysis, we showed that overexpression of *HRD1* allows for self-remodeling of the HRD complex, allowing Hrd1 to retrotranslocate ERAD-M substrates without Dfm1 (Neal et al., 2020); in normal circumstance, ERAD-M retrotranslocation is completely dependent on Dfm1, with no involvement of Hrd1. Thus, elucidating the mechanisms of *dmf1Δ* suppression led to the discovery of new functions for the HRD complex and an expanded view of Hrd1's molecular abilities. Given the considerable genetic and biochemical insight produced by this approach, we wondered if a similar pathway to suppression could be identified in the case of *sec61-2* toxicity.

To expose cells to constitutive proteotoxic stress, we transformed strains with a stably integrating plasmid on which *sec61-2-GFP* expression is driven by the strong *TDH3* promoter. When this plasmid was transformed into an *asi1Δhrd1Δ* null, all resultant transformants bore the plasmid growth marker but were non-fluorescent, suggesting strong selection for those transformants that had lost substrate expression (not shown). To circumvent this issue, we pursued a 5-FOA counterselection strategy. We first introduced *HRD1* on a *URA3 CEN*/*ARS* plasmid into an *asi1Δhrd1Δ* null. As expected, this *HRD1*-complimented strain phenocopied an *asi1Δ* null, and it

was therefore able to stably express not only Sec61-GFP but also proteotoxic Sec61-2-GFP on a *TDH3* promoter (Figure 6A, -Trp -Ura). These viable, *HRD1*-complimented strains were then grown on 5-FOA to bring about removal of the HRD1 plasmid. In effect, 5-FOA selects for cells that spontaneously lose *URA3 CEN*/*ARS* plasmids (i.e. it counterselects such plasmids), and in this way, 5-FOA allowed us to rapidly unveil an *asi1Δhrd1Δ* genotype. On 5-FOA, the strain expressing wild-type SEC61-GFP produced lawn growth, indicating that the unveiled *asi1Δhrd1Δ* strain was viable (Figure 6A, -Trp 5-FOA). On the other hand, the strain expressing Sec61-2-GFP produced only a small number of non-optical colonies, indicating that the unveiled *asi1Δhrd1Δ* strain suffered the expected lethal proteotoxic stress. We reasoned that the rare "escaper" colonies that eventually emerged would be suppressees.

After extended outgrowth on 5-FOA plates, the newly generated *asi1Δhrd1Δ* nulls gave rise to a small number of suppressees that were optically bright. In strong contrast to *dfm1Δ* suppressors, these strains continued to express high levels of Sec61-2-GFP and did not regain their ability to degrade the substrate (Figure 6B). Thus, whereas *dfm1Δ* suppressees harness additional modes of ERAD retrotranslocation, *asi1Δhrd1Δ* suppressees remained unable to degrade the stressing substrate, suggesting that no additional modes of INMAD retrotranslocation were available to cells, at least by the genetic mechanisms available to growth-restored escapers

As mentioned above, *dfm1Δ* suppressees uniformly acquire a duplication of chromosome XV, which allows acquisition of a novel route of restored ERAD-M (Neal et al., 2018; Neal et al., 2020). We wondered if *asi1Δhrd1Δ* suppression relied upon similar genetic mechanism. We therefore isolated four suppressed strains and subjected them to high-throughput genome sequencing. This uncovered two classes of suppressed strain (Figure 6C). In the first class, the complete chromosome V was duplicated. In the second class, both chromosome V and XIV were fully duplicated, suggesting a sequential suppression pathway. Together, these data demonstrated that the

membrane stress imposed by Sec61-2 can indeed induce a novel, aneuploidy-based suppression pathway that allows for the tolerance of high levels of membrane proteotoxic stress. Intriguingly, chromosome XIV contains *ASI3*, perhaps indicating that this INMAD component acts to mitigate stress. The observation of a suppression pathway indicates that this novel physiological stress is surmountable and thus amenable to study by understanding the processes that are altered to restore normal growth.

Discussion

Though ERAD-M is entirely Dfm1 dependent, in these studies we found that INMAD was Dfm1 independent. This was true of all INMAD substrates tested, including the ASI-HRD substrate Sec61-2-GFP, the pure ASI substrate Erg11, and the ASI-DOA substrate Asi2. Notably, these substrates allowed us to test the Dfm1 dependence of all INMAD pathways characterized to date. This includes both the Asi1-Asi3 and Asi1-Asi2-Asi3 configurations of the ASI complex, which target sec61-2 and Erg11, respectively. In every case, INMAD proceeds in the absence of Dfm1.

To further corroborate these data, we performed *in vivo* biochemical analyses of Sec61-2 degradation by ERAD and INMAD pathways. We directly demonstrated Hrd1- and Asi-mediated ubiquitination of Sec61-2 *in vivo*, and we showed that Sec61-2 is extracted from lipid bilayers by both HRD and ASI pathways in an *in vivo* retrotranslocation assay. In both cases, retrotranslocation was completely Cdc48-dependent, and involved removal of the full-length transmembrane Sec61-2 protein from the lipid bilayer. This thermodynamically impressive feat is a hallmark of all ERAD and INMAD substrates tested to date.

To our knowledge, these studies constitute the first demonstrations of *in vivo* ubiquitination and retrotranslatiocation of a full-length, transmembrane Asi substrate. Thus, it is clear that that

Sec61-2-GFP is an extraordinarily tractable tool for exploring INM retrotranslocation and the stresses that are mitigated by those pathways.

More generally, this study and others suggest that a growing number of proteins possess the ability to retrotranslocate quality-control substrates out of or through lipid bilayers. These include, but as we show are not limited to, Hrd1, Dfm1, Doa10, and the Asi complex (Baldridge and Rapoport, 2016; Natarajan, et al., 2020; Neal et al., 2018; Neal et al., 2020; Schmidt et al., 2020; Schoebel et al., 2017; Vasic et al., 2020; Wu et al., 2020). While redundancy is a common feature of protein quality control pathways, it will be interesting to further dissect the biochemical and cell-biological nuances that necessitate these dedicated channels.

One possible benefit to a broad collection of retrotranslocons is the ability to couple ubiquitination and retrostranslocation in some instance and to decouple them in others. For instance, Hrd1 both ubiquitinates and retrotranslocates ER luminal proteins by forming a pore (Baldridge and Rapoport, 2016; Carvalho et al., 2006; Schoebel et al., 2017; Vasic et al., 2020), but retrotranslocation of Hrd1 itself is entirely Dfm1 dependent (Neal et al., 2018). Recent *in vitro* analysis suggests that the ASI complex is similarly unable to affect self-retrotranslocation: whereas the reconstituted ASI complex is fully competent to retrotranslocate a transmembrane Erg11-derived degron, polyubiquitinated Asi3 is not extracted from proteoliposomes (Natarajan et al., 2020). Similarly, degradation of Asi1 is ASI complex independent (Pantazopoulou, et al., 2016). It seems that, while ubiquitin ligases are often efficient retrotranslocons, they do not affect their own retrotranslocation, perhaps as a means to prevent runaway self-degradation.

While separation of E3 functions may necessitate numerous retrotranslocons, it does not account for Dfm1's inability to participate in INMAD. It could be that Dfm1 simply cannot pass through nuclear pores to access the INM. That restriction could be enforced by multimerization with the HRD complex (Stolz, et al., 2010) and/or some intrinsic feature of Dfm1 structure, but a definitive

illustration of Dfm1 localization will require electron microscopy. It is also possible that the INM presents a unique biochemical challenge for retrotranslocation. Indeed, the INM has a distinct lipid composition that may require a distinct mode of retrotranslocation and distinct retrotranslocons (Romanauska, et al., 2018). This is a particularly interesting possibility with derlin-based retrotranslocation, which may involve lipid biophysics as an underlying mechanism, rather than classic pore formation (Greenblatt et al., 2010; Wu et al., 2020). It will be intriguing to identify functionally important transmembrane motifs of INM retrotranslocons as they are discovered, and to compare and contrast them with the WR and GxxxG motifs of Dfm1. It is also possible that the distinct composition of the INM requires a distinct mechanism for retrotranslocation, or a lipid modulating factor tailored for INM lipid composition.

These studies also described the apparent autonomy of INMAD retrotranslocation. This autonomy may stem from the fact that, once ubiquitinated, substrates would be sterically trapped inside the nuclear subcompartment of the cytosol. A key feature of nuclear pore restriction appears to be the simple steric rubric of cytoplasmic domains needing to be less than ~60 kD (Ohba et al., 2004; Smoyer et al., 2016). Even four ubiquitin molecules in a chain would add over 30 kD to the cytoplasmic size of the modified protein. The resulting entrapment within a compartment would further necessitate the existence of dedicated, INM-localized retrotranslocons. Consistent with this idea, there was a precipitous decrease in Sec61-2 retrotranslocation in a *dfm1Δ* null background (Figure 4B, lanes 4-6) despite robust Hrd1-dependent ubiquitination. Moreover, when we compared *hrd1Δ* and *dfm1Δhrd1Δ* null backgrounds, there was no apparent decrease in retrotranslocation in the double null to indicate the loss of substrates that are ubiquitinated in the ER and retrotranslocated in the INM (Figure 4B, lanes 7-9). These data demonstrate an epistatic relationship between *HRD1* and *DFM1*, which suggests that Dfm1 alone can retrotranslocate Hrd1-ubiquitinated Sec61-2-GFP.

These studies also provide a means of separating the ERAD and INMAD components of the DOA pathway. We have demonstrated elsewhere that a *dfm1Δ* null background ablates the ERAD-M component of the DOA pathway. Here we showed that the INMAD component of the DOA pathway remains intact in Dfm1's absence. In this way, a *dfm1Δ* null could prove useful in separating the two channels of DOA degradation. For instance, Sbh2 is found in the ER and INM and is degraded by the DOA pathway (Habeck, et al., 2015; Smoyer et al., 2016). A *dfm1Δ* null background could be used to discern whether this substrate is degraded in the ER or INM. The ability to detect compartment-specific degradation could, in turn, allow for the discovery of compartment specific determinants of degradation.

While these studies evinced a number of ways INMAD and ERAD are functionally distinct, it remains the case that these two pathways are interconnected and mutually supportive. We demonstrated that Sec61-2-GFP imposes a lethal proteotoxicity when the HRD and ASI pathways are disrupted in tandem. Notably, this indicates a very specific role for shared maintenance of membrane protein proteostasis, whereas the *asi1Δhrd1Δire1Δ* synthetic lethality (Foresti et al., 2014; Khmelinskii, Blaszczak et al., 2014) demonstrates a more general proteostatic network shared between the ER and INM. As importantly, this cell-death phenotype has great potential for screening. A whole-genome array could be used to cross a *hrd1Δ* null strain bearing *pGal1::sec61-2* to the deletion collection, with components of INMAD phenocopying a cross to the *asi1Δ* and *asi3Δ* nulls. Along with putative retrotranslocon, such a screen could unveil novel components of the INMAD-mitigated stress pathways.

Finally, we demonstrated that prolonged Sec61-2 toxicity elicits a novel suppression pathway involving the duplication of chromosomes V and XIV. This is distinct from suppression of *dfm1Δ*, which requires the duplication of chromosome XV. Moreover, suppression of Sec61-2

toxicity did not result in renewed degradation of the substrate, whereas dfm1 suppression fully restores retrotranslocation and degradation of all ERAD-M substrates.

Taken together, these results imply the existence of distinct INM machinery that mediates retrotranslocation and mitigates proteotoxicity. One final, intriguing possibility is that ERAD and INMAD retrotranslocons play both of these roles, not only removing substrates from membranes but also detoxifying them upon biding. Indeed, Dfm1 is responsible for the retrotranslocation of all known integral ER membrane substrates, and in the absence of Dfm1, those substrates induce considerable proteotoxic stress (Neal et al., 2020; Neal et al., 2018). Perhaps the Asi1-Asi3 confirmation of the ASI complex has similar properties. As mentioned above, *ASI3* is duplicated as part of chromosome XIV in our suppressees, without restoration of degradation. Perhaps upon duplication, overexpressed Asi3 gains the ability to adequately detoxify Sec61-2-GFP, even in the absence of Asi1 and functional INMAD. If Asi1 and Asi3 do form a retrotranslocon, it will be of great interest to investigate how the complex effects retrotranslocation and to elucidate why some transmembrane substrates require recognition by Asi2 while others are completely Asi2 independent.

Materials and Methods

Yeast and Bacteria Growth Media

Unless otherwise stated, yeast strains were grown in either minimal medium (Difco yeast nitrogen base with necessary amino acids and nucleic acids) with 2% glucose or rich medium (YPD) and were grown at 30° C with aeration. For expression of constructs under the control of the galactose-inducible promoter in liquid culture, yeast cells were first grown for at least 24 hours in minimal medium with 2% raffinose and 0.1% dextrose before being diluted into medium with 2% raffinose and no dextrose and grown into log phase. Cells were then induced for two hours by the addition of galactose at a final concentration of 0.2%.

All *Escherichia coli* DH5α were grown in LB plus ampicillin at 37°.

Plasmids and Strains

All plasmids used in these studies are listed in Table S1. Plasmids were constructed using standard molecular-biological techniques, as previously described (Sato et al., 2009). Primer information can be provided upon request. All plasmids made for this study were sequenced verified (Eton Biosciences). The YCp *URA3 HRD1* plasmid was a gift from Ernst Jarosch (MDC Berlin, Berlin, Germany).

All strains used in these studies are listed in Table S2. Strains are derived from either S288C (RHY2863) or BY4741. Yeast were transformed with plasmids or PCR products using the standard LiOAc method (Ito et al., 1983). Null strains were either obtained from the yeast deletion collection (Winzeler, Shoemaker, Astromoff, Liang, et al., 1999) or generated using a PCR-mediated knockout strategy. Briefly, yeast were transformed with an amplicon comprised of a selectable marker (NatMX, KanMX, or HphMX) flanked by 50bp directly upstream and downstream of the gene to be deleted. Transformants were recovered on YPD plates, then replica plated to selection plates containing CloNat/nourseothricin, G418, or hygromycin. All deletions were confirmed using diagnostic PCR.

Flow Cytometry

A BD Accuri C6 flow cytometer (BD Biosciences) was used to measure GFP fluorescence as previously described (Garza et al., 2009b). All readings comprise 10,000 cells, and statistics were acquired from BD Accuri software.

Whole Cell Lysates and Western Blotting

Three OD eq cells were harvested by centrifugation at 14,000 x g for 5 min. Pellets were resuspended in 100 µL SUME (SDS, Urea, MOPS, ETDA) buffer (1% SDS, 8 M urea, 10 mM MOPS, 10 mM EDTA, pH 6.8) with protease inhibitors (PIs) (1 mM phenylmethylsulfonyl fluoride, 260 mM 4-(2-aminoethyl) benzenesulfonyl fluoride hydrochloride, 100 mM leupeptin hemisulfate, 76 mM pepstatin A, 5 mM 6-aminocaproic acid, 5 mM benzamidine, and 142 mM TPCK), and 0.5 mm glass beads were added to the meniscus. Cells were lysed three times for 1-min intervals on a multi-vortexer at room temperature with 1 min on ice in between. After the addition of 100 µL 2x urea sample buffer (2x USB: 8 M urea, 4% SDS, 200 mM dithiothreitol, 125 mM Tris, pH 6.8), samples were heated at 95° C for 10 minutes and clarified by centrifugation at 14,000 x g for 5 min. Samples were resolved by SDS-PAGE, transferred to nitrocellulose in 12% methanol, and blotted with mouse monoclonal anti-GFP antibody (Living Colors), anti-HA antibody (Thermo Fisher Scientific) or anti-PGK1 antibody (Molecular Probes) (loading control) followed by goat anti-mouse HRP-conjugated secondary antibody (Jackson ImmunoResearch).

Cycloheximide Chase

Cycloheximide chases were performed as described elsewhere (Sato et al., 2009). Yeast strains were grown in minimal media to early log phase (OD_{600} < 0.3) prior to the addition of cycloheximide at a final concentration of 50 µg/mL. In MG132 experiments, MG132 was added to 25 µg/mL, or an equal volume of DMSO vehicle control was used. Samples were taken at the indicated time points and subjected to lysis, resolution by SDS-PAGE, and immunoblotting.

***In Vivo* Ubiquitination Assay**

Western blotting to detect in vivo ubiquitination was performed as described previously (Garza et al., 2009). Briefly, yeast strains were grown to log phase (OD600 of 0.2 to 0.3) and treated

with MG132 for 2 hours. 15 OD equivalents of cells were pelleted by centrifugation and resuspended in lysis buffer (0.24 M sorbitol, 1 mM EDTA, 20 mM KH2PO4, pH 7.5) with PIs, after which 0.5 mm glass beads were added to the meniscus. The cells were lysed by vortexing in 1-min cycles at 4o C, with 1 min on ice in between, for 6 to 8 cycles. Lysates were clarified by centrifugation at 2,500 x g for 5 min. The clarified lysates were moved to fresh tubes, and 600 µL immunoprecipitation buffer (IPB; 15mM Na2HPO4, 150mM NaCl, 2% Triton X-100, 0.1% SDS, 0.5% deoxycholate, 10mM EDTA, pH 7.5) and 15 µL of rabbit polyclonal anti-GFP antisera (C. Zucker, University of California San Diego) were added. Samples were incubated on ice for 5 min, clarified by centrifugation at 14,000 x g for 5 min, and moved to a fresh tube. Tubes were incubated at 4o C overnight with rocking followed by the addition of 100 µL of equilibrated Protein A-Sepharose in IPB (50% w/v). Samples were then incubated at 4o C for 2 hours with rocking. Beads were washed twice with IPB and then washed once with IP wash buffer (50 mM NaCl, 10 mM Tris, pH 7.5). Beads were aspirated to dryness, resuspended in 55 µL 2x USB, and incubated at xxo C for 10 minutes. Samples were resolved by SDS-PAGE on 8% gels, transferred to nitrocellulose, and immunoblotted with monoclonal anti-ubiquitin (Fred Hutchinson Cancer Research Institute) and anti-GFP (Living Colors) primary antibodies followed by goat anti-mouse (Jackson ImmunoResearch Laboratories) or goat anti-rabbit (Bio-Rad) HRP conjugated secondary antibody.

In Vivo Retrotranslocation Assay

In vivo retrotranslocation assay was adapted from Neal et al., 2018. Cells in log phase (OD_{600} 0.2-0.3) were treated with MG132 (benzyloxycarbonyl-Leu-Leu-aldehyde, Sigma) at a final concentration of 25 µg/mL (25 mg/mL stock dissolved in DMSO) for 2 hours at 30°C. Cells were resuspended in H_20, centrifuged and lysed with the addition of 0.5 mm glass beads and 400 µL of XL buffer (1.2 M sorbitol, 5 mM EDTA, 0.1 M KH_2PO_4, final pH 7.5) with PIs, followed by vortexing in 1 minute intervals for 6-8 min at 4°C. Lysates were combined and clarified by

centrifugation at 2,500 g for 5 min. Clarified lysate was ultracentrifuged at 100,000 g for 15 min to separate pellet (P100) and supernatant fraction (S100). P100 pellet was resuspended in 200 µL SUME (1% SDS, 8 M Urea, 10 mM MOPS, pH 6.8, 10 mM EDTA) with PIs and 5 mM N-ethyl maleimide (NEM, Sigma) followed by addition of 600 µL immunoprecipitation buffer (IPB) with PIs and NEM. S100 supernatant was added directly to IPB with PIs and NEM. 15 µL of rabbit polyclonal anti-GFP antisera (C. Zuker, University of California, San Diego) was added to P100 and S100 fractions for immunoprecipitation (IP) of Sec61-2-GFP. Samples were incubated on ice for 5 minutes, clarified at 14,000 g for 5 min and removed to a new eppendorf tube and incubated overnight at 4ºC. 100 µL of equilibrated Protein A-Sepharose in IPB (50% w/v) (Amersham Biosciences) was added and incubated for 2 h at 4ºC. Proteins A beads were washed twice with IPB and washed once more with IP wash buffer (50 mM NaCl, 10 mM Tris), aspirated to dryness, resuspended in 2x Urea sample buffer (8 M urea, 4% SDS, 1mM DTT, 125 mM Tris, pH 6.8), and incubated at 55ºC for 10 min. IPs were resolved by 8% SDS-PAGE, transferred to nitrocellulose, and immunoblotted with monoclonal anti-ubiquitin (Fred Hutchinson Cancer Center, Seattle) and anti-GFP (Clontech, Mountain View, CA). Goat anti-mouse (Jackson ImmunoResearch, West Grove, PA) and goat anti-rabbit (Bio-Rad) conjugated with horseradish peroxidase (HRP) recognized the primary antibodies. Western Lightning® Plus (Perkin Elmer, Watham, MA) chemiluminescence reagents were used for immunodetection.

Proteolytic Removal of Ubiquitin from Retrotranslocated Sec61-2-GFP

Ubiquitin removal was accomplished with the broadly active Usp2 ubiquitin protease as previously described Neal et al., 2018, except that human recombinant Usp2Core (LifeSensors Inc., Malvern, PA) was used, and leupeptin and NEM were excluded from all buffers. Briefly, 100 µL of S100 supernatant containing in vivo retrotranslocated Sec61-2-GFP was incubated with 20 µL of Usp2Core (5 µg) for 1 hr at 37ºC. The reaction was quenched with 200 µl of SUME (1% SDS, 8 M

Urea, 10 mM MOPS, pH 6.8, 10 mM EDTA) *with PIs and retrotranslocated Sec61-2-GFP was immunoprecipitated as described above. 20 μL of IP was used for detection of Sec61-2-GFP with α-GFP.*

Spot-Dilution Growth Assay

Growth assays were carried out as described previously (Neal et al., 2020). Briefly, cells were grown into log phase (OD_{600} 0.2-0.3) in medium with 2% dextrose. Cells were then diluted to 0.015 OD/mL and subjected to 5-fold serial dilutions in a 96-well plate. An 8 x 12 pinning tool was then used to spot dilutions onto SC -Ura plates with either 2% dextrose or 2% galactose. Plates were incubated at 30° C and imaged at day four and day seven.

5-FOA Counterselection and Suppressee Generation

Strains to be counterselected were initially maintained on selective plates lacking uracil. Strains were then patched to YPD to allow loss of *URA3* plasmids, and cells from these patches were subsequently streaked either onto plates lacking uracil or plates with 5-FOA.

Outgrowth time for suppressees was variable. 5-FOA plates were incubated at 30° C for up to seven days, and plates were examined daily for bright colonies using a GFP-visualizing platform (Cronin, S. R., and Hampton, R. Y., 1999). Such colonies were picked and re-streaked to 5-FOA plates to verify viability before use.

Yeast Genome Sequencing and Analysis

Sequencing and analysis were performed as described elsewhere (Neal et al., 2018). Briefly, genomic DNA was collected using the MasterPure Yeast DNA purification kit (Epicenter). Genomic DNA was then tagmented using Nextera DNA Sample Preparation Kit (Illumina) with Tn5 (Tagment DNA Enzyme 1). Samples were purified using ChIP DNA Clean and Concentrate kit (Zymo

Research) and barcoded using PCR. Libraries were size-selected by gel isolation and sequenced SE75 on a NextSeq 2500 (Illumina). 3’ end adaptor sequences were trimmed and reads were aligned with bowtie 2 (version 2.3; default parameters) (Langmead and Salzberg, 2012) to the S. cerevisiae genome (sacCer3). HOMER (Heinz et al., 2010) was used to tile the genome and to generate normalized read densities using the annotatePeaks.pl command.

ACKNOWLEDGEMENTS

Chapter III, in full, has been submitted for publication of the material as it may appear in Molecular Biology of the Cell, 2020, Matthew P. Flagg, Margaret A. Wangeline, Sarah R. Holland, Sascha H. Duttke, Christopher Benner, Sonya Neal, Randolph Y. Hampton, American Society for Cell Biology, 2020. The dissertation author was the primary investigator and first author of this paper, and permission from all other authors has been obtained.

The authors would also like to acknowledge all members of the Hampton lab past and present for their intellectual and technical support. Cycloheximide chases were perform by M.A.W and M.P.F. *In vivo* retrotanslocation and ubiquitin stripping assays were performed by S.E.N. Pinning assays were performed by S.R.H. and counterselection assays were performed by M.P.F. Sequencing was performed by S.H.D. and M.P.F. These studies were conceptualized by R.H.Y., S.E.N., and M.P.F. The manuscript was written by M.P.F. with contributions to the materials and methods from M.A.W. and S.E.N. The manuscript was then edited by M.P.F., R.H.Y., and S.E.N. These studies were supported by and NIH grants (K99 GM135515) to S.H.D. and (R01 GM134366) to C.B., NIH grant 1R35GM133565-01 and Burroughs Wellcome Fund 1013987 (to S.E.N.) and 5R37DK051996-18 (to R.Y.H.).

Figures

Figure 3.1: Sec61-2-GFP is quality-control substrate of Hrd1 and Asi1.

(A) Depiction of the contiguous ER and inner-nuclear membrane (INM). A subset of ER proteins can diffuse through nucleoporins into the INM. Both the 26S proteosome and Cdc48 can access the nucleoplasm through nucleoporins, and cell physiology thus supports ERAD retrotranslocation into the cytoplasm and INMAD retrotranslocation into the nucleoplasm.

(B) Sec61-GFP is stable, whereas sec61-2 GFP is a degraded. Isogenic strains expressing Sec61-GFP or Sec61-2-GFP were grown into log phase and degradation of each protein was measured using cycloheximide chase (CHX). After adding CHX, cells were collected and lysed at the indicated times. Lysates were analyzed by SDS-PAGE and immunoblotting with α-GFP and α-Pgk1. Densitometry was performed using ImageJ, and α-GFP signal was normalized to α-Pgk1 signal. t=0 was taken as 100% and data plotted are mean ± SD from three experiments.

(C) Sec61-2-GFP is stabilized by the proteasome inhibitor MG132. A *pdr5*Δ strain expressing Sec61-2-GFP was grown into log phase then treated with either MG132 (25 µg/mL) or DMSO. Degradation was then measure by CHX. After adding CHX, cells were collected and lysed at the indicated times. Lysates were analyzed by SDS-PAGE and immunoblotting with α-GFP and α-Pgk1. Data plotted are mean ± SD from three experiments.

(D) Sec61-2-GFP degradation depends on both Hrd1 and Asi1. WT, *hrd1Δ*, *asi1Δ*, and *hrd1Δasi1Δ* strains expressing Sec61-2-GFP were subjected to CHX. After adding CHX, cells were collected and lysed at the indicated times. Lysates were analyzed by SDS-PAGE and immunoblotting with α-GFP and α-Pgk1. Data plotted are mean ± SD from three experiments.

(E) Sec61-2-GFP degradation requires the Cdc48 ATPase. WT, *hrd1Δasi1Δ*, and retrotranslocation deficient *cdc48-2* strains expressing Sec61-2-GFP were subjected to CHX. After adding CHX, cells were collected and lysed at the indicated times. Lysates were analyzed by SDS-PAGE and immunoblotting with α-GFP and α-Pgk1. Data plotted are mean ± SD from three experiments.

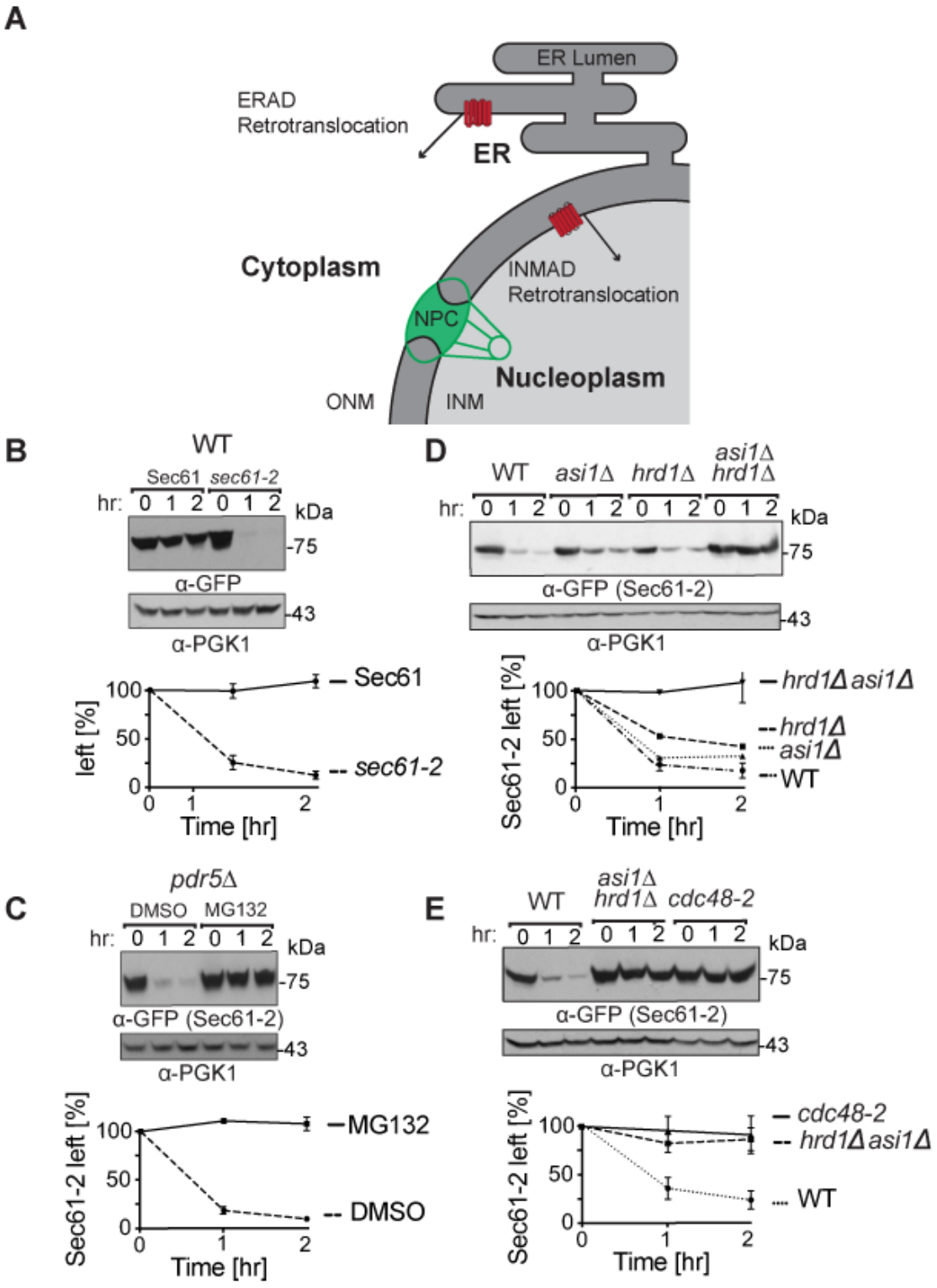
A
ER Lumen
ERAD
Retrotranslocation
ER
Cytoplasm
INMAD
Retrotranslocation
NPC
Nucleoplasm
ONM
INM
B
WT
Sec61 sec61-2
hr: 0 1 2 0 1 2
kDa
75
α-GFP
43
α-PGK1
Sec61
sec61-2
left [%]
Time [hr]
C
pdr5Δ
DMSO MG132
hr: 0 1 2 0 1 2
kDa
75
α-GFP (Sec61-2)
43
α-PGK1
MG132
DMSO
Sec61-2 left [%]
Time [hr]
D
WT asi1Δ hrd1Δ asi1Δ hrd1Δ
hr: 0 1 2 0 1 2 0 1 2 0 1 2
kDa
75
α-GFP (Sec61-2)
43
α-PGK1
hrd1Δ asi1Δ
hrd1Δ
asi1Δ
WT
Sec61-2 left [%]
Time [hr]
E
WT asi1Δ hrd1Δ cdc48-2
hr: 0 1 2 0 1 2 0 1 2
kDa
75
α-GFP (Sec61-2)
43
α-PGK1
cdc48-2
hrd1Δ asi1Δ
WT
Sec61-2 left [%]
Time [hr]

Figure 3.2: INMAD proceeds independently of Dfm1.

(A) Dfm1 acts downstream of Hrd1 and in parallel with the Asi-complex. WT, *dfm1Δ*, *hrd1Δdfm1Δ*, and *asi1Δdfm1Δ* strains expressing Sec61-2-GFP were subjected to CHX. After adding CHX, cells were collected and lysed at the indicated times. Lysates were analyzed by SDS-PAGE and immunoblotting with α-GFP and α-Pgk1. Data plotted are mean ± SD from three experiments.

(B) Sec61-2-GFP degradation is recapitulated by flow cytometry. WT, *dfm1Δ*, *hrd1Δdfm1Δ*, and *asi1Δdfm1Δ* strains expressing Sec61-2-GFP were subjected to CHX. After adding CHX, cells were assayed for fluorescence by flow cytometry, and at each timepoint, the mean fluorescence of 10,000 cells was measured. t=0 was taken as 100%, and data plotted are the mean ± SD from three experiments.

(C) Erg11-3HA degradation is Dfm1 independent. WT, *dfm1Δ*, and *asi1Δ* strains expressing Erg11-3HA were subjected to CHX. After adding CHX, cells were collected and lysed at the indicated times. Lysates were analyzed by SDS-PAGE and immunoblotting with α-HA and α-Pgk1. Data plotted are mean ± SD from three experiments.

(D) HA-Asi2 is stabilized in neither *dfm1Δ* nor *doa10Δ* strains. WT, *dfm1Δ*, and *doa10Δ* strains were subjected to CHX. After adding CHX, cells were collected and lysed at the indicated times. Lysates were analyzed by SDS-PAGE and immunoblotting with α-HA and α-Pgk1. Data plotted are mean ± SD from three experiments.

(E) HA-Asi2 degradation by Doa10 and the Asi-complex is Dfm1 independent. WT, *asi1Δ*, *asi1Δdfm1Δ*, and *asi1Δdoa10Δ* strains were subjected to CHX. After adding CHX, cells were collected and lysed at the indicated times. Lysates were analyzed by SDS-PAGE and immunoblotting with α-HA and α-Pgk1. Data plotted are mean ± SD from three experiments.

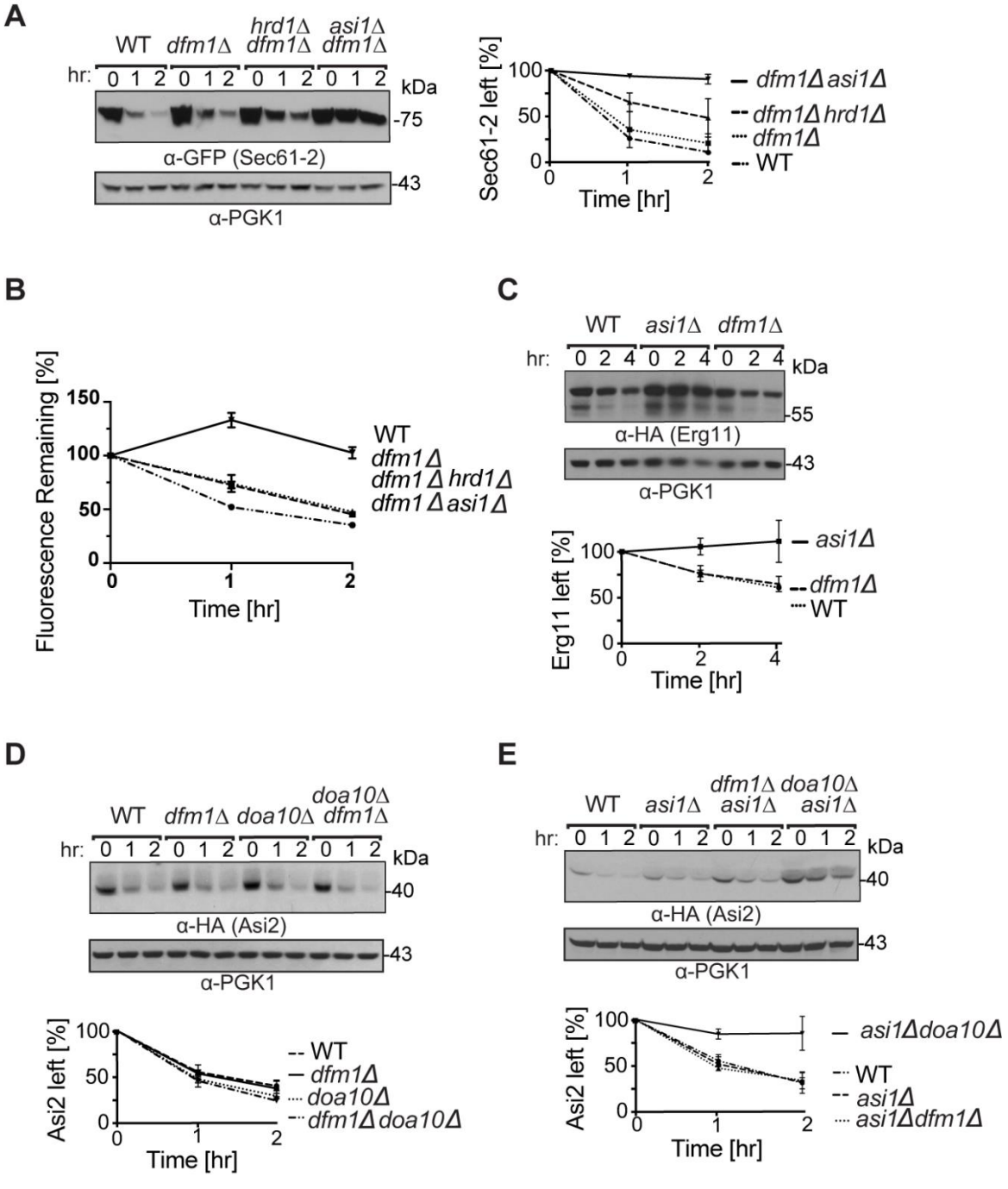
A
WT
dfm1Δ
hrd1Δ dfm1Δ
asi1Δ dfm1Δ
hr: 0 1 2 0 1 2 0 1 2 0 1 2
kDa
-75
α-GFP (Sec61-2)
-43
α-PGK1
Sec61-2 left [%]
100
50
0
0 1 2
Time [hr]
dfm1Δ asi1Δ
dfm1Δ hrd1Δ
dfm1Δ
WT
B
Fluorescence Remaining [%]
150
100
50
0
0 1 2
Time [hr]
WT
dfm1Δ
dfm1Δ hrd1Δ
dfm1Δ asi1Δ
C
WT
asi1Δ
dfm1Δ
hr: 0 2 4 0 2 4 0 2 4
kDa
55
α-HA (Erg11)
43
α-PGK1
Erg11 left [%]
100
50
0
0 2 4
Time [hr]
asi1Δ
dfm1Δ
WT
D
WT
dfm1Δ
doa10Δ
doa10Δ dfm1Δ
hr: 0 1 2 0 1 2 0 1 2 0 1 2
kDa
40
α-HA (Asi2)
43
α-PGK1
Asi2 left [%]
100
50
0
0 1 2
Time [hr]
WT
dfm1Δ
doa10Δ
dfm1Δ doa10Δ
E
WT
asi1Δ
dfm1Δ doa10Δ
asi1Δ asi1Δ
hr: 0 1 2 0 1 2 0 1 2 0 1 2
kDa
40
α-HA (Asi2)
43
α-PGK1
Asi2 left [%]
100
50
0
0 1 2
Time [hr]
asi1Δdoa10Δ
WT
asi1Δ
asi1Δdfm1Δ

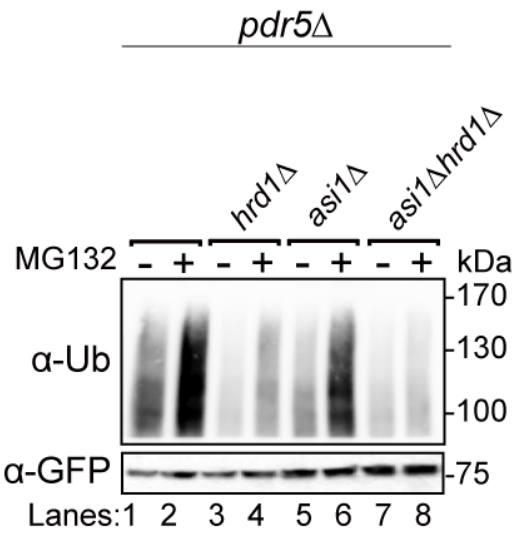

Figure 3.3: Both Asi1 and Hrd1 ubiquitinate Sec61-2-GFP *in vivo*.

Indicated strains expressing Sec61-2-GFP were grown into log phase and treated with MG132 or a vehicle control (DMSO). Cells were lysed, and microsomes were collected and immunoprecipitated with α-GFP. Samples were then subjected to SDS-PAGE and immunoblot by α-Ubiquitin and α-GFP. One of three biological replicates is shown.

Figure 3.4: Retrotranslocation of full-length Sec61-2-GFP.

(A) *In vivo* retrotranslocation of Sec61-2-GFP through both Hrd1 and Asi channels. WT, *hrd1Δ*, *asi1Δ*, and *cdc48-2* strains expressing Sec61-2-GFP were grown into log phase and treated with MG132 (25 µg/mL). Crude lysates were ultracentrifuged to separate Sec61-2-GFP that has been retrotranslocated into the soluble fraction (S) and Sec61-2-GFP that has not been retrotranslocated from membrane (P). Sec61-2-GFP was immunoprecipitated from both fractions, then analyzed by SDS-PAGE and immunoblotting with α-GFP and α-ubiquitin. One representative of three biological replicates is shown.

(B) *In vivo* retrotranslocated Sec61-2-GFP is full length. WT, *hrd1Δ*, *asi1Δ*, and *cdc48-2* strains expressing Sec61-2-GFP were grown into log phase and treated with MG132 (25 µg/mL). Crude lysates were ultracentrifuged to separate Sec61-2-GFP to collect retrotranslocated Sec61-2-GFP from soluble fractions. Solubilized Sec61-2-GFP was then immunoprecipitated and then either treated with either buffer (–) or the catalytic core of the deubiquitinase Usp2 (+). Samples were analyzed by SDS-PAGE and immunoblotted with α-GFP and α-ubiquitin. One representative of three biological replicates is shown.

(C) *In vivo* retrotranslocation of Sec61-2-GFP through Asi1 is Dfm1 independent. WT, *dfm1Δ*, *dfm1Δhrd1Δ*, *dfm1Δasi1Δ*, and *cdc48-2* strains expressing Sec61-2-GFP were grown into log phase and treated with MG132 (25 µg/mL). Crude lysates were ultracentrifuged to separate Sec61-2-GFP that has been retrotranslocated into the soluble fraction (S) and Sec61-2-GFP that has not been retrotranslocated from membrane (P). Sec61-2-GFP was immunoprecipitated from both fractions, then analyzed by SDS-PAGE and immunoblotting with α-GFP and α-ubiquitin. One representative of three biological replicates is shown.

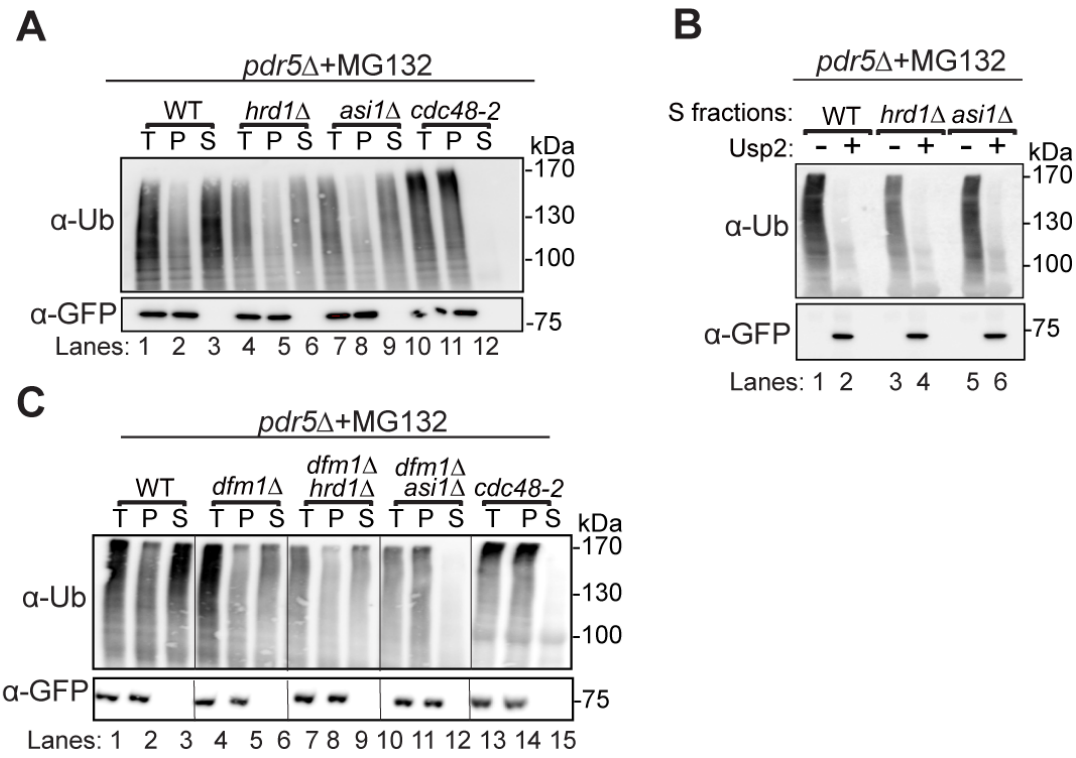
A
pdr5Δ+MG132
WT
hrd1Δ
asi1Δ
cdc48-2
T P S T P S T P S T P S
kDa
170
130
100
α-Ub
α-GFP
75
Lanes: 1 2 3 4 5 6 7 8 9 10 11 12
B
pdr5Δ+MG132
S fractions:
WT
hrd1Δ
asi1Δ
Usp2: - + - + - +
kDa
170
130
100
α-Ub
α-GFP
75
Lanes: 1 2 3 4 5 6
C
pdr5Δ+MG132
WT
dfm1Δ
dfm1Δ hrd1Δ
dfm1Δ asi1Δ
cdc48-2
T P S T P S T P S T P S T P S
kDa
170
130
100
α-Ub
α-GFP
75
Lanes: 1 2 3 4 5 6 7 8 9 10 11 12 13 14 15

Figure 3.5: Sec61-2-GFP is lethal to cells lacking INMAD and ERAD.

(A-B) Galactose-induced Sec61-2-GFP expression is lethal to *asi1Δhrd1Δ* cells. WT, *asi1Δ*, *hrd1Δ*, and *asi1Δhrd1Δ* cells bearing empty vector (–), GAL-driven Sec61-GFP, or GAL-driven Sec61-2-GFP were monitored for growth by dilution assay. 5-fold dilutions of each strain were spotted onto glucose- or galactose-containing plates to induce Sec61-GFP and Sec61-2-GFP overexpression. Plates were incubated at 30° C and imaged at the indicated times.

(C) Galactose-induced Sec61-2-GFP expression is also lethal to *asi3Δhrd1Δ* cells. WT, *asi3Δ*, *hrd1Δ*, and *asi1Δhrd1Δ* cells bearing GAL-driven Sec61-GFP or GAL-driven Sec61-2-GFP were monitored for growth by dilution assay. 5-fold dilutions of each strain were spotted onto glucose- or galactose-containing plates to induce Sec61-GFP and Sec61-2-GFP overexpression. Plates were incubated at 30° C and imaged at the indicated times.

(D) Galactose-induced Sec61-2-GFP expression is not lethal to *asi2Δhrd1Δ* cells. WT, *asi3Δ*, *hrd1Δ*, and *asi2Δhrd1Δ* cells bearing GAL-driven Sec61-GFP or GAL-driven Sec61-2-GFP were monitored for growth by dilution assay. 5-fold dilutions of each strain were spotted onto glucose- or galactose-containing plates to induce Sec61-GFP and Sec61-2-GFP overexpression. Plates were incubated at 30° C and imaged at the indicated times.

(E-F) Asi1 catalytic activity is required to prevent Sec61-2-GFP lethality. WT, *asi1Δ*, *hrd1Δ*, and *asi1Δhrd1Δ* cells bearing GAL-driven Sec61-2-GFP were co-transformed with empty vector (–), wild-type *ASI1*, or RING-dead ASI1 (RD-Asi1). These strains were then monitored for growth by dilution assay. 5-fold dilutions of each strain were spotted onto glucose- or galactose-containing plates to induce Sec61-GFP and Sec61-2-GFP overexpression. Plates were incubated at 30° C and imaged at the indicated times.

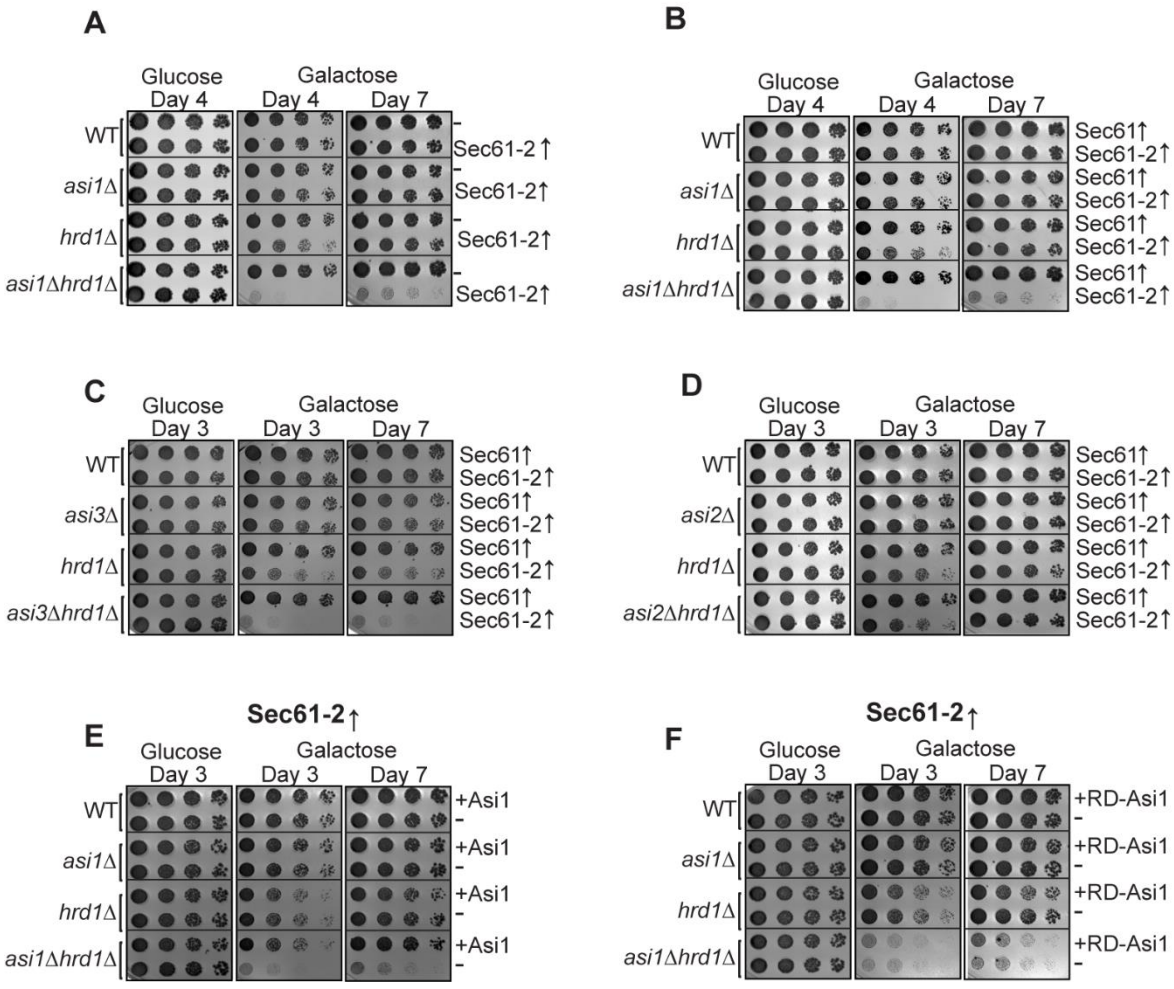
A
Glucose
Day 4
Galactose
Day 4
Day 7
WT
asi1Δ
hrd1Δ
asi1Δhrd1Δ
Sec61-2↑
B
Glucose
Day 4
Galactose
Day 4
Day 7
WT
asi1Δ
hrd1Δ
asi1Δhrd1Δ
Sec61↑
Sec61-2↑
C
Glucose
Day 3
Galactose
Day 3
Day 7
WT
asi3Δ
hrd1Δ
asi3Δhrd1Δ
Sec61↑
Sec61-2↑
D
Glucose
Day 3
Galactose
Day 3
Day 7
WT
asi2Δ
hrd1Δ
asi2Δhrd1Δ
Sec61↑
Sec61-2↑
E
Sec61-2↑
Glucose
Day 3
Galactose
Day 3
Day 7
WT
asi1Δ
hrd1Δ
asi1Δhrd1Δ
+Asi1
-
F
Sec61-2↑
Glucose
Day 3
Galactose
Day 3
Day 7
WT
asi1Δ
hrd1Δ
asi1Δhrd1Δ
+RD-Asi1
-

Figure 3.6: Suppressees of Sec61-2-GFP lethality are ChrV and XIV aneuploids.

(A) Constitutive over-expression of Sec61-2-GFP is lethal to *asi1Δhrd1Δ* cells. Left, schematic denoting the genotypes of each strain tested before exposure to 5-FOA. Center and right, the indicated strains were streaked onto plates that either selected (-Trp -Ura) or counterselected the *URA3* plasmids. Plates were incubated at 30° C for two days prior to imaging.

(B) Lethality suppressees cannot degrade the Sec61-2-GFP. Four suppressees and a WT strain expressing Sec61-2-GFP were subjected to CHX chase. After adding CHX, cells were assayed for fluorescence by flow cytometry, and at each timepoint, the mean fluorescence of 10,000 cells was measured. t=0 was taken as 100%, and data plotted are the mean ± SD from three experiments.

(C) Genome profiling reveals duplications of ChrV and XIV in suppressees. Chromosome profiles of whole-genome sequencing are mapped across the yeast genome. Copy number is indicated on the y-axis and chromosome number is indicated on the x-axis. Reads from each of four suppressees are shown.

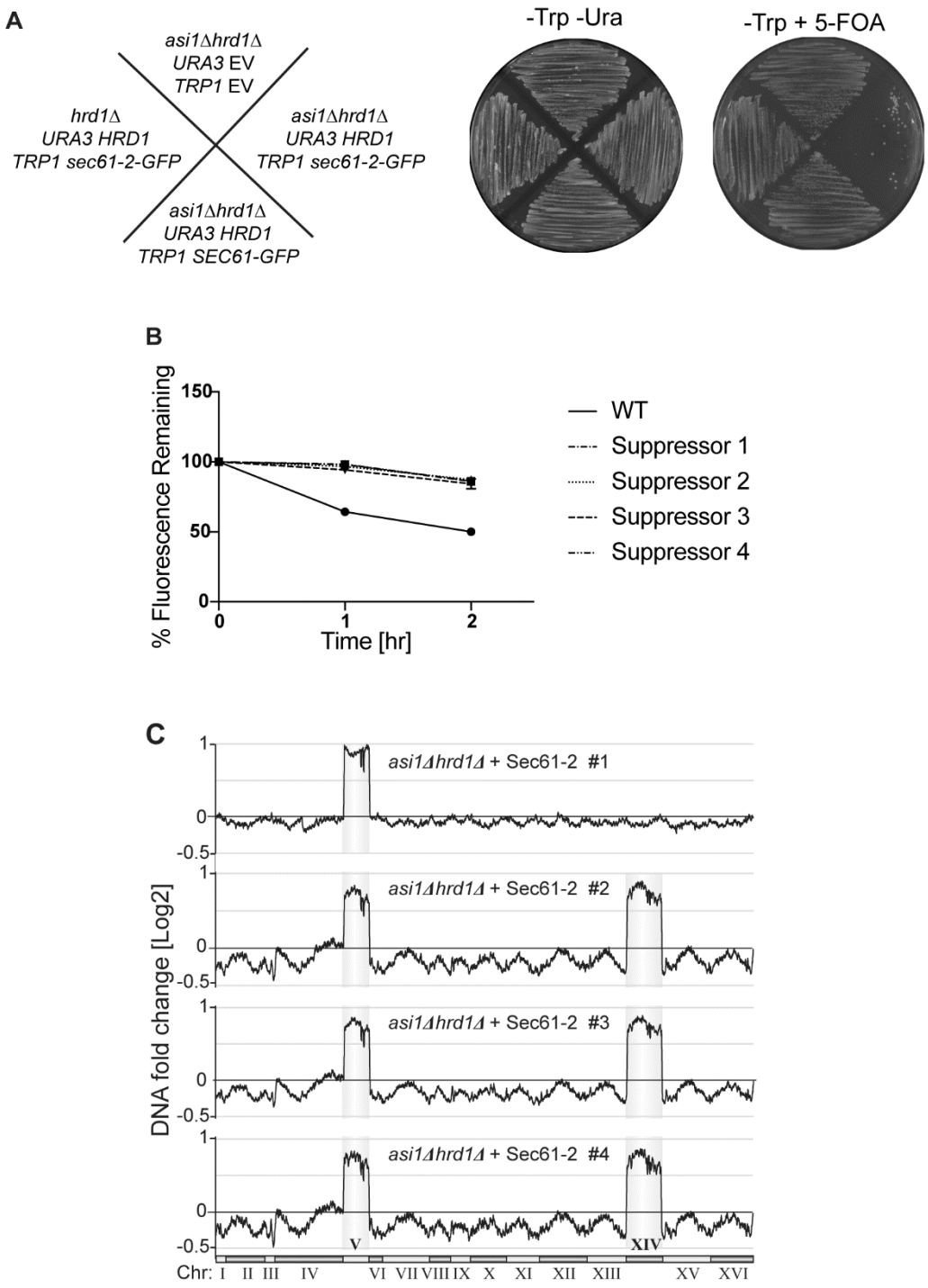
A
asi1Δhrd1Δ
URA3 EV
TRP1 EV
hrd1Δ
URA3 HRD1
TRP1 sec61-2-GFP
asi1Δhrd1Δ
URA3 HRD1
TRP1 sec61-2-GFP
asi1Δhrd1Δ
URA3 HRD1
TRP1 SEC61-GFP
-Trp -Ura
-Trp + 5-FOA
B
% Fluorescence Remaining
150
100
50
0
0
1
2
Time [hr]
WT
Suppressor 1
Suppressor 2
Suppressor 3
Suppressor 4
C
DNA fold change [Log2]
asi1Δhrd1Δ + Sec61-2 #1
asi1Δhrd1Δ + Sec61-2 #2
asi1Δhrd1Δ + Sec61-2 #3
asi1Δhrd1Δ + Sec61-2 #4
1
0
-0.5
V
XIV
Chr: I II III IV VI VII VIII IX X XI XII XIII XV XVI

Supplemental Figures

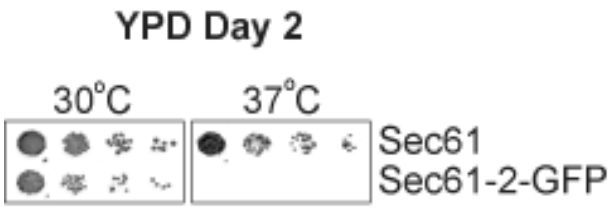

Figure 3.S1: *sec61-2-GFP* causes temperature sensitivity.

WT cells and cells with *sec61-2-GFP* integrated at the endogenous SEC61 locus were monitored for growth by dilution assay. 5-fold dilutions of each strain were spotted onto YPD, the cells were grown at the indicated temperatures and imaged at the indicated time.

Supplemental Tables

Table 3.S1: Plasmids used in this study

Plasmid	**Gene**	**Reference**
pRH311	YIp *TRP1*	Sikorski et. al., 1989
pRH316	Ycp *LEU2*	Sikorski et. al., 1989
pRH317	YCp *URA3*	Sikorski et. al., 1989
pRH2431	pFA6a-3HA-His3MX6	Longtine et al., 1998
pRH2497	YCp *URA3 HIS3 pHRD1::HRD1-13xMyc::tHRD1*	Gift from the Ernst Jarosch lab
pRH2846	YIp *TRP1 pTDH3::sec61-2-GFP::tADH1*	This study
pRH2879	YCp *URA3 pGAL1::sec61-2-GFP::tADH1*	This study
pRH2880	YIp *TRP1 pTDH3::SEC61-GFP::tADH1*	This study
pRH2881	YCp *URA3 pGAL1::SEC61-GFP::tADH1*	This study
pRH2977	YIp *URA3 TRP1 pGAL1::sec61-2-GFP::tADH1*	This study
pRH2978	YIp *URA3 TRP1 pGAL1::sec61-2-GFP::tADH1*	This study
pRH3131	YIp *TRP1 pASI2::3xHA-ASI2::tASI2*	This study
pRH3160	YCp *LEU2 pASI1::asi1-C583S-C585S::tADH1*	This study
pRH3146	YCp *LEU2 pASI1::ASI1-3xHA::tASI1*	This study

Table 3.S2: Yeast strains used in this study

Strain	Genotype	Reference
RHY2863	MATa *ade2-101 met2 lys2-801 his3Δ200 ura3-52 trp1Δ::hisG leu2Δ*	
RHY7447	BY4741	
RHY10825	RHY2863 *asi1Δ::HphMX hrd1Δ::KanMX* pRH311 (YIp *TRP1)* pRH317 (YCp *URA3)*	This study
RHY10828	RHY2863 *hrd1Δ::KanMX* pRH2846 (YIp *TRP1 pTDH3::sec61-2-GFP::tADH1*) pRH2497 (YCp *URA3 HIS3 pHRD1::HRD1-13xMyc::tHRD1*)	This study
RHY10829	RHY2863 *asi1Δ::HphMX hrd1Δ::KanMX* pRH2497 pRH2846	This study
RHY10830	RHY2863 *asi1Δ::HphMX hrd1Δ::KanMX* pRH2497 pRH2880 (YIp *TRP1 pTDH3::SEC61-GFP::tADH1*)	This study
RHY11597	RHY2863 pRH2977 (YIp *URA3 TRP1 pGAL1::sec61-2-GFP::tADH1)*	This study
RHY11598	RHY2863 *asi1Δ::HphMX* pRH2977	This study
RHY11599	RHY2863 *hrd1Δ::KanMX* pRH2977	This study
RHY11600	RHY2863 *asi1Δ::HphMX hrd1Δ::KanMX* pRH2977	This study
RHY11603	RHY2863 *hrd1Δ::KanMX dfm1::NatMX* pRH2977	This study
RHY11604	RHY2863 *cdc48-2* pRH2977	This study
RHY11609	RHY2863 *pdr5*Δ::HIS3 pRH2977	This study
RHY11645	RHY2863 *asi1Δ::HphMX pdr5Δ::HIS3* pRH2977	This study
RHY11646	RHY2863 *dfm1::NatMX pdr5Δ::HIS3* pRH2977	This study
RHY11647	RHY2863 *hrd1Δ::KanMX pdr5Δ::HIS3* pRH2977	This study
RHY11648	RHY2863 *asi1Δ::HphMX hrd1Δ::KanMX pdr5Δ::HIS3* pRH2977	This study
RHY11650	RHY2863 *hrd1Δ::KanMX dfm1::NatMX pdr5Δ::HIS3* pRH2977	This study
RHY11664	RHY2863 *dfm1::NatMX* pRH2977	This study
RHY11665	RHY2863 *ERG11-3HA*	This study
RHY11666	RHY2863 *asi1Δ::HphMX ERG11-3HA*	This study
RHY11667	RHY2863 dfm1::NatMX *ERG11-3HA*	This study
RHY11679	RHY2863 *cdc48-2 pdr5Δ::HIS3* pRH2977	This study
RHY11681	RHY2863 pRH3131 (YIp *TRP1 pASI2::3xHA-ASI2::tASI2*)	This study
RHY11687	RHY7447 pRH2879 (YCp *URA3 pGAL1::sec61-2-GFP::tADH1*)	This study
RHY11688	BY4741 *asi1Δ::KanMX* pRH2879	This study
RHY11689	BY4741 *asi2Δ::KanMX* pRH2879	This study
RHY11690	BY4741 *asi3Δ::KanMX* pRH2879	This study
RHY11691	BY4741 *hrd1Δ::KanMX* pRH2879	This study

Strain	Genotype	Reference
RHY11693	RHY7447 pRH2881 (YCp *URA3 pGAL1::SEC61-GFP::tADH1*)	This study
RHY11694	BY4741 *asi1Δ::KanMX* pRH2881	This study
RHY11695	BY4741 *asi2Δ::KanMX* pRH2881	This study
RHY11696	BY4741 *asi3Δ::KanMX* pRH2881	This study
RHY11697	BY4741 *hrd1Δ::KanMX* pRH2881	This study
RHY11703	RHY2863 *doa10Δ::HphMx* pRH3131	This study
RHY11704	RHY2863 *dfm1::NatMX* pRH3131	This study
RHY11705	RHY2863 *dfm1::NatMX doa10Δ::HphMx*	This study
RHY11716	RHY2863 *asi1Δ::HphMX dfm1::NatMX* p pRH2977	This study
RHY11718	RHY2863 *asi1Δ::HphMX dfm1::NatMX pdr5Δ::HIS3* pRH2977	This study
RHY11719	BY4741 *asi1Δ::KanMX hrd1Δ::NatMX* pRH2879	This study
RHY11720	BY4741 *asi2Δ::KanMX hrd1Δ::NatMX* pRH2879	This study
RHY11721	BY4741 *asi3Δ::KanMX hrd1Δ::NatMX* pRH2879	This study
RHY11723	BY4741 *asi1Δ::KanMX hrd1Δ::NatMX* pRH2881	This study
RHY11724	BY4741 *asi2Δ::KanMX hrd1Δ::NatMX* pRH2881	This study
RHY11725	BY4741 *asi3Δ::KanMX hrd1Δ::NatMX* pRH2881	This study
RHY11855	RHY2863 *asi1Δ::HphMX* pRH3131	This study
RHY11856	RHY2863 *asi1Δ::HphMX dfm1::NatMX* pRH3131	This study
RHY11857	RHY2863 asi1Δ::HphMX doa10Δ::NatMX	This study
RHY11862	RHY7447 pRH317	This study
RHY11863	BY4741 *asi1Δ::KanMX* pRH317	This study
RHY11865	BY4741 *hrd1Δ::KanMX* pRH317	This study
RHY11866	BY4741 *asi1Δ::KanMX hrd1Δ::NatMX* pRH317	This study
RHY11880	RHY7447 pRH2879 pRH3146 (YCp *LEU2 pASI1::ASI1-3xHA::tASI1*)	This study
RHY11881	RHY7447 pRH2879 pRH3146 (YCp *LEU2*)	This study
RHY11884	BY4741 *asi1Δ::KanMX* pRH2879 pRH3146	This study
RHY11885	BY4741 *asi1Δ::KanMX* pRH2879 pRH316	This study
RHY11892	BY4741 *hrd1Δ::KanMX* pRH2879 pRH3146	This study
RHY11893	BY4741 *hrd1Δ::KanMX* pRH2879 pRH316	This study
RHY11896	BY4741 *asi1Δ::KanMX hrd1Δ::NatMX* pRH2879 pRH3146	This study
RHY11897	BY4741 *asi1Δ::KanMX hrd1Δ::NatMX* pRH2879 pRH316	This study
RHY12000	RHY7447 pRH2879 pRH3160 (YCp *LEU2 pASI1::asi1-C583S-C585S::tADH1*)	This study
RHY12001	BY4741 *asi1Δ::KanMX* pRH2879 pRH3160	This study
RHY12002	BY4741 *hrd1Δ::KanMX* pRH2879 pRH3160	This study
RHY12003	BY4741 *asi1Δ::KanMX hrd1Δ::NatMX* pRH2879 pRH3160	This study

References

Baldridge, R. D., & Rapoport, T. A. (2016). Autoubiquitination of the Hrd1 Ligase Triggers Protein Retrotranslocation in ERAD. *Cell*, 166(2), 394–407.

Biederer, T., Volkwein, C., & Sommer, T. (1996). Degradation of subunits of the Sec61p complex, an integral component of the ER membrane, by the ubiquitin-proteasome pathway. *EMBO J*, 15(9), 2069–2076.

Boban, M., Pantazopoulou, M., Schick, A., Ljungdahl, P. O., & Foisner, R. (2014). A nuclear ubiquitin-proteasome pathway targets the inner nuclear membrane protein Asi2 for degradation. *J Cell Sci*, *127*(16), 3603–3613.

Boban, M., Pantazopoulou, M., Schick, A., Ljungdahl, P. O., & Foisner, R. (2014). A nuclear ubiquitin-proteasome pathway targets the inner nuclear membrane protein Asi2 for degradation. *J Cell Sci*, 127(16), 3603–3613.

Boban, M., Zargari, A., Andréasson, C., Heessen, S., Thyberg, J., & Ljungdahl, P. O. (2006). Asi1 is an inner nuclear membrane protein that restricts promoter access of two latent transcription factors. *J Cell Biol*, 173(5), 695–707.

Braun, S., & Matuschewski, K. (2002). Role of the ubiquitin-selective CDC48UFD1/NPL4 chaperone (segregase) in ERAD of OLE1 and other substrates. *EMBO J*. 21(4), 615-621.

Carvalho, P., Goder, V., & Rapoport, T. A. (2006). Distinct Ubiquitin-Ligase Complexes Define Convergent Pathways for the Degradation of ER Proteins. *Cell*, 126(2), 361–373.

Chen, L., Romero, L., Chuang, S. M., Tournier, V., Joshi, K. K., Lee, J. A., Kovvali, G., Madura, K. (2011). Sts1 plays a key role in targeting proteasomes to the nucleus. *J Biol Chem*, 286(4), 3104–3118.

Cronin, S. R., & Hampton, R. Y. (1999). Measuring protein degradation with green fluorescent protein. *Methods Enzymol*, 302(1993), 58–73

Deng, M., & Hochstrasser, M. (2006). Spatially regulated ubiquitin ligation by an ER/nuclear membrane ligase. *Nature*, 443(7113), 827–831.

Foresti, O., Rodriguez-Vaello, V., Funaya, C., & Carvalho, P. (2014). Quality control of inner nuclear membrane proteins by the Asi complex. *Science*, 346(6210), 751–755.

Gallagher, P. S., Clowes Candadai, S. V., & Gardner, R. G. (2014). The requirement for Cdc48/p97 in nuclear protein quality control degradation depends on the substrate and correlates with substrate insolubility. *J Cell Sci*, 127(9), 1980–1991.

Garza, R. M., Sato, B. K., & Hampton, R. Y. (2009a). In vitro analysis of Hrd1p-mediated retrotranslocation of its multispanning membrane substrate 3-hydroxy-3-methylglutaryl (HMG)-CoA reductase. *J Biol Chem*, 284(22), 14710–14722.

Garza, R. M., Tran, P. N., & Hampton, R. Y. (2009b). Geranylgeranyl pyrophosphate is a potent regulator of HRD-dependent 3-hydroxy-3-methylglutaryl-CoA reductase degradation in yeast. *J Biol Chem*, 284(51), 35368–35380.

Greenblatt, E. J., Olzmann, J. A., & Kopito, R. R. (2010). Derlin-1 is a rhomboid pseudoprotease required for the dislocation of mutant α-1 antitrypsin from the endoplasmic reticulum. *Nat Struct and Mol Biol*. 18, 1147–1152 (2011)

Habeck, G., Ebner, F. A., Shimada-Kreft, H., & Kreft, S. G. (2015). The yeast ERAD-C ubiquitin ligase Doa10 recognizes an intramembrane degron. *J Cell Biol*, 209(2), 261–273.

Hampton, R. Y., & Garza, R. M. (2009). Protein quality control as a strategy for cellular regulation: lessons from ubiquitin-mediated regulation of the sterol pathway. *Chem Rev*, 109(4), 1561–1574.

Heinz S., Benner C., Spann N., Bertolino E., Lin Y.C., Laslo P., Cheng J.X., Murre C., Singh H., Glass C.K. (2010). Simple Combinations of Lineage-Determining Transcription Factors Prime cis-Regulatory Elements Required for Macrophage and B Cell Identities. *Mol Cell*, 38(4), 576–589.

Huh, W. K., Falvo, J. V., Gerke, L. C., Carroll, A. S., Howson, R. W., Weissman, J. S., & O'Shea, E. K. (2003). Global analysis of protein localization in budding yeast. *Nature*, 425(6959), 686–691.

Ito, H., Fukuda, Y., Murata, K., & Kimura, A. (1983). Transformation of intact yeast cells treated with alkali cations. *Journal Bacteriol*, 153(1), 163–168.

Kandel R.R., Neal S.E. The role of rhomboid superfamily members in protein homeostasis: Mechanistic insight and physiological implications. *Biochim Biophys Acta Mol Cell Res*. 2020 Oct;1867(10):118793.

Khmelinskii, A., Blaszczak, E., Pantazopoulou, M., Fischer, B., Omnus, D. J., Le Dez, G., Brossard, A., Gunnarsson, A., Barry, J.D., Meurer, M., et al. (2014). Protein quality control at the inner nuclear membrane. *Nature*, 516(7531), 410–413.

Langmead, B., & Salzberg, S. L. (2012). Fast gapped-read alignment with Bowtie 2. *Nat Methods*, 9(4), 357–359.

Longtine, M. S., McKenzie, A., Demarini, D. J., Shah, N. G., Wach, A., Brachat, A., Philippsen P., Pringle, J. R. (1998). Additional modules for versatile and economical PCR-based gene deletion and modification in Saccharomyces cerevisiae. *Yeast*, 14, 953–961

Natarajan, N., Foresti, O., Wendrich, K., Stein, A., & Carvalho, P. (2020). Quality Control of Protein Complex Assembly by a Transmembrane Recognition Factor. *Mol Cell*, 77(1), 108-119.e9.

Neal, S., Jaeger, P. A., Duttke, S. H., Benner, C. K., Glass, C., Ideker, T., & Hampton, R. (2018). The Dfm1 Derlin Is Required for ERAD Retrotranslocation of Integral Membrane Proteins. *Mol Cell*, 69(2), 306-320.e4.

Neal, S., Syau, D., Nejatfard, A., Nadeau, S., & Hampton, R. Y. (2020). HRD complex self-remodeling enables a novel route of membrane protein retrotranslocation. *iScience*, 23(9), 101493.

Ohba, T., Schirmer, E. C., Nishimoto, T., & Gerace, L. (2004). Energy- and temperature-dependent transport of integral proteins to the inner nuclear membrane via the nuclear pore. *J Cell Biol*, 167(6), 1051–1062.

Omnus, D. J., & Ljungdahl, P. O. (2014). Latency of transcription factor Stp1 depends on a modular regulatory motif that functions as cytoplasmic retention determinant and nuclear degron. *Mol Biol Cell*, 25(23), 3823–3833.

Pantazopoulou, M., Boban, M., Foisner, R., & Ljungdahl, P. O. (2016). Cdc48 and Ubx1 participate in a pathway associated with the inner nuclear membrane that governs Asi1 degradation. *J Cell Sci*, 129(20), 3770–3780.

Plemper, R. K., Egner, R., Kuchler, K., & Wolf, D. H. (1998). Endoplasmic reticulum degradation of a mutated ATP-binding cassette transporter Pdr5 proceeds in a concerted action of Sec61 and the proteasome. *J Biol Chem*, 273(49), 32848–32856.

Richly, H., Rape, M., Braun, S., Rumpf, S., Hoege, C., & Jentsch, S. (2005). A series of ubiquitin binding factors connects CDC48/p97 to substrate multiubiquitylation and proteasomal targeting. *Cell*, 120(1), 73–84.

Romanauska, A., & Köhler, A. (2018). The Inner Nuclear Membrane Is a Metabolically Active Territory that Generates Nuclear Lipid Droplets. *Cell*, 174(3), 700-715.e18.

Ryu, K. Y., Baker, R. T., & Kopito, R. R. (2006). Ubiquitin-specific protease 2 as a tool for quantification of total ubiquitin levels in biological specimens. *Anal Biochem*, 353(1), 153–155.

Sato, B. K., & Hampton, R. Y. (2006). Yeast Derlin Dfm1 interacts with Cdc48 and functions in ER homeostasis. *Yeast*, 23(14–15), 1053–1064.

Sato, B. K., Schulz, D., Do, P. H., & Hampton, R. Y. (2009). Misfolded Membrane Proteins Are Specifically Recognized by the Transmembrane Domain of the Hrd1p Ubiquitin Ligase. *Mol Cell*, 34(2), 212–222.

Schmidt, C. C., Vasic, V., & Stein, A. (2020). Doa10 is a membrane protein retrotranslocase in er-associated protein degradation. *ELife*, 9, 1–31.

Schoebel, S., Mi, W., Stein, A., Ovchinnikov, S., Pavlovicz, R., DImaio, F., Baker, D., Chambers, M.G., Su H., Li D., et al. (2017). Cryo-EM structure of the protein-conducting ERAD channel Hrd1 in complex with Hrd3. *Nature*, 548(7667), 352–355.

Smoyer CJ, Katta SS, Gardner JM, Stoltz L, McCroskey S, Bradford WD, McClain M, Smith SE, Slaughter BD, Unruh JR, et al. (2016). Analysis of membrane proteins localizing to the inner nuclear envelope in living cells. *J Cell Biol*, 215(4), 575–590.

Smoyer, C. J., & Jaspersen, S. L. (2019). Patrolling the nucleus: inner nuclear membrane-associated degradation. *Curr Genet*, 65(5):1099-1106

Stolz, A., Schweizer, R. S., Schäfer, A., & Wolf, D. H. (2010). Dfm1 Forms Distinct Complexes with Cdc48 and the ER Ubiquitin Ligases and Is Required for ERAD. *Traffic*, 11(10), 1363–1369.

Sun, Z., & Brodsky, J. L. (2019). Protein quality control in the secretory pathway. *J Cell Biol*, 218(10), 3171–3187.

Swanson, R., Locher, M., & Hochstrasser, M. (2001). A conserved ubiquitin ligase of the nuclear envelope/endoplasmic reticulum that functions in both ER-associated and Mat α2 repressor degradation. *Genes Dev*, 2(20), 2660–2674.

Vashist, S., & Ng, D. T. W. (2004). Misfolded proteins are sorted by a sequential checkpoint mechanism of ER quality control. *J Cell Biol*, 165(1), 41–52.

Vasic, V., Denkert, N., Schmidt, C. C., Riedel, D., Stein, A., & Meinecke, M. (2020). Hrd1 forms the retrotranslocation pore regulated by auto-ubiquitination and binding of misfolded proteins. *Nat Cell Biol*, 22(3), 274–281.

Winzeler, E. A., Shoemaker, D. D., Astromoff, A., Liang, H., Anderson, K., Andre, B., Bangham R., Benito R., Boeke J.D., Bussey H., et al. (1999). Functional characterization of the S. cerevisiae genome by gene deletion and parallel analysis. *Science*, 285(5429), 901–906.

Wu, X., Siggel, M., Ovchinnikov, S., Mi, W., Svetlov, V., Nudler, E., Liao M., Hummer G., Rapoport, T. A. (2020). Structural basis of ER-associated protein degradation mediated by the Hrd1 ubiquitin ligase complex. *Science* 368(6489)

Ye, Y., Meyer, H. H., & Rapoport, T. A. (2001). The AAA ATPase Cdc48/p97 and its partners transport proteins from the ER into the cytosol. *Nature*, 414(6864), 652–656.

Zargari, A., Boban, M., Heessen, S., Andréasson, C., Thyberg, J., & Ljungdahl, P. O. (2007). Inner nuclear membrane proteins Asi1, Asi2, and Asi3 function in concert to maintain the latent properties of transcription factors Stp1 and Stp2. *J Biol Chem*, 282(1), 594–605.

CHAPTER IV

Structure-Misfunction Analysis of Cytoplasmic Proteins Unveils the Complexity of Minimal Protein Misfolding

Abstract

Misfolded and otherwise aberrant proteins are recognized, ubiquitinated, and degraded by the protein quality-control (PQC) arm of the ubiquitin-proteasome system (UPS). While decades of research have uncovered the components and mechanisms of UPS-mediated PQC, misfolded proteins themselves remain poorly understood. This is particularly true of the full-length, functional-but-misfolded proteins that underlie a broad range of human diseases, such as cystic fibrosis. To address these shortcomings, we have designed a screen for minimally misfolded proteins that we call "Structure-Misfunction" analysis. Structure-Misfunction analysis leverages optics and yeast genetic to identify point mutants of a protein of interest that retain function but are nonetheless recognized and degraded by PQC. This genetic and cell-biological approach to quality-control analysis yielded a wide range of PQC substrates. Upon closer characterization, these substrates bore the same classical disruptions to protein folding—such as buried charge—that are found in many disease-causative mutants. Our substrates also allowed us to demonstrate the "local" nature of minimal misfolding. To our surprise, different amino-acid substitutions within a single domain could elicit recognition and degradation by distinct PQC pathways. Contrastingly, a single pathway mediated degradation when destabilizing mutations occupied one hydrophobic pocket or a single amino acid position. Thus, Structure-Misfunction analysis unveiled underlying "rules" of PQC recognition and misfolding. The screen also allowed us to create a simple model of pharmacological chaperoning. We isolated mutants of the classic allosteric protein chorismate mutase that are stabilized by the allosteric effector tryptophan. Mutational disruption of the allosteric binding site completely abrogated this effect. In sum, structure-misfunction analysis is a broadly applicable platform for investigating UPS-mediated PQC and misfolding itself.

Introduction

As a part of protein quality control (PQC), the ubiquitin-proteasome system (UPS) recognizes, ubiquitinates, and degrades aberrant proteins (Dikic, I., 2017; Jayaraj, G. G., et al., 2020). In this role, the UPS must specifically degrade misfolded versions of a given protein while sparing the correctly folded form. This exquisite specificity is affected by E3 ubiquitin ligases, which recognize PQC substrates, facilitate their ubiquitination, and thereby target them to the 26S proteasome for degradation (Zheng, N., and Shabek, N., 2017). Remarkably, the array of abnormal proteins produced by environmental stress, mutations, and translational errors are recognized by a relatively small number of PQC ligases. We refer to the ability of these ligases to accurately select a wide range of misfolded substrates as "broad specificity." This feature of degradative PQC is absolutely central to the UPS's role in supporting cellular and organismal health, and defects in the UPS are a hallmark of aging as well as a growing list of human diseases (Klaips, C. L., et al., 2018).

Given this biomedical relevance, there have been sustained efforts to understand not only PQC E3 ligases but also the PQC substrates they recognize. Studies of the latter most often hinge on model substrates collected from a variety of sources. One source is point mutants that destabilize a protein and cause its degradation. Often, these are initially identified as loss-of-function or temperature-sensitive mutants: the point mutation affects function and/or causes PQC degradation that leads to a decrease in abundance (Biederer, T., et al., 1996; Farzin Khosrow-Khavar, et al., 2012; Gardner, R. G., et al., 2005; Ravid, T., et al., 2006). A related source is truncated versions of full-length proteins. These polypeptides are unlikely to ever achieve a folded state and are often rapidly degraded by the UPS (Fredrickson, E. K., et al., 2011; Heck et al., 2010; Rosenbaum, J. C., et al., 2011). Finally, a variant of PQC substrates are naturally degraded proteins. These appear to display structural features of quality control as part of cellular regulation of their abundance (Foresti, O., et al., 2013; Foresti, O., et al., 2014; Hampton, R.Y., et al., 1996; Khmelinskii, A., et al., 2014;

Swanson, R., et al., 2001; Wangeline, M.A., et al., 2017; Zelcer, N., et al., 2014). Together, substrates from each of these categories have allowed the field to define numerous key and conserved quality-control pathways. However, this relatively small collection of often disparate substrates has made it difficult to define the features of biologically relevant misfolding and the PQC response to it.

To create more comprehensive collections of PQC substrates, investigators have developed and refined a number of screening and genetic approaches. For instance, several groups have designed screens to discover "degrons," short amino-acid sequences that confer degradation upon a reporter protein (Geffen, Y., et al. 2016; Gilon, T., et al., 2000; Maurer, M. J. et al., 2016). A recent example of this approach used high-throughput analysis of cytosolic reporter-protein levels and function as a readout of degradation and thereby uncovered 130 degrons targeted by the PQC E3 ligase Doa10, 13 of which were derived from segments of native proteins (Geffen, Y., et al. 2016). In parallel experiments, a nuclear-localized reporter protein fused to 30,000 unique sequences was significantly enriched for degrons targeted by the nuclear PQC E3 ligase San1 (Geffen, Y., et al. 2016). These data highlight the breadth of substrates recognized by individual ligases and demonstrate that a small collection of E3s can indeed recognize a large variety of degrons. As importantly, the substrate collections generated by degron screens and other studies have revealed structural features that indicate the basis of E3 recognition. These include amphipathic helices in the case of Doa10 and its mammalian homolog MARCH6 (Chua, N. K., et al., 2017; Johnson, P. R., et. al, 1998; Geffen, Y., et al., 2016) and hydrophobicity and disorder in the case of San1 (Fredrickson, E. K., et al., 2011; Fredrickson, E. K., et al., 2013; Rosenbaum, J. C., et al., 2011). In other approaches, the sequence of a structurally characterized protein is directly altered, introducing amino-acid substitutions predicted to cause quality control degradation (Abildgaard, A. B., et al., 2019; Nielsen, S. V., et. al, 2017). We sought to combine the facility of screening for bona fide PQC

substrates with a focus on proteins with known structures. By doing so, we hoped to explore a key but so far under-explored class of substrates that we call minimally misfolded proteins.

Minimally misfolded proteins bear an individual missense mutation that brings about quality-control degradation without ablating protein function. Such minimal structural changes can have important clinical outcomes stemming from degradation, with perhaps the most famous case being the cystic fibrosis variant CFTRΔF508 (Guerriero, C. J., and Brodsky, J. L., 2012). Indeed, it is possible that minimally misfolded proteins underlie a swath of human diseases. Studies combining *in vitro* and computational data suggest that the majority of monogenic diseases are caused by mutations that destabilize protein structure, often by a ΔΔG of little as 1-3kcal/mol (Redler, R. L., et al., 2016; Yue, P., et al., 2005). Recently, systematic, *in vivo* approaches have corroborated that destabilizing mutations lower protein abundance (Matreyek, K. A., et al., 2018), and two recent studies show that such mutations can result in UPS-mediated degradation (Abildgaard, A. B., et al., 2019; Nielsen, S. V., et. al, 2017). A broader collection of minimally misfolded substrates stands to demonstrate that PQC E3 ligases broadly recognize subtle disease-causative mutations.

Minimally misfolded proteins also reflect amino-acid substitutions produced during translation. Recent studies in bacteria demonstrate that misincorporations occur at frequencies as high as 1 in 1000 residues and that the resultant substitutions cause an average ΔΔG of 1.45 kcal/mol (Garofalo, R., et al., 2019; Mordret, E., et al., 2019). Thus, insights from both disease states and normal biology imply that minimally misfolded point mutants are a large and highly relevant class of quality control substrate that would benefit from more intense and encompassing study. Furthermore, minimally misfolded proteins that retain their native function offer the possibility of referring to the proteins' native structures to understand the structural changes that cause recognition by a given PQC E3 or E3s.

In this work, we devised a screen to identify point mutants that convert a stable protein into a minimally perturbed PQC substrate. Our goal was to discover the types of structural alterations that trigger quality control, the UPS pathways that are involved in degradation, and the features that define biologically relevant misfolding. To facilitate structural interpretation, we constrained the screen to soluble, monomeric proteins with solved crystal structures, and we isolated only point mutants that retained enzymatic function. In homage to classical "structure-function" analysis, We named this approach a "structure-misfunction" analysis.

Structure-misfunction analysis produced a range of mutations that cause a given protein to undergo degradation without losing its function. By referencing crystal structures, we determined that these mutants represent the same canonical disruptions of protein folding found in disease alleles. We isolated instances of buried charges and polar groups, losses of charge-polar interactions, cavity formation, and over packing, amongst others (Yue, P., et al., 2005). To our surprise, seemingly identical structural perturbations can elicit remarkably diverse PQC responses, even within a single domain. Intriguingly, amino-acids substitutions that elicit distinct PQC responses cluster together in a protein's tertiary structure. These data suggest that, rather than causing "global" unfolding, spatially clustered perturbations can create a "local" lesion bearing a distinct PQC determinant (Stein, A., et al., 2019). Structure-misfuncton analysis unveils the broad ability of PQC ligases to recognize destabilizing mutations and indicates the considerable complexity within the seemingly restricted category of minimally misfolded mutants of a single protein.

An additional, intriguing feature of some minimally misfolded proteins is the ability for ligand binding to promote their folding or misfolding. Classically, a number of orthosteric and allosteric ligands have been demonstrated to facilitate integral cell-membrane protein folding and maturation (Leidenheimer, N. J., and Ryder, K. G., 2014). Such ligands are referred to as pharmacological chaperones, and they represent a mode of intervention for diseases such as cystic

fibrosis (Van Goor, F., et al., 2009; Van Goor, F., et al., 2011). Our lab has discovered an instance of ligand binding that produces the opposite effect. The yeast HMG-CoA reductase (HMGR) isozyme Hmg2 is subject to UPS-mediated degradation when a sterol pathway metabolite binds to it and causes it to undergo reversible misfolding (Garza, R. M., et al., 2009; Shearer, A. G., and Hampton, R. Y., 2005; Wangeline and Hampton, 2018). We have named this mode of degradative feedback regulation "mallostery" due to its many similarities to classic allosteric regulation (Wangeline, M. A., and Hampton, R. Y., 2018). We wondered if structure-misfunction analysis could identify a point mutation that would unveil a direct evolutionary path from allosteric modulation of protein activity to allosteric modulation of protein degradation. Surprisingly, by analyzing the classic and extremely well-studied allosteric enzyme chorismate mutase (CM), we uncovered two individual point mutations that render CM a target of ligand modulated degradation. In these instances, the CM allosteric activator, tryptophan, markedly stabilized the protein. Structure misfunction analysis not only uncovered a path from allosteric regulation of activity to allosteric regulation of degradation, it also demonstrated that one can be converted into the other by a single mutation.

Overall, structure-misfunction analysis generates a biomedically relevant class of quality-control substrate and reveals the extraordinary complexity of the quality-control code that lurks in even one domain of a simple globular protein. Our results also demonstrate that structure-misfunction analysis is a widely applicable discovery platform capable of facilitating inquiry into a broad array subtle but biomedically critical PQC phenomena.

Results

An Optical Screen for Minimally Misfolded Point Mutants

Our first goal was to screen for point mutations that converted a stable protein into a PQC substrate. In preparation for the screen, candidate point mutants were made by mutagenizing a coding region of interest with error-prone PCR, and this mutagenized product was used for yeast

recombination cloning (Figure 4.1A). This strategy produces thousands of yeast colonies that each bear a unique, plasmid-born mutant, and it allows for colony-level screening for phenotypes of interest (Muhlrad, D., et al., 1992). In our screen, mutagenized coding region is recombined with a plasmid bearing GFP, yielding GFP-tagged mutants and fluorescent colonies.

A signal phenotype of degraded point mutants is reduced protein steady-state levels compared to the stable, wild-type protein. Accordingly, a degraded, GFP-tagged mutant produces a dim colony compared to the bright colonies of the wild-type protein and stable mutants. These fluorescence phenotypes can be observed using a simple GFP visualizing platform, allowing us to identify dim colonies in a primary screen for new PQC substrates (Cronin, S. R., and Hampton, R. Y., 1999).

While this primary screen eliminated most stable mutants, dim candidates included mutations that merely reduced expression levels without effecting stability. This is also true of other preliminary indicators of PQC degradation, such as temperature-sensitive growth (Farzin Khosrow-Khavar, et al., 2012). We therefore designed a secondary screen for UPS-dependent degradation. Specifically, we wanted to test dim candidates for increased steady-state levels when proteasome activity was compromised. This was facilitated by use of a hypomorphic *RPN1*/*HRD2* allele of the 26S proteasome, *hrd2-1*, which markedly stabilizes a broad range of quality control substrates (Hampton, R. Y., et al., 1996; Murray, B. P., and Correia, M. A., 2001; Wilhovsky, S., et al., 2000).

To directly test candidates for stabilization in *hrd2-1* strains, we designed a yeast counterselection strategy. The primary screen for dim colonies was performed in a *hrd2-1* strain bearing a *URA3-HRD2* plasmid, which fully complements the *hrd2-1* mutant. Once dim colonies have been isolated, the *HRD2* plasmid can be removed by counterselection of the *URA3* marker with 5-FOA, thereby imposing 26S-proteasome deficiency in the plasmid-cleared colonies. In this uncovered *hrd2-1* background, increased colony fluorescence indicates UPS substrate (Figure 4.1B).

This counterselection scheme yielded a strong phenotype that was apparent upon visual inspection (Figure 4.1C).

Because we sought to identify even very slowly degraded mutants, we isolated candidates with any increase in fluorescence in the *hrd2-1* background. Even with this permissive approach, the secondary screen typically identified two to five putative substrates from ~1000 colonies. These putative substrates were then subjected to a preliminary cycloheximide chase using a flow cytometer. Mutants that passed the secondary screen and showed degradation during a chase were then sequenced, and the screen was repeated until it produced consensus point mutants, a benchmark usually attained after screening ~20,000 colonies in the case of a ~1kb gene.

This workflow can isolate any mutation that causes PQC degradation, but we constrained the screen to isolate minimally misfolded, functional-but-degraded point mutants. As mentioned above, such substrates model disease alleles and mistranslation events. Such mutants also promised to support an overarching goal of these studies: unveiling connections between the apparent effect of a substitution on protein structure the PQC pathway(s) elicited. We reasoned that X-ray crystal structures would prove invaluable in that efforts, and that functional mutants would bear a closer resemblance to the native structure than non-functional mutants, which could be grossly misfolded or unfolded. Assays for mutant functionality were therefore added to the screen, as detailed below.

Screening of *ADE1* Produces Minimally Misfolded UPS Substrates

To further support structural analysis, we chose to isolate minimally misfolded substrates derived from simple, well-studied proteins. We searched protein databases for soluble, monomeric proteins with solved crystal structures and easy-to-score functions. Ade1 met these criteria. Ade1 catalyzes an intermediate step of adenine biosynthesis, and *ade1Δ* nulls cannot grow on plates lacking adenine (Roman, H., 1956). This nutritional requirement facilitated a simple readout of Ade1-mutant

function: when expressed in an *ade1Δ* null, functional *ade1* mutants support growth on plates lacking adenine. Structurally, Ade1 is a stable (Figure 4.S1), cytosolic monomer with a two-domain structure revealed by crystallography (Huh, W. K., et al., 2003; Levdikov, V. M., et al., 1998). Finally, *ADE1-GFP* fully compliments *ade1Δ* nulls (Figure 4.2), allowing us to assess both optics and function while screening.

We mutagenized the *ADE1* ORF and generated mutant-expressing colonies in a *HRD2*/*hrd2-1 ade1Δ* null background. To assess the quality of this plate-based library, we grew transformed cells on plates with adenine, picked fifty colonies at random, and recovered plasmids. Sequencing confirmed a desired low rate of mutagenesis (0.6 mutations per mutant recovered) that facilitated isolation of point mutants from the screen (Table S1). Critically, randomly selected mutations were distributed throughout the *ADE1* ORF, as observed in other analyses of the Mutazyme II kit (Wong, T. S., et al., 2006). Having confirmed the quality of our library, we screened ~20,000 colonies grown on plates with adenine. Dim colonies were then isolated and incubated at a permissive temperature on plates lacking adenine. Mutants that supported growth were preliminarily scored as functional, and these were screened for UPS-dependent degradation. Roughly 40 candidates retained function, increased in fluorescence in the secondary screen, and evinced degradation in a preliminary cycloheximide chase conducted on a flow cytometer (data not shown). In total, we isolated nine destabilizing point mutations at seven distinct residues, and we recovered most mutants on multiple occasions, indicating that we approached or achieved screen saturation.

To confirm that these nine point mutants were minimally misfolded PQC substrates, we transformed each into standard lab strains and assayed each mutant protein for enzymatic function and UPS-mediated degradation. First, we retested mutants for function by expressing each in an *ade1Δ* null. All mutants supported growth on plates lacking adenine and we thus scored as functional (Figure 4.2). Each mutant was then tested for UPS-mediated degradation using cycloheximide chase

in the presence or absence of the proteasome inhibitor MG132. The inhibitor stabilized all mutants, confirming the efficacy of the secondary screen (Figure 4.3 A-C). Cycloheximide chase also demonstrated the breadth of degradation kinetics detected by our optical screen. Substrate half-lives ranged from roughly thirty minutes to over six-and-a-half hours. Thus, even our most rapidly degraded Ade1 mutants conformed to our definition of a minimally misfolded UPS substrate, supporting reference to the Ade1 crystal structure during structural analysis.

As an additional, independent test for minimal misfolding, we subjected each Ade1 mutant to *in vivo* treatment with glycerol, a chemical chaperone. Chemical chaperones favor protein folding and stabilize misfolded substrates *in vivo* (Auton, M., and Bolen, D. W., 2015; Shearer, A. G., and Hampton, R. Y., 2004; Zhao, Y., et al., 2013). By contrast, chemical chaperones have no *in vivo* effect on proteins that are permanently misfolded or unfolded, such as the severely misfolded 6myc-Hmg2 and the non-folding mutant CPY* (Shearer, A. G., and Hampton, R. Y., 2004). Strikingly, all mutants were stabilized in the presence of glycerol, further indicating minimal misfolding and a close resemblance to the stable, wild-type structure (Figure 4.S2).

Because the newly isolated Ade1 PQC substrates met all our criteria for minimal misfolding, we used the Ade1 crystal structure to infer their destabilizing effect(s) of the various amino acid substitutions. The majority of isolated mutants (L32R, G54E, G54R, W64R, A195D) introduced charge or polarity into the interior of the folded structure. Two other mutations introduced prolines into secondary structures, one on an α helix (L102P), one on a β strand in a β sheet (L32P). Another mutation (D37V) abrogated hydrogen bonds to both a nearby sidechain and nearby peptide backbone, and a final mutation (G54V) caused a steric clash at a position that cannot accommodate bulky residues, polarity (G54E), or charge (G54R). As with destabilizing mutations that lower PTEN steady-state levels (Matreyek, K. A., et al., 2018), these perturbations occurred preferentially on secondary structures (six out of seven positions). Our screen uncovered a variety of the structural

perturbations commonly caused by disease alleles (Yue, P., et al., 2005). In sum, our *ade1* mutants juxtapose canonically disrupted protein folding and intact enzymatic function, an intriguing property of many disease alleles (Guerriero, C. J., and Brodsky, J. L., 2012; Nielsen, S. V., et. al, 2017; Takahashi, M., et al., 2007).

All Ade1 Mutants are Degraded by The Same Combination of E3 Ligases

We next characterized the PQC pathway(s) elicited by each of our minimally misfolded Ade1 mutants. Because no predictive frameworks for PQC recognition exists, there are few indicators to predict which E3 ligase or ligases will recognize a novel substrate. Relatedly, and perhaps more intriguingly, there have been few opportunities to identify the degradative pathway(s) that recognize different mutants of the same protein. It was unclear if a common pathway would degrade all variants, or if different pathways would degrade different variants, perhaps according to the distinct biochemical properties unveiled by distinct structural perturbations.

We therefore tested a variety of E3 ligases for their role in degrading Ade1 substrates. In *S. cerevisiae*, the major E3 ligases that mediate cytosolic PQC are the soluble E3 ligase Ubr1, the ER-transmembrane ligase Doa10, and the nuclear ligase San1. These E3s are often functionally redundant, especially San1 and Ubr1, which almost always act in parallel (Heck et al., 2010). However, it is also well-documented that PQC ligases can recognize distinct degrons that other ligases cannot (Geffen, Y., et al., 2016; Swanson, R., et al., 2001). Therefore, a given cytosolic substrate may be recognized by one, two, or all three ligases depending on the PQC determinants displayed upon misfolding.

We assayed ade1-D37V, -G54E, and -W64R for Doa10-, San1-, Ubr1-dependent degradation by subjecting each to cycloheximide chase in *doa10Δ, san1Δ*, *ubr1Δ*, null backgrounds.

In all cases, the absence of individual ligases did little to stabilize the mutants (Figure 4.4 A-C i). This suggested combinatorial recognition by two or more cytosolic ligases.

We next performed cycloheximide chase in *san1Δubr1Δ* and *san1Δubr1Δdoa10Δ* backgrounds. In the past, we have demonstrated that many substrates are subject to parallel recognition by San1 and Ubr1 (Heck et al., 2010), and to some degree this was also the case for Ade1 mutants. Each was partially stabilized in a *san1Δubr1Δ* background (Figure 4.4 A-C ii). By contrast, the *san1Δubr1Δdoa10Δ* null background stabilized all mutants tested to roughly the same degree as MG132 ((Figure 4.4 A-C ii). We therefore concluded that *ade1* mutants are uniformly subject to multi-pathway degradation, with each mutant eliciting recognition by San1, Ubr1, and Doa10 simultaneously. Taken alone, these data imply that all destabilized variants of a protein elicit the same PQC pathways, even when variants cause a variety of disruptions. We wondered if this was a general feature of degradative PQC, or merely a reflection of the limited number of degrons within one small, monomeric protein.

Lys1 Mutants are Degraded by Distinct UPS Pathways, Even Within a Domain

To expand our analysis of minimal misfolding, we screened a second protein, Lys1. Lys1 catalyzes the final step of lysine biosynthesis. Accordingly, *lys1Δ* nulls cannot grow on plates lacking lysine, and functional Lys1 mutants rescue this nutritional phenotype, again allowing function to be scored by growth (Hawthorne, D. C., and Mortimer, R. K., 1960; Saunders, P. P., and Broquist, H. P., 1966). Like Ade1, Lys1 is a two-domain, soluble, monomeric protein with a solved crystal structure (Burk, D. L., et al., 2007). A minor drawback of Lys1, its native localization to the peroxisome, is easily overcome by a C'-terminal GFP fusion. GFP blocks the protein's peroxisomal localization sequence, thereby rendering Lys1-GFP a stable (Figure 4.S3) cytosolic protein that retains its function (Al-Saryi, N. A., et al., 2017). Lys1-GFP provided another opportunity to study minimal misfolding in a simple context.

We screened ~20,000 colonies expressing mutated Lys1-GFP, and we isolated eight point mutations at seven distinct residues. These met our criteria for functional, misfolded UPS substrates. In subsequent testing, each Lys1 mutant complemented *lys1Δ* null, though some mutants required multi-copy plasmids to achieve adequate protein steady-state levels (Figure 4.5). As importantly, each was stabilized by proteasome inhibitor (Figure 4.6), and each was stabilized *in vivo* by glycerol (Figure 4.S4). Again, our screening strategy isolated novel, minimally misfolded point mutants.

We therefore used the Lys1 crystal structure to infer the destabilizing effect(s) of each mutation. In this case, mutations introduced charge or polarity into hydrophobic pockets of the protein (V26D, W151R, P194Q, I254N, W353R) or interfered with secondary structures (L29P, L146P, W151G). As with our Ade1 mutants, Lys1 mutants were preferentially located on secondary structures (six out of seven positions).

We also noticed that several mutations clustered in the Lys1 3D structure. W151R, P194Q, and I254N are within five angstroms of one another and constitute a hydrophobic pocket in the second domain. While it does not occupy this pocket, L146P is on the same α-helix as W151R. L29P and V26D represent a similar grouping in the first domain, with both substitutions occurring on the same α-helix. Such clustering of destabilizing mutants is reminiscent of degraded variants of MSH2, which tended to occupy the protein's C-terminal ATPase domain (Nielsen, S. V., et. al, 2017). A final mutant, W353R is somewhat more isolated. The first domain of Lys1 contains both the N- and C-terminus of the protein. Lys1-W353 is on the final N'-terminal alpha-helix of the protein whereas Lys1-L29 and Lys1-V26 are on the first, C-terminal alpha-helix. Nevertheless, the Chimera distance tool estimates that the closest atoms of the Lys1-W353 and -L29 sidechains are separated by only nine angstroms.

We proceeded to uncover the PQC pathways involved in degrading Lys1 mutants. We first tested the mutants that clustered in the second domain (W151R, P194Q, I254N, and L146P) using

single and multiple nulls, as above. Each of these mutants was partially stabilized in *san1Δ* and *ubr1Δ* nulls and fully stabilized in a *san1Δubr1Δ* null, as evinced by cycloheximide chase (Figure 4.7). Each of these spatially related substitutions elicited degradation by the same UPS pathways.

We next proceeded to characterize the lone W353R mutant. This mutant, too, was partially stabilized in *san1Δ* and *ubr1Δ* nulls and fully stabilized in a *san1Δubr1Δ* null, as evinced by cycloheximide chase (Figure 4.8A). Thus, the majority of our Lys1 mutants represented classical substrates of the parallel Ubr1 and San1 pathways.

V26D and L29P provided a striking contrast. When each was introduced into a *san1Δubr1Δ* null background, we were unable to detect any stabilization of the substrate (Figure 4.8B-C). Different destabilizing mutations uncovered distinct PQC determinants within a domain.

We wondered if we could predict an additional mutation that, like V26D and L29P, would elicit San1-Ubr1-indendent degradation. Investigating the Lys1 crystal structure, we found that V26 is within five angstroms of I36. I36 occupies the face of a β strand that projects R groups towards the α-helix occupied by V26 and L29; I36 and V26 contribute to the same hydrophobic pocket. We substituted I36 with an aspartic acid, and the resultant point mutant showed identical proteasome-dependent, San1-Ubr1-independent degradation (Figure 4.8D-E). V26D, L29P, and I36D form a similarly uniform grouping to W151R, I245N, and P194Q, suggesting that individual hydrophobic pockets can bear distinct PQC determinants.

All Destabilizing Substitutions at Lys1-W151 Elicit Ubr1-San1 Recognition

In the above screens, random mutagenesis created mutations throughout *ADE1* and *LYS1*, as desired, but it also created two or three different substitutions of some residue positions (ade1-L32P and L32R; ade1-G54E, G54R, and G54V; along with lys1-W151G and W151R). We were intrigued

to find that different destabilizing substitutions at these positions were recognized by the same PQC ligases, and we wondered if this applied to all destabilizing mutations at a residue.

To pursue this question, we turned to saturation mutagenesis. We first sought a position that would be destabilized by most substitutions and thereby yield a broad panel of PQC substrates. Lys1-W151 had already yielded two substrates and these were subject to relatively straightforward recognition by San1 and Ubr1 in parallel. As a preliminary check for the restrictiveness of this position, we used recombination cloning to introduce a random codon at W151. Briefly, we ordered a primer with an NNK codon and appropriate homology for recombination, and we transformed plasmid and fragments into our hrd2-1/HRD2 screening strain. This preliminary check yielded predominantly dim colonies that increased in fluorescence upon HRD2 counterselection, indicating that, indeed, few substitutions were tolerated and most led to destabilization. We collected both substrates and stable mutants from this screen, then used recombination to create rarer codons, such as those for Met and Lys.

This collection of iso-positional mutants was then transformed into ligase nulls to determine the PQC pathways responsible for degradation. Only three mutants were identical to Lys1-GFP: W151F, W151Y, and W151H. Thus, saturation mutagenesis demonstrated a requirement for not only space filling at this position but also, perhaps, aromaticity. All other mutants evinced varying degrees of degradation. This ranged from the largely stable W151L, which had roughly 90% protein remaining at three hours, to the relatively strongly destabilized W151P, which had roughly reached its half-life by three hours. Strikingly, in every case, degradation depended entirely upon San1 and Ubr1 for degradation (Figure 4.9). The same PQC pathways recognized every destabilizing substitution, ranging from buried charges to cavity formers to helix breakers. It would seem, then, that the decision for which E3 ligase(s) are used for these substrates has more to do with residue position than thermodynamic perturbation.

Misfolded Aro7 Mutants that Can Be Stabilized by An Allosteric Ligand

Some functional-but-degraded mutants can be treated by inhibiting degradation; upon inhibition, protein abundance is increased, and adequate function is restored. Though such treatments could target the UPS, successful drugs often bind to the mutant protein and facilitate its folding (Pedemonte, N., et al., 2020; Van Goor, F., et al., 2009; Van Goor, F., et al., 2011). These drugs have been named pharmacological chaperones, an allusion to their site-specific binding and their chaperone-like ability to promote maturation and stability. We wondered if pharmacological chaperoning could stabilize a simple, minimally misfolded protein derived from our screen.

We reasoned that an ideal parent protein would be a soluble, allosteric protein with a scorable function, known structure, and well-defined allosteric binding site. We therefore chose perhaps the simplest allosteric protein known, the enzyme chorismate mutase (CM). CM (known as Aro7 in yeast) occupies a branch point in the synthesis of tyrosine and tryptophan; it commits chorismate to tyr synthesis and diverts it from trp synthesis. To balance trp and tyr levels, CM activity is regulated by a simple allosteric mechanism: trp activates it—favoring production of tyr—while tyr inhibits it—favoring production of trp. The structural basis of this trp- and tyr-mediated regulation is extraordinarily well-studied (Sträter, N., et al., 1996; Xue, Y., et al., 1994). CM is a homodimer with a ligand binding site at the interface of the subunits, and a number of structure-function analyses have identified mutations that block or disable allosteric binding (Schnappauf, G., et al., 1998). As importantly, *aro7Δ* nulls are tyrosine and phenylalanine auxotrophs, again allowing us to test mutant function with growth assays (Tang, Y., et al., 1991). CM has the useful characteristics of Ade1 and Lys1, and it allowed us to explore the possibility of creating proteins that undergo ligand-dependent changes in PQC degradation.

We screened ~20,000 ARO7 mutants and recovered three point mutants that met our criteria for minimal misfolding: each was a functional UPS substrate (data not shown and figure 4.9A).

Examining the Aro7 crystal structure, we found that two of the mutated residues (R33 and D147) hydrogen bond to one another in the native protein. The remaining mutant (S155G) represents a helix breaker on the same alpha helix as D147. For a third time, the screen yielded classically destabilized mutants that nonetheless retained function.

We tested these CM mutants for *in vivo* stabilization by trp and/or tyr. To do so, we assayed for changes in steady state levels during log phase growth. Neither the mutants nor the wild-type protein responded to tyr (not shown). Similarly, Aro7-GFP did not respond to trp (Figure 4.10B). On the other hand, we recorded a dose-responsive increase in Aro7-R33G-GFP steady-state levels after treatment with 20 and 200 µM trp (Figure 4.10B).

In other cases of pharmacological chaperoning, mutants are stabilized by interactions between the drug and a bona-fide binding site (Generoso, S. F., et al., 2015; Tapper, A. R., et al., 2004). Accordingly, we evaluated the role of CM's trp-binding site in mutant stabilization. It has been demonstrated elsewhere that the point mutation G141S blocks the allosteric binding site of Aro7 (Schnappauf, G., et al., 1998). To test if this mutant would also prevent the stabilizing effect of trp, we made a double mutant R33G, G141S construct and tested its response to trp. Remarkably, G141S almost completely reversed the stabilizing effects of trp (figure 4.10B), indicating the role of allosteric-site-specific binding in stabilization.

Discussion

In this study, we designed a screen for minimally misfolded proteins and subjected three proteins to it: Ade1, Lys1, and Aro7. In each case, the screen isolated point mutants that were not only subject to UPS-mediated degradation but were also functional and could be stabilized *in vivo* by the chemical chaperone glycerol. Within this seemingly restricted category, the screen isolated a spectrum of substrates as judged by their half-lives, which ranged from 30 minutes to roughly eight

hours, and by their modes of destabilization, which included buried charge and polarity, helix breaking, cavity formation, and loss of side-chain hydrogen bonding.

Ade1 and Lys1 offer contrasting collections of PQC substrates. All Ade1 mutants tested entered a UPS pathway mediated in parallel by Doa10, San1, and Ubr1. These data could support two difficult to distinguish models (Stein, A., et al., 2019). The first is that, when destabilized, Ade1 becomes globally unfolded, making one or more degrons equally available in all cases. Thus, all destabilizing mutations elicit the same UPS response. Mutant function and glycerol-mediated stabilization suggest more subtle misfolding, but unfolding cannot be ruled out. The second possibility is that the substitutions unveiled by the screen led to local misfolding, and this local misfolding unveiled a single degron that elicits the observed UPS response. This model is supported by the relative proximity of many of the destabilizing mutations, which were closely juxtaposed in the Ade1 tertiary structure. To resolve between these possibilities, future studies could look deeper into the mutational landscape of Ade1. Our structure-misfunction analysis was limited by the substitutions made by an error-prone polymerase and the requirement that mutants retain function. It could be intriguing to investigate mutations that are predicted to be highly destabilizing. Perhaps these will yield substrates that elicit a distinct UPS pathway, ruling out, to some extent, a role for global unfolding. Rather than pursuing this possibility, we proceeded to screen Lys1.

In many ways, our Lys1 mutants closely resemble our Ade1 mutants in their breadth of degradation kinetics, their intact enzymatic function, and their canonical forms of destabilizing substitution. However, Lys1 mutants clustered to several distinct parts of the protein in both the first and second domain. Mutants in the second domain were uniform Ubr1-San1 substrates with varying degradation kinetics. Several of these mutations were grouped very closely together, suggesting they contribute to a single hydrophobic pocket with, perhaps, one buried degron. When we pursued saturation mutagenesis at one of these positions, W151, we found that destabilizing mutations again

led to a range of degradation kinetics but uniform recognition by San1 and Ubr1. One of the three substitutions in the first domain, W353R, yielded a similar San1-Ubr1 substrate, again raising the prospect of global unfolding.

The remaining substitutions in Lys1 domain I, V26D and L29P, provided a striking contrast. Both V26D and L29P elicited degradation by a UPS pathway that is entirely San1 and Ubr1 independent. These observations strongly suggest that these mutants unveil a degron or degrons that are biochemically distinct from those unveiled by W353R. Thus, Structure-Misfunction analysis of Lys1 provided a compelling demonstration of local misfolding wherein different mutations with a single domain can yield distinct UPS substrates.

Further leveraging the Lys1 crystal structure, we were then able to isolate an additional substitution that caused San1-Ubr1-independent degradation, I36D. These data, as well as the clustered mutations in Lys1 domain II, strongly suggest that minimal misfolding may occur at discrete hydrophobic pockets throughout a protein. The ability to discern such clusters with a crystal structure also insinuate that local misfolding represents a perturbation to the folded protein structure rather than a folding intermediate, though there are almost certainly exceptions to this model. Nevertheless, we were able to use a crystal structure to predict novel substitutions that caused particular PQC outcomes.

Together, these results also complicate some previous suggestions about the relative positions of a destabilizing amino-acid substitution and the degron it unveils. For instance, a destabilized mutant of Ura3 elicited San1-mediated degradation, and the amino-acids proximal to the destabilizing substitutions yielded San1-dependent degradation when fused to GFP^{NLS} (Frederickson, E., et al., 2011). While this model could explain Lys1-V26D, -L29P, and -I36D, which are relatively nearby one another in the Lys1 primary structure, it is somewhat more difficult to apply to Lys1-L146P, -W151R, -P194Q, and -I245N, which are distant in the primary structure but closely

juxtaposed in the Lys1 tertiary structure. Perhaps given their distinct PQC character, the V26D, L29P, I36D degron could be elucidated by making GFP fusions. On the other hand, it remains somewhat unclear if such analysis would be efficacious in the case of San1-Ubr1 substrates given that those ligases recognize the majority of cytosolic PQC substrates analyzed here and elsewhere (Heck, J., et al., 2010). Perhaps full-length misfolded mutants are better subjected to methods such as hydrogen-deuterium exchange (HDX), which can rely upon solved crystal structures, whereas cis analysis can only assume that native structures are retained in isolated segments.

Whereas global misfolding suggests that a mutant may never be refolded or regain function, local and minimal misfolding pose the possibility of thermodynamically favoring the folded state and, with it, function. Indeed, "corrector" molecules that facilitate CFTRΔF508 continue to represent some of the most promising treatments for cystic fibrosis (Rowe, S.M. and Verkman A.S., 2013). To further support the model of minimal misfolding as a local and correctable lesion, we sought to identify a novel UPS substrate that could be stabilized (or destabilized) by a small molecule. We therefore performed structure misfunction analysis on chorismate mutase, known as Aro7 in *S. cerevisiae*. Remarkably, Aro7-R33G-GFP showed dose-responsive stabilization by the allosteric effector Trp. This effect was reversed when a second mutation that blocks the Trp binding site was introduced. The use of small molecule correctors may be a broadly applicable approach for minimally misfolded proteins, and as with our other mutants, it would be intriguing to perform HDX on this mutant in the presence and absence of trp.

Overall, it is clear that our screen isolated minimally misfolded, functional-but-degraded mutants. In this way, structure-misfunction analysis presents a broadly applicable discovery platform given an appropriate gene of interest. One additional, intriguing target is the protein Erg11-GFP. Erg11 is an essential, single-pass transmembrane protein with a solved crystal structure (Monk, B. C., et al., 2014). *ERG11-GFP* strains are viable, and Erg11-GFP seems to be restricted to the ER;

Erg11-GFP is not subject to Asi-complex mediated degradation, though 3HA-Erg11 is (Foresti, O., et al., 2014; Khmelinskii, A., Blaszczak, E., et al., 2014). For these reasons, the Erg11-GFP transmembrane domain is ripe for structure misfunction analysis and could provide insight into the poorly understood determinants of transmembrane protein destabilization.

Materials and Methods

Yeast and Bacteria Growth Media

Yeast strains were grown at 30° C with aeration in minimal medium (Difco yeast nitrogen base with necessary amino acids and nucleic acids) with 2% glucose or rich medium (YPD). *Escherichia coli* DH5α were grown at 37° in LB medium with ampicillin.

Plasmids and Strains

Plasmids from these studies are listed in Table S1. Plasmids were constructed using standard molecular-biological techniques as previously described (Sato et al., 2009) or, in the case of mutants isolated from the screen, using yeast recombination and an integrating after CEN excision approach described elsewhere (Flagg et al., 2019). Oligo sequences can be provided upon request. Plasmids and screening candidates made during this study were sequenced verified (Eton Biosciences).

Strains from these studies are listed in Table S2. The screen strain was derived from S288C (RHY2863), whereas all other strains are derived from BY4741. Yeast transformation followed thestandard LiOAc method (Ito et al., 1983). Null strains were from the yeast deletion collection (Winzeler, Shoemaker, Astromoff, Liang, et al., 1999) or were createded using PCR-mediated knockout in which yeast were transformed with an amplicon containing a selectable marker (NatMX, KanMX, or HphMX) flanked by 50bp directly upstream and downstream of the gene to be deleted. Transformants were grown out on YPD plates followed by replica plating to selection by CloNat/nourseothricin, G418, or hygromycin. Diagnostic PCR was used to confirm all deletions.

Random Mutagenesis

The Mutazyme II (Agilent) was used to perform random mutagenesis according to the manufacturer's instructions for low rates of mutagenesis, including a reduced number of PCR cycles and high concentration of template DNA. PCR results were quantitated by gel electrophoresis, imaging, and band quantitation (Protein Simple). Sample with mutated DNA was then treated with DpnI (NEB) to remove template DNA, and this sample was then used as an amplicon for an additional, non-mutagenic PCR using high-fidelity Phusion polymerase (NEB). The product of this PCR was then used as the insert in yeast recombination cloning for the screen, and new product was generated from the original mutated stock, as needed.

Structure-Misfunction Screening

A relevant screen strain was transformed with BamHI-XhoI digested pRH2940 and the appropriate mutated amplicon at a 1:9 ration. Transformants were selected on -Leu -Ura plates that selected only for the recombined plasmid and the *HRD2-URA3 CEN* plasmid. Transformants were grown for three days before observation beneath a GFP visualizing platform described elsewhere (Cronin, S. R., and Hampton, R. Y., 1999). Dim colonies were picked and patched to -Leu -Ade, -Leu -Lys, or -Leu -Tyr plates for Ade1, Lys1, and Aro7 mutants, respectively. Plates with transformants were then allowed to grow overnight at room temperature before rescreening for and picking of additional dim colonies. In this stage, only putatively functional mutants support outgrowth of patches.

Grown patches were then streaked to both -Leu -Ura and -Lue 5-FOA plates for overnight growth. Throughout the following day, corresponding patches were monitored for increased fluorescence on the -Leu 5-FOA plates. Patches bearing putative substrates were then repatched from -Leu -Ura and -Leu 5FOA to -Lue plates. The next day, direct side-by-side comparisons were made,

and patches that were brighter after counterselection were isolated for flow cytometry, plasmid isolation, and *CEN* excision, as described elsewhere (Flagg et al., 2019).

Flow Cytometry

GFP fluorescence was measured using a BD Accuri C6 flow cytometer (BD Biosciences) as previously described (Garza et al., 2009). 10,000 cells are analyzed in all readings. Statistics were recorded from BD Accuri software.

***In Vivo* stabilization by glycerol**

Relevant yeast strains were grown into log phase, pelleted at 5,000 rpm in a microcentrifuge for five minutes, then resuspended in YNB -Leu +20% glycerol medium. Time zero fluorescnce readings were then taken on a flow cytometer. Cells were then incubated for 6 hours at 30° C with aeration, after which final reading were taken on a flow cytometer. All readings represent 10,000 cells.

Whole Cell Lysates and Western Blotting

At each timepoint, three OD eq of cells were harvested and centrifuged at 14,000 x g for 2 min. Cell pellets were then resuspended in 100 µL SUME buffer (1% SDS, 8 M urea, 10 mM MOPS, 10 mM EDTA, pH 6.8) with protease inhibitors (1 mM phenylmethylsulfonyl fluoride, 260 mM 4-(2-aminoethyl) benzenesulfonyl fluoride hydrochloride, 100 mM leupeptin hemisulfate, 76 mM pepstatin A, 5 mM 6-aminocaproic acid, 5 mM benzamidine, and 142 mM TPCK). Silica beads were then added, and cells were lysed on a multivortexer (three repeats of 1 minute of vortexing at room temperature followed by 1 min on ice). 100 µL of 2X urea sample buffer (8 M urea, 4% SDS, 200 mM dithiothreitol, 125 mM Tris, pH 6.8) was added to each lysed sample, which were then boiled at 95° C for 8 minutes and centrifuged at 14,000 x g for 5 min.

Samples were resolved on 10% acrylamide gels by SDS-PAGE, transferred to nitrocellulose in 13% methanol, and blotted with mouse monoclonal anti-GFP antibody (Living Colors) or anti-PGK1 antibody (Molecular Probes) followed by goat anti-mouse HRP-conjugated secondary antibody (Jackson ImmunoResearch).

Cycloheximide Chase

Cycloheximide chases were performed as described elsewhere (Sato et al., 2009). Yeast strains were grown in minimal media to early log phase (OD_{600} < 0.3) prior to the addition of cycloheximide at a final concentration of 50 µg/mL. In MG132 experiments, MG132 was added to 25 µg/mL, or an equal volume of DMSO vehicle control was used. Samples were taken at the indicated time points and subjected to lysis, resolution by SDS-PAGE, and immunoblotting.

***In Vivo* Stabilization by Trp**

Cells were grown in minimal media to log phase, then diluted to ~0.05 OD. Cells were then incubated for an additional one to two hours to allow stabilization of Aro7 and Aro7-mutant steady-state levels. The appropriate dosage of Trp was then spike into the medium from a 2mM solution. Steady-state fluorescence levels were then monitored by flow cytometry.

ACKNOWLEDGEMENTS

Chapter IV, in full, is currently being prepared for submission to ELife. Matthew P. Flagg, Breanna Lam, Yousif I. Slaiwa, Andy Kao, Darren K. Lam, Randolph Y. Hampton. The dissertation author was the primary investigator and first author of this paper, and permission from all other authors has been obtained.

Figure 4.1: The Structure-Misfunction screen.

(A) Generation of a colony-based mutant library. Schematic depicting how random mutagenesis (left) can be paired with yeast recombination cloning (middle) to generate hundreds of colonies, each bearing a unique mutant (right).

(B) Secondary screen for proteasome dependence. Schematic depicting the workflow of the HRD2-counterselection methodology. Yeast colonies with low fluorescence bear a putative substrate (left). These are subjected to 5-FOA counterselection (middle arrow), which leads to the loss of HRD2. The resultant, proteasome-deficient hrd2-1 strain is bright if it bears a PQC substrate (right).

(C) The secondary screen yields a strong optical phenotype. HRD2/hrd2-1 strains bearing GFP, an empty vector (EV), or the cytosolic PQC substrate ΔssCPY*-GFP were spotted onto plates before and after 5-FOA counterselection. Plates were then imaged using an Amersham Typhoon scanner. Image is in greyscale where dark pixels indicate bright fluorescence.

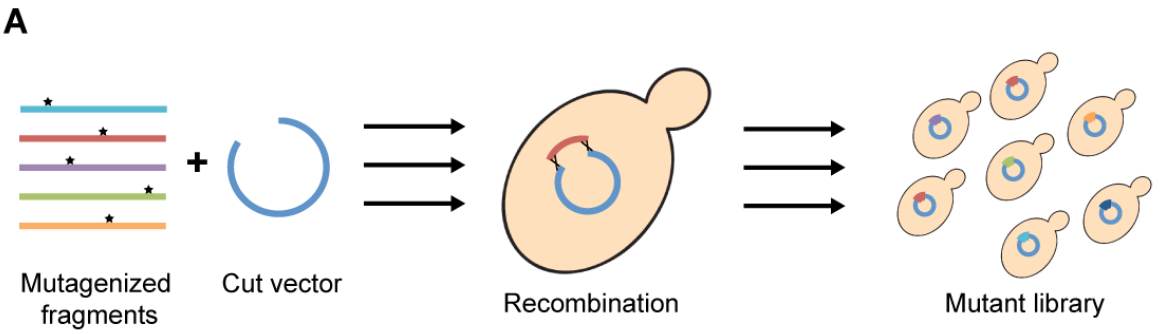
A
Mutagenized fragments
Cut vector
Recombination
Mutant library

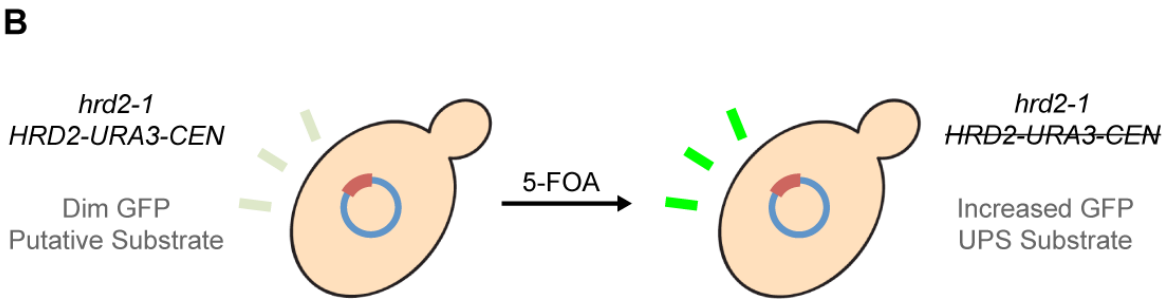
B
hrd2-1
HRD2-URA3-CEN
Dim GFP
Putative Substrate
5-FOA
hrd2-1
HRD2-URA3-CEN
Increased GFP
UPS Substrate

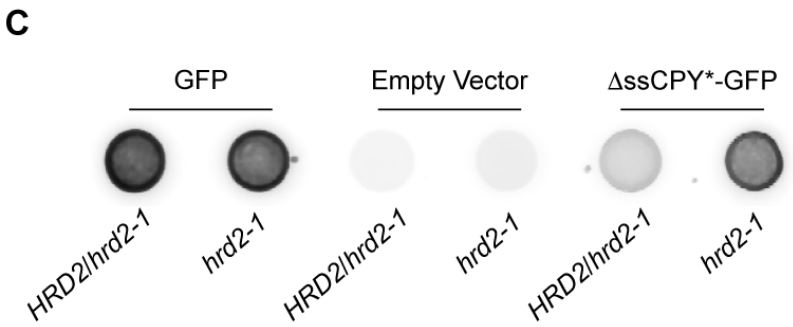
C
GFP
Empty Vector
ΔssCPY*-GFP
HRD2/hrd2-1
hrd2-1
HRD2/hrd2-1
hrd2-1
HRD2/hrd2-1
hrd2-1

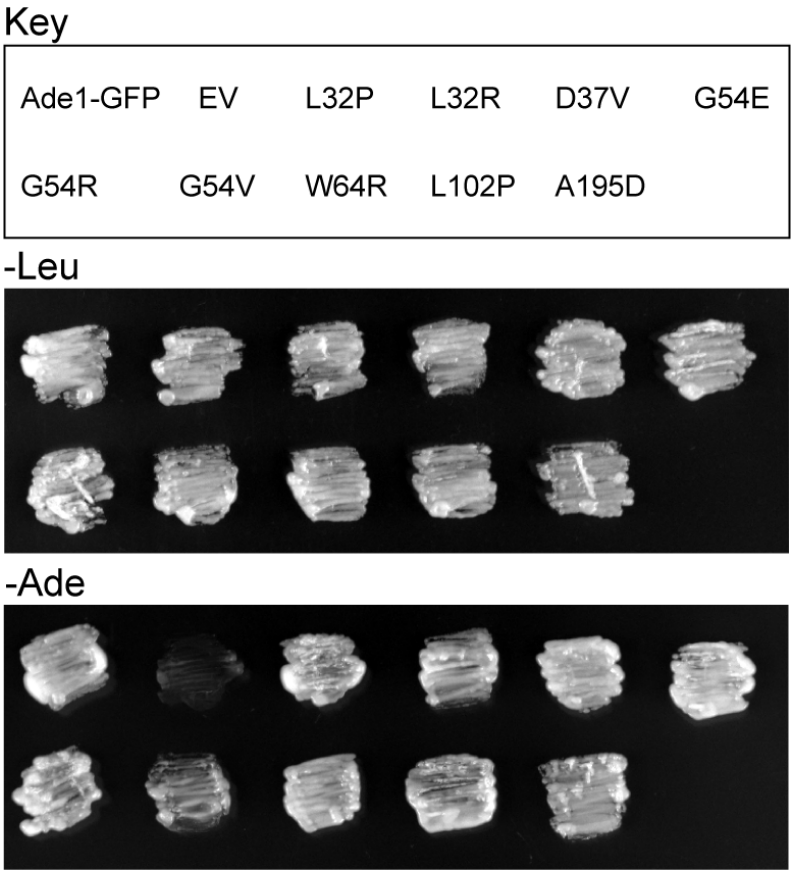

Figure 4.2: Ade1 mutants retain function.

Ade1Δ strains were transformed with WT Ade1-GFP, an empty vector (EV), or the indicated Ade1 mutant (top). Resultant strains were then patched onto plates that were permissive for growth (-Leu) or plates that required Ade1 function for growth (-Ade). Cells were grown for two days at 30° C before imaging.

Figure 4.3: Degradation of Ade1 mutants is proteasome dependent.

(A-B) Ade1-L32P-GFP and Ade1-L32R-GFP are stabilized by the proteasome inhibitor MG132. *pdr5Δ* strains expressing either Ade1-L32P-GFP (A) or Ade1-L32R-GFP (B) were grown into log phase and treated with either MG132 (25 µg/mL) or vehicle control (DMSO). Cycloheximide (CHX) was then added to assay for degradation. After adding CHX, cells were collected and lysed at the indicated times. Lysates were analyzed by SDS-PAGE and immunoblotting with α-GFP and α-Pgk1. FIJI was used to perform densitometry. GFP densitometry was normalized to Pgk1 densitometry, and timepoints were normalized to t=0, which is shown as 100% protein remaining. Data plotted are mean ± SD from three experiments.

(C) Remaining Ade1 mutants are also stabilized by the proteasome inhibitor MG132. *pdr5Δ* strains expressing the indicated Ade1-GFP mutant were subjected to CHX. After adding CHX, cells were assayed for fluorescence by flow cytometry. At each timepoint, the mean fluorescence of 10,000 cells was measured. t=0 was taken as 100%, and data plotted are the mean ± SD from three experiments.

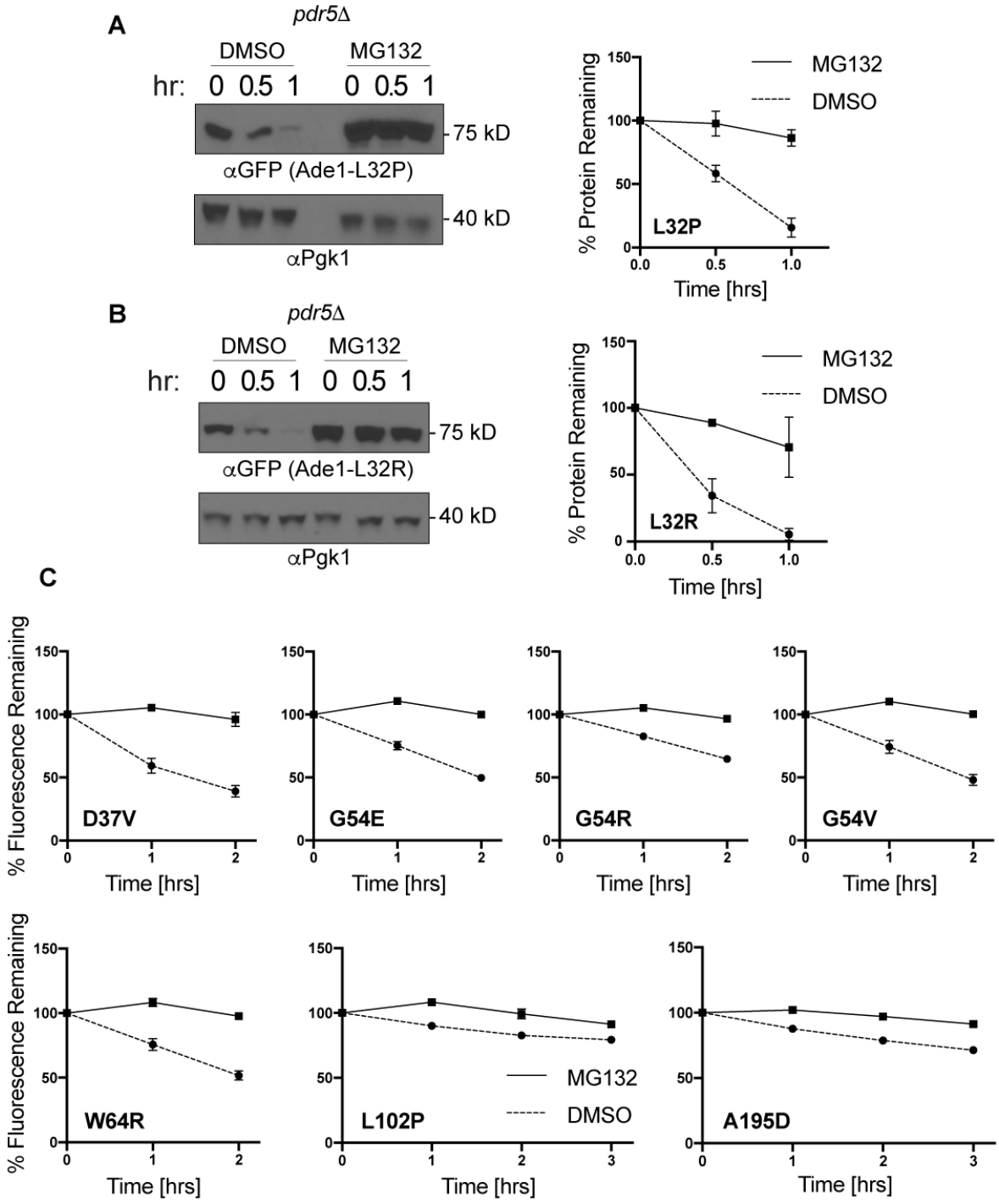
A
pdr5Δ
DMSO
MG132
hr: 0 0.5 1 0 0.5 1
75 kD
αGFP (Ade1-L32P)
40 kD
αPgk1
% Protein Remaining
MG132
DMSO
L32P
Time [hrs]
B
pdr5Δ
DMSO
MG132
hr: 0 0.5 1 0 0.5 1
75 kD
αGFP (Ade1-L32R)
40 kD
αPgk1
% Protein Remaining
MG132
DMSO
L32R
Time [hrs]
C
% Fluorescence Remaining
D37V
G54E
G54R
G54V
W64R
L102P
A195D
MG132
DMSO
Time [hrs]

Figure 4.4: Ade1 mutants are recognized by San1, Ubr1, and Doa10.

(A) Ade1-D37V-GFP is a San1-Ubr1-Doa10 substrate. WT, *san1Δ*, *ubr1Δ*, and *doa10Δ* (i) or WT, *san1Δubr1Δ*, and *doa10Δsan1Δubr1Δ* expressing Ade1-D37V-GFP were subjected to CHX. Cells were collected at the indicated times and subjected to flow cytometry. At each timepoint, the mean fluorescence of 10,000 cells was measured. t=0 was taken as 100%, and data plotted are the mean ± SD from three experiments.

(B) Ade1-G54E-GFP is a San1-Ubr1-Doa10 substrate. WT, *san1Δ*, *ubr1Δ*, and *doa10Δ* (i) or WT, *san1Δubr1Δ*, and *doa10Δsan1Δubr1Δ* expressing Ade1-G54E-GFP were subjected to CHX. Cells were collected at the indicated times and subjected to flow cytometry. At each timepoint, the mean fluorescence of 10,000 cells was measured. t=0 was taken as 100%, and data plotted are the mean ± SD from three experiments.

(C) Ade1-W64R-GFP is a San1-Ubr1-Doa10 substrate. WT, *san1Δ*, *ubr1Δ*, and *doa10Δ* (i) or WT, *san1Δubr1Δ*, and *doa10Δsan1Δubr1Δ* expressing Ade1-W64R-GFP were subjected to CHX. Cells were collected at the indicated times and subjected to flow cytometry. At each timepoint, the mean fluorescence of 10,000 cells was measured. t=0 was taken as 100%, and data plotted are the mean ± SD from three experiments.

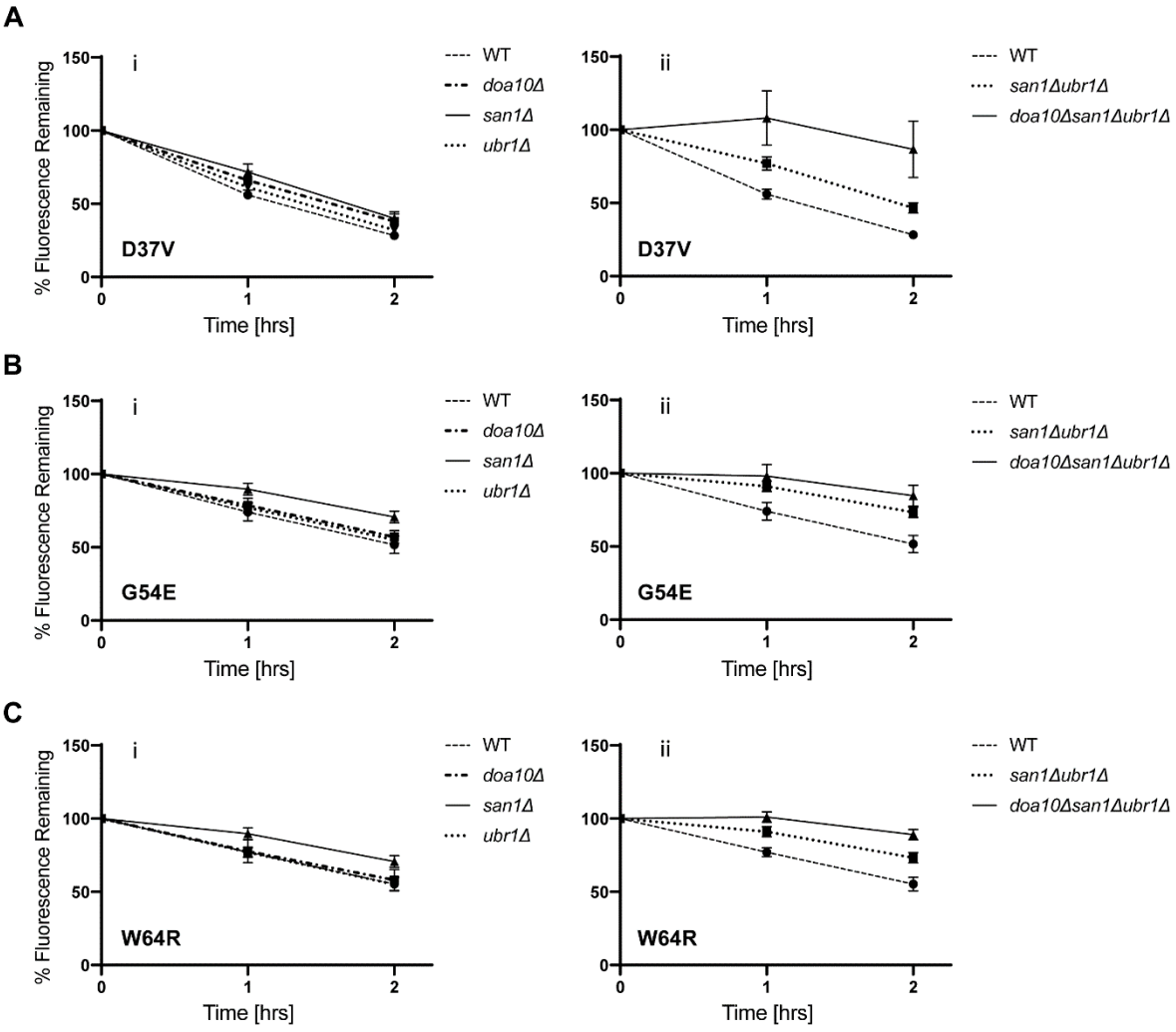
A
i
ii
% Fluorescence Remaining
Time [hrs]
D37V
WT
doa10Δ
san1Δ
ubr1Δ
san1Δubr1Δ
doa10Δsan1Δubr1Δ
B
G54E
C
W64R
0
50
100
150
1
2

Figure 4.5: Lys1 mutants are functional.

(A) A single copy of most Lys1 mutants support growth in the absence of lysine. *lys1Δ* strains were transformed with WT Lys1-GFP, an empty vector (EV), or the indicated Lys1 mutant (top) by single-copy genomic integration. Resultant strains were then patched onto plates that were permissive for growth (-Leu) or plates that required Lys1 function for growth (-Lys). Cells were grown at 30° C for two days on -Leu and four days for -Lys before imaging.

(B) Multiple copies of the remaining Lys1 mutants support growth in the absence of lysine. *lys1Δ* strains were transformed with WT Lys1-GFP, an empty vector (EV), or the indicated Lys1 mutant (top) on a multi-copy *CEN* plasmid. Resultant strains were then patched onto plates that were permissive for growth (-Leu) or plates that required Lys1 function for growth (-Lys). Cells were grown at 30° C for two days on -Leu and four days for -Lys before imaging.

A

Key: single-copy genomic integration

Lys1-GFP	EV	V26D	L29P	L146P
W151G	W151R	P194Q	I245N	W353R

-Leu

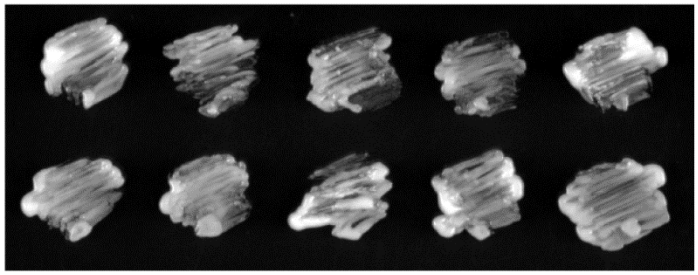

-Lys

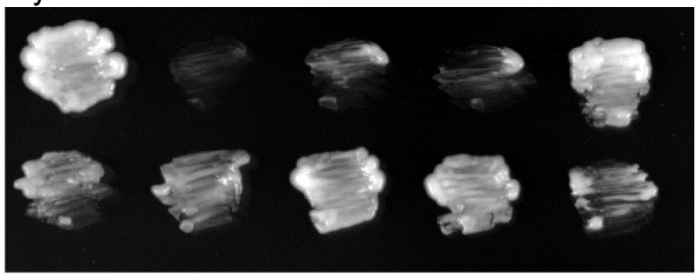

B

Key: multi-copy *CEN* plasmid

Lys1-GFP	EV	V26D	L29P
W151G	W151R	W353R	

-Leu

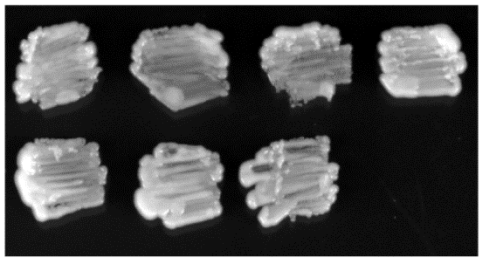

-Lys

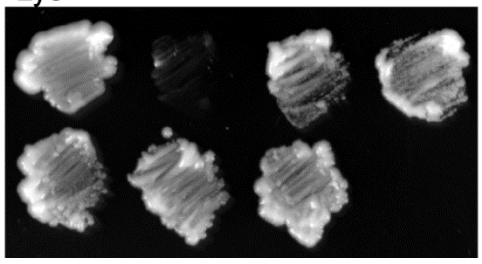

Figure 4.6: Lys1 mutant degradation is proteasome dependent.

(A-B) Lys1-V26D-GFP and Ade1-L29P-GFP are stabilized by the proteasome inhibitor MG132. *pdr5Δ* strains expressing either Lys1-V26D-GFP (A) or Lys1-L29P-GFP (B) were grown into log phase and treated with either MG132 (25 µg/mL) or vehicle control (DMSO) then subjected to CHX. Cells were then collected and lysed at the indicated times. Lysates were analyzed by SDS-PAGE and immunoblotting with α-GFP and α-Pgk1. FIJI was used to perform densitometry. GFP densitometry was normalized to Pgk1 densitometry, and timepoints were normalized to t=0, which is shown as 100% protein remaining. Data plotted are mean ± SD from three experiments.

(C) Remaining Lys1 mutants are also stabilized by the proteasome inhibitor MG132. *pdr5Δ* strains expressing the indicated Lys1-GFP were subjected to CHX. After adding CHX, cells were assayed for fluorescence by flow cytometry. At each timepoint, the mean fluorescence of 10,000 cells was measured. t=0 was taken as 100%, and data plotted are the mean ± SD from three experiments.

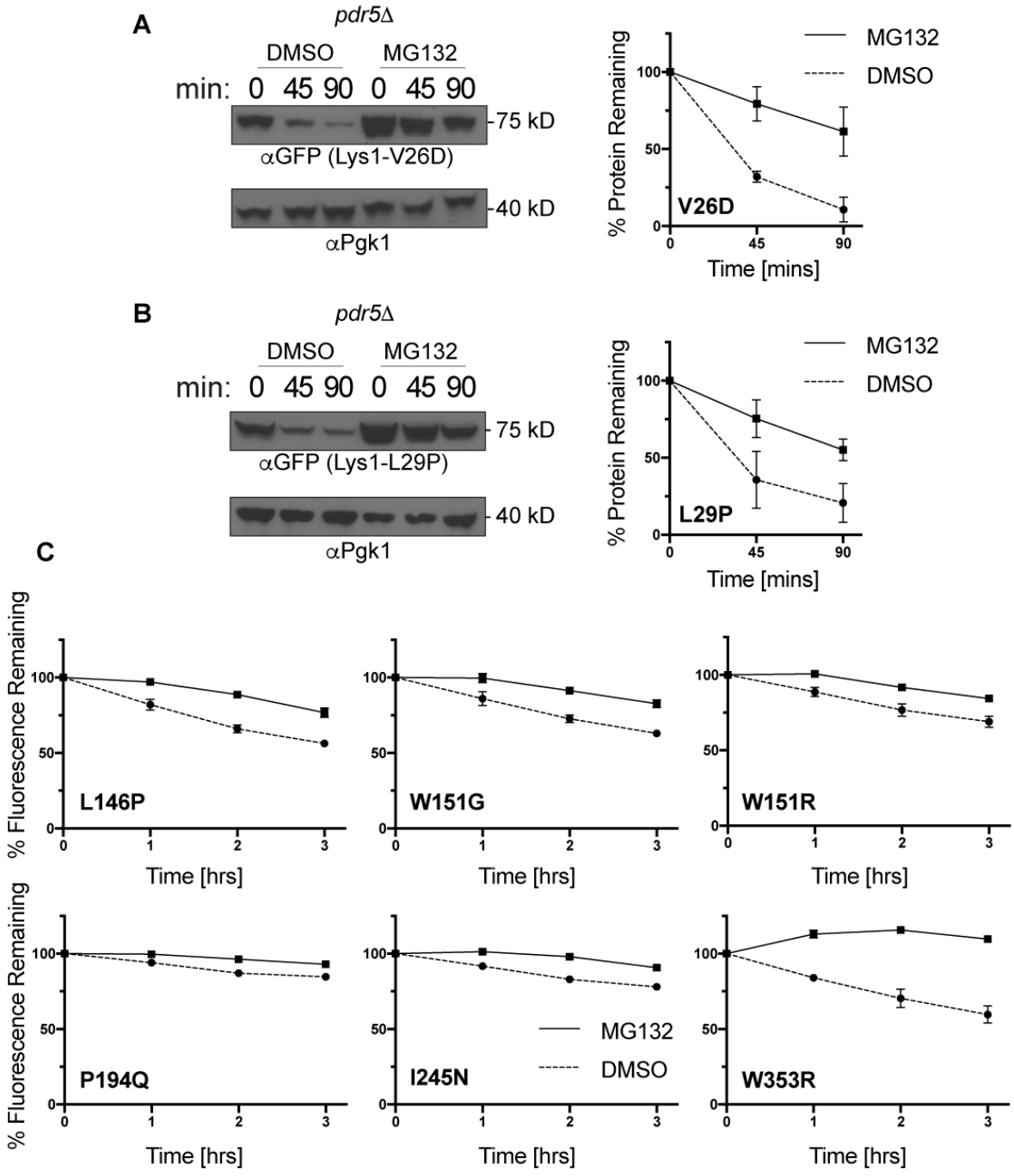
A
pdr5Δ
DMSO
MG132
min: 0 45 90 0 45 90
75 kD
αGFP (Lys1-V26D)
40 kD
αPgk1
% Protein Remaining
MG132
DMSO
V26D
Time [mins]
B
pdr5Δ
DMSO
MG132
min: 0 45 90 0 45 90
75 kD
αGFP (Lys1-L29P)
40 kD
αPgk1
% Protein Remaining
MG132
DMSO
L29P
Time [mins]
C
% Fluorescence Remaining
L146P
W151G
W151R
P194Q
I245N
W353R
MG132
DMSO
Time [hrs]

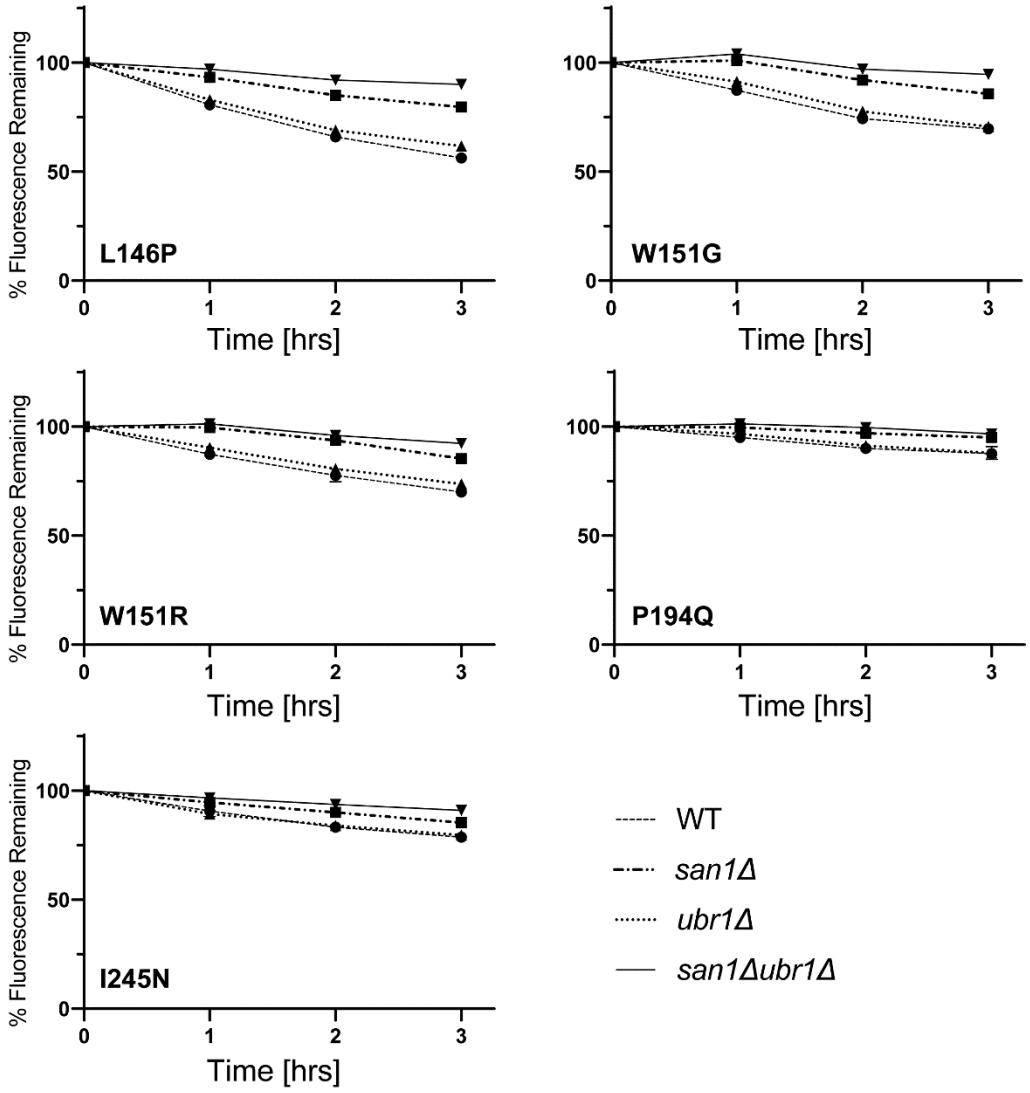

Figure 4.7: Mutations in domain II of Lys1 are recognized by San1 and Ubr1.

WT, *san1Δ*, *ubr1Δ*, and *san1Δubr1Δ* strains expressing the indicated mutant were subjected to CHX. Cells were then collected at the indicated times and subjected to flow cytometry. At each timepoint, the mean fluorescence of 10,000 cells was measured. t=0 was taken as 100%, and data plotted are the mean ± SD from three experiments.

Figure 4.8: Mutations in domain I of Lys1 are recognized by two distinct PQC pathways.

(A) Lys1-W353R-GFP is a San1-Ubr1 substrate. WT, *san1Δ*, *ubr1Δ*, and *san1Δubr1Δ* strains expressing Lys1-W353R-GFP were subjected to CHX. Cells were collected at the indicated times and subjected to flow cytometry. At each timepoint, the mean fluorescence of 10,000 cells was measured. t=0 was taken as 100%, and data plotted are the mean ± SD from three experiments.

(B-C) Lys1-V26D-GFP and Lys1-L29P-GFP degradation is San1 and Ubr1 independent. WT and *san1Δubr1Δ* strains expressing Lys1-V26D-GFP (B) or Lys1-L29P-GFP (C) were subjected to CHX. Cells were then collected and lysed at the indicated times. Lysates were analyzed by SDS-PAGE and immunoblotting with α-GFP and α-Pgk1. FIJI was used to perform densitometry. Data plotted are mean ± SD from three experiments.

(D) Lys1-I36D-GFP degradation is proteasome dependent. A *pdr5Δ* strains expressing Lys1-I36D-GFP (A) was treated with either MG132 (25 μg/mL) or vehicle control (DMSO) then subjected to CHX. Cells were then collected and lysed at the indicated times. Lysates were analyzed by SDS-PAGE and immunoblotting with α-GFP and α-Pgk1. FIJI was used to perform densitometry. Data plotted are mean ± SD from three experiments.

(E) Lys1-I36D-GFP degradation is San1 and Ubr1 independent. WT and *san1Δubr1Δ* strains expressing Lys1-I36D-GFP were subjected to CHX. Cells were collected and lysed at the indicated times. Lysates were analyzed by SDS-PAGE and immunoblotting with α-GFP and α-Pgk1. FIJI was used to perform densitometry. Data plotted are mean ± SD from three experiments.

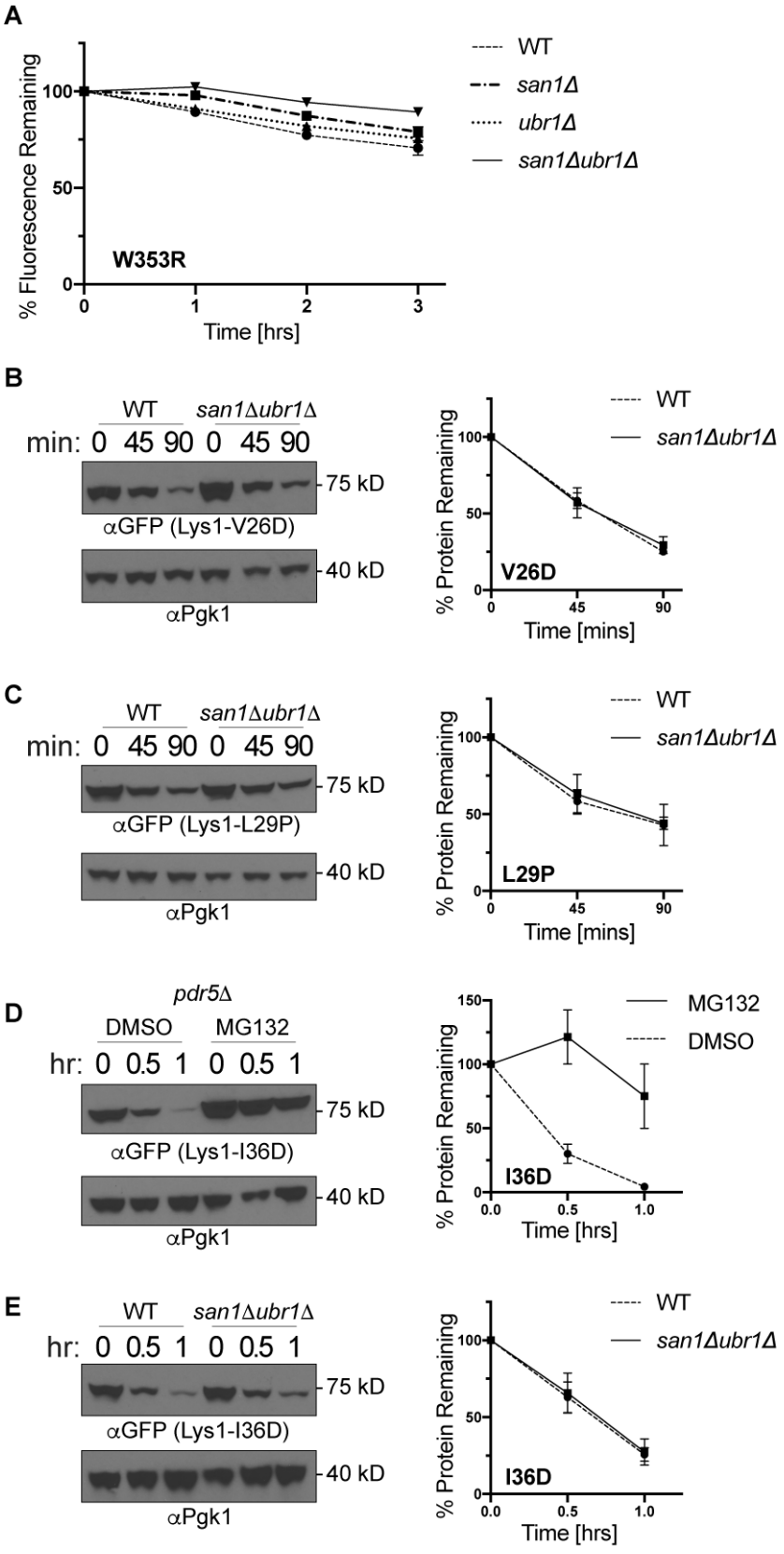
A
WT
san1Δ
ubr1Δ
san1Δubr1Δ
% Fluorescence Remaining
100
50
0
W353R
0
1
2
3
Time [hrs]
B
WT
san1Δubr1Δ
min: 0 45 90 0 45 90
75 kD
αGFP (Lys1-V26D)
40 kD
αPgk1
WT
san1Δubr1Δ
% Protein Remaining
100
50
0
V26D
0
45
90
Time [mins]
C
WT
san1Δubr1Δ
min: 0 45 90 0 45 90
75 kD
αGFP (Lys1-L29P)
40 kD
αPgk1
WT
san1Δubr1Δ
% Protein Remaining
100
50
0
L29P
0
45
90
Time [mins]
D
pdr5Δ
DMSO
MG132
hr: 0 0.5 1 0 0.5 1
75 kD
αGFP (Lys1-I36D)
40 kD
αPgk1
MG132
DMSO
% Protein Remaining
150
100
50
0
I36D
0.0
0.5
1.0
Time [hrs]
E
WT
san1Δubr1Δ
hr: 0 0.5 1 0 0.5 1
75 kD
αGFP (Lys1-I36D)
40 kD
αPgk1
WT
san1Δubr1Δ
% Protein Remaining
100
50
0
I36D
0.0
0.5
1.0
Time [hrs]

Figure 4.9: All destabilizing mutations at Lys1 position 151 are recognized by San1 and Ubr1.

WT, *san1Δ*, *ubr1Δ*, and *san1Δubr1Δ* strains expressing the indicated mutant were subjected to CHX. Cells were then collected at the indicated times and subjected to flow cytometry. At each timepoint, the mean fluorescence of 10,000 cells was measured. t=0 was taken as 100%, and data plotted are the mean ± SD from three experiments.

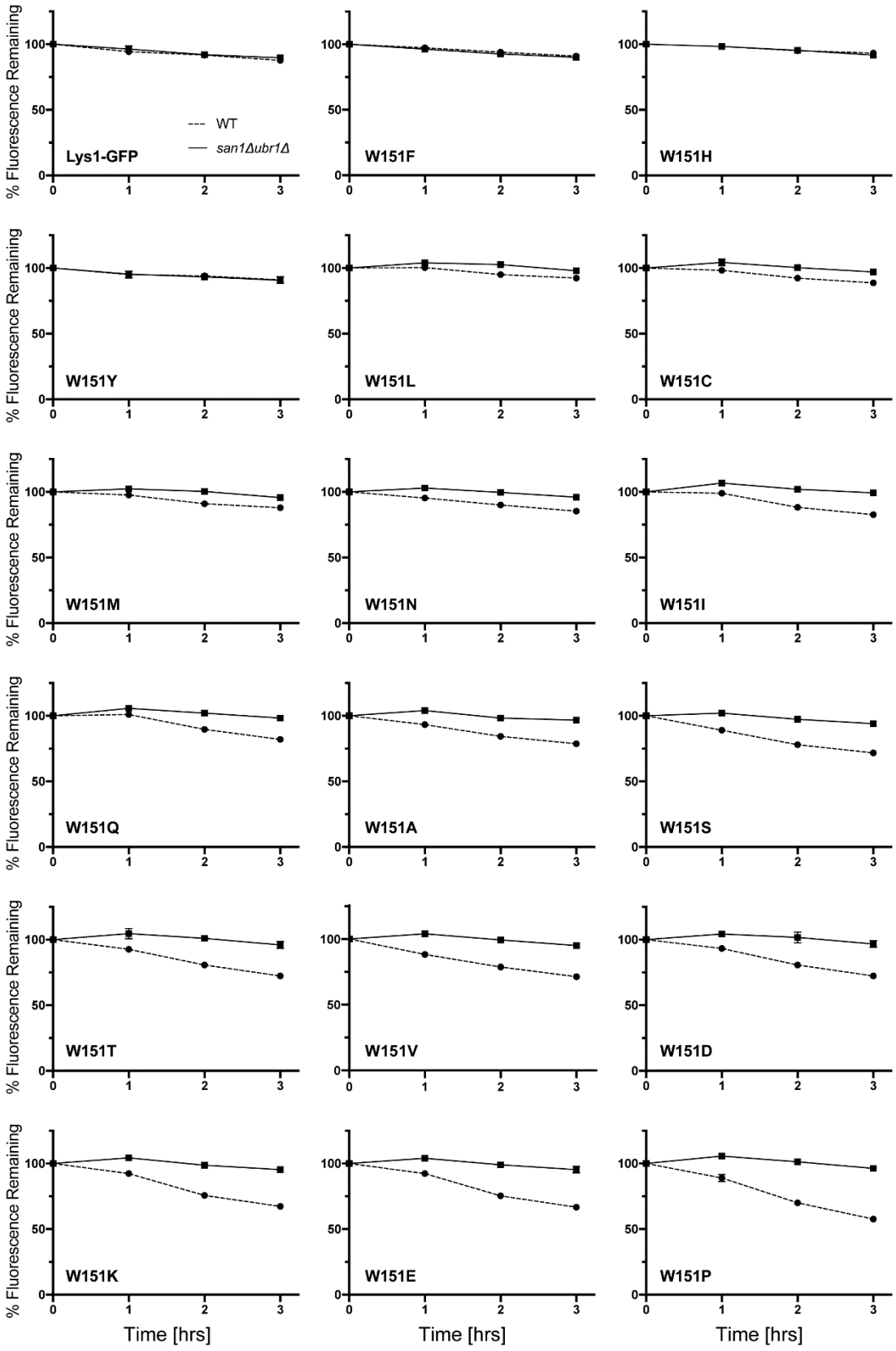
% Fluorescence Remaining
100
50
0
0
1
2
3
--- WT
—— san1Δubr1Δ
Lys1-GFP
W151F
W151H
W151Y
W151L
W151C
W151M
W151N
W151I
W151Q
W151A
W151S
W151T
W151V
W151D
W151K
W151E
W151P
Time [hrs]

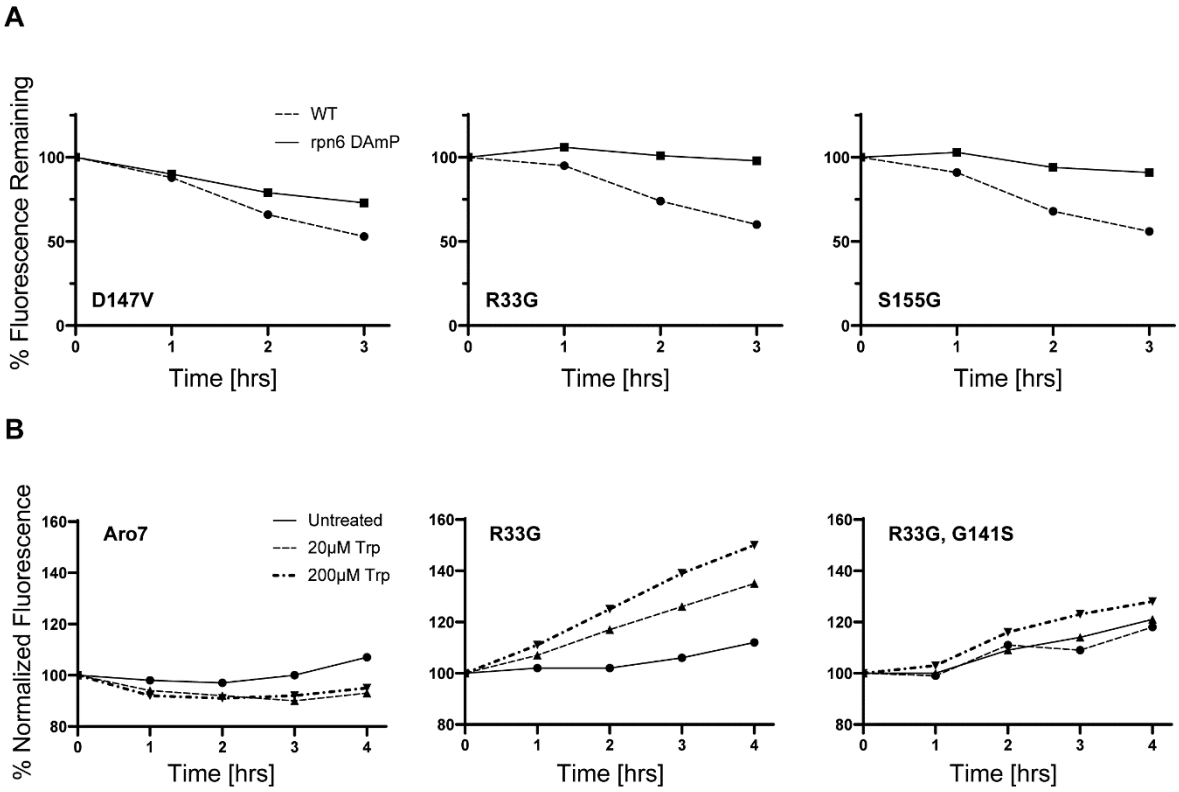

Figure 4.10: Aro7 mutants are degraded by the UPS and stabilized by Trp *in vivo*.

(A) Degradation of Aro7 mutants is proteasome dependent. WT or proteasome-deficient rpn6-DAmP strains expressing the indicated Aro7 mutants were subjected to CHX. Cells were collected at the indicated times and subjected to flow cytometry. At each timepoint, the mean fluorescence of 10,000 cells was measured. t=0 was taken as 100%, and data plotted are the mean of one experiment.

(B) Aro7-R33G-GFP is stabilized by allosteric Trp binding. WT cells expressing Aro7-GFP, Aro7-R33G-GFP, or Aro7-R33G, G141S-GFP were grown into log phase then spiked with the indicated amount of trp. Cells were then subjected to flow cytometry at the indicated timepoints. Readings are normalized to t = 0 hrs and the mean fluorescence of 10,000 cells is shown from one experiment.

Tables

Table 4.1: Randomly selected *ade1* mutants.

Isolate	Mutation(s)	Nucleotide Position(s)	Nucleotide Change(s)
1	0	-	-
2	1	19bp	G to A
3	0	-	-
4	1	104bp	C to A
5	0	-	-
6	0	-	-
7	1	94bp	C to A
8	0	-	-
9	1	428bp	A to G
10	2	-	-
11	2	27bp; 295bp	C to T; A to G
12	0	583bp; 747bp	G to C; T to C
13	1	324bp	G to A
14	1	879bp	A to C
15	1	110bp	A to G
16	1	257bp	Deletion
17	0	-	-
18	0	-	-
19	0	-	-
20	1	322bp	T to A
21	0	-	-
22	0	-	-
23	2	407bp; 676bp	Deletion; C to T
24	0	-	-
25	0	-	-
26	2	207bp; 208bp	C to T; A to G
27	1	894bp	A to C
28	0	-	-
29	0	-	-
30	1	894bp	A to G
31	1	681bp	T to A
32	2	7bp; 496bp	A to G; G to T
33	0	-	-
34	1	413bp	C to T

Table 4.1 continued: Randomly selected *ade1*-mutant sequencing

Isolate	Mutation(s)	Nucleotide Position(s)	Nucleotide Change(s)
35	2	326bp; 777bp	T to C; T to C
36	0	-	-
37	0	-	-
38	0	-	-
39	3	34bp; 99bp; 633bp	T to A; T to G; C to G
40	0	-	-
41	0	-	-
42	0	-	-
43	0	-	-
44	2	6bp ; 43bp	A to G; G to A
45	0	-	-
46	1	76bp	G to A
47	0	-	-
48	0	-	-
49	0	-	-
50	0	-	-

Supplemental Figures

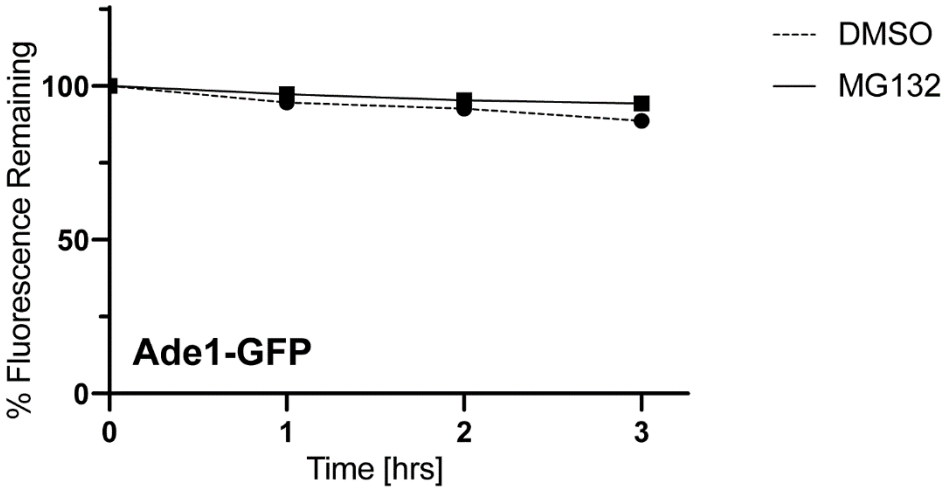

Figure 4.S1: Ade1-GFP is stable.

A *pdr5Δ* strains expressing Ade1-GFP mutant was subjected to CHX. After adding CHX, cells were assayed for fluorescence by flow cytometry. At each timepoint, the mean fluorescence of 10,000 cells was measured. t=0 was taken as 100%, and data plotted are the mean ± SD from three experiments.

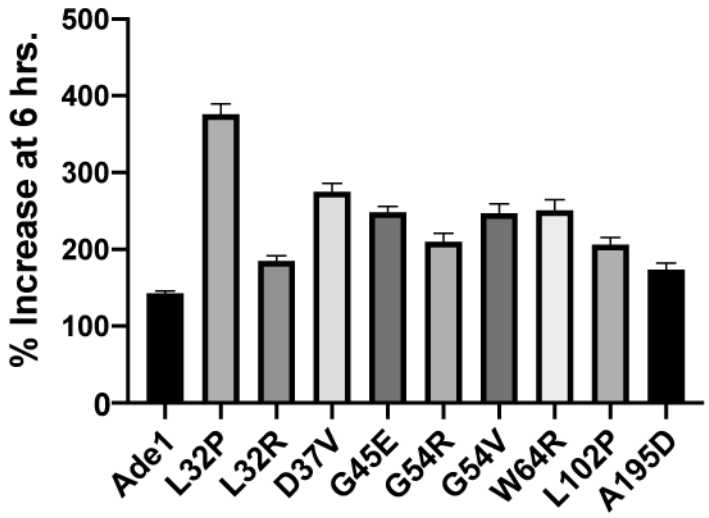

Figure 4.S2: Ade1 mutants are stabilized by glycerol *in vivo*.

WT strains expressing either Ade1-GFP or the indicated Ade1-GFP mutant were grown into log phase, pelleted, and resuspended in medium with 20% glycerol. Cell fluorescence was measured by flow cytometry immediately after transfer to glycerol-containing medium and after six hours of incubation at 30° C. Readings at six hours were then normalized to initial readings. Data plotted are the mean ± SEM from three experiments.

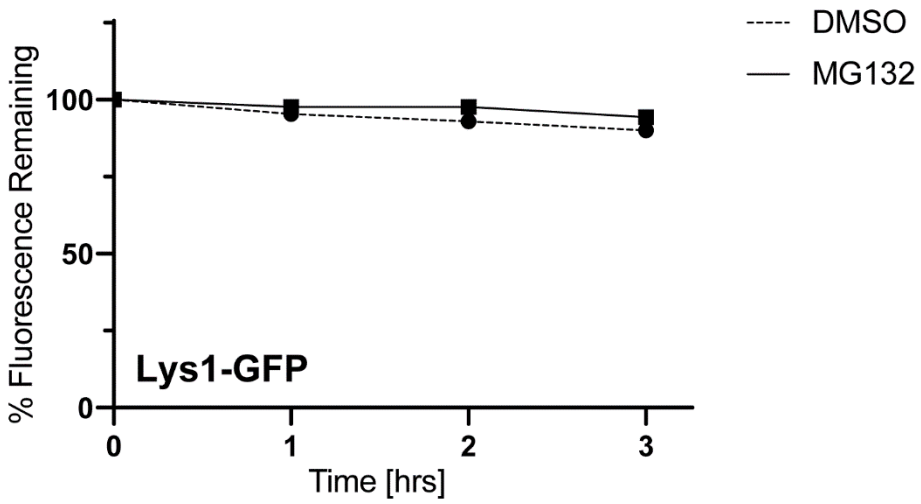

Figure 4.S3: Lys1-GFP is stable.

A *pdr5Δ* strains expressing Lys1-GFP mutant was subjected to CHX. After adding CHX, cells were assayed for fluorescence by flow cytometry. At each timepoint, the mean fluorescence of 10,000 cells was measured. t=0 was taken as 100%, and data plotted are the mean ± SD from three experiments.

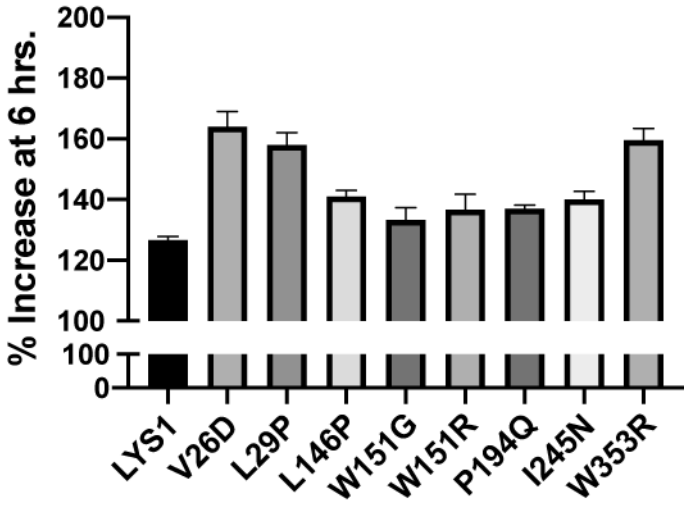

Figure 4.S2: Lys1 mutants are stabilized by glycerol *in vivo*.

WT strains expressing either Lys1-GFP or the indicated Lys1-GFP mutant were grown into log phase, pelleted, and resuspended in medium with 20% glycerol. Cell fluorescence was measured by flow cytometry immediately after transfer to glycerol-containing medium and after six hours of incubation at 30° C. Readings at six hours were then normalized to initial readings. Data plotted are the mean ± SEM from three experiments.

Supplemental Tables

Table 4.S1: Plasmids used in this study

Plasmid	Gene	Reference
pRH2940	ICE Plasmid *AED2-LUE2 pTDH3::ARO7-GFP::tADH1*	This study
pRH2941	YIp *AED2-LUE2 pTDH3::ARO7-GFP::tADH1*	This study
pRH2946	YCp *URA3 pHRD2::HRD2::tHRD2*	This study
pRH2961	YIp *AED2-LUE2 pTDH3::LYS1-GFP::tADH1*	This study
pRH3002	YIp *AED2-LUE2 pTDH3::lys1-W353R-GFP::tADH1*	This study
pRH3015	YIp *AED2-LUE2 pTDH3::lys1-L29P-GFP::tADH1*	This study
pRH3016	YIp *AED2-LUE2 pTDH3::lys1-V26D-GFP::tADH1*	This study
pRH3038	YIp *AED2-LUE2 pTDH3::lys1-L146P-GFP::tADH1*	This study
pRH3039	YIp *AED2-LUE2 pTDH3::lys1-W151G-GFP::tADH1*	This study
pRH3040	YIp *AED2-LUE2 pTDH3::lys1-W151R-GFP::tADH1*	This study
pRH3041	YIp *AED2-LUE2 pTDH3::lys1-W151P-GFP::tADH1*	This study
pRH3042	YIp *AED2-LUE2 pTDH3::lys1-W151E-GFP::tADH1*	This study
pRH3043	YIp *AED2-LUE2 pTDH3::lys1-W151S-GFP::tADH1*	This study
pRH3044	YIp *AED2-LUE2 pTDH3::lys1-W151T-GFP::tADH1*	This study
pRH3045	YIp *AED2-LUE2 pTDH3::lys1-W151C-GFP::tADH1*	This study
pRH3046	YIp *AED2-LUE2 pTDH3::lys1-W151L-GFP::tADH1*	This study
pRH3047	YIp *AED2-LUE2 pTDH3::lys1-W151H-GFP::tADH1*	This study
pRH3048	YIp *AED2-LUE2 pTDH3::lys1-W151Y-GFP::tADH1*	This study
pRH3053	YIp *AED2-LUE2 pTDH3::lys1-W151A-GFP::tADH1*	This study
pRH3054	YIp *AED2-LUE2 pTDH3::lys1-W151F-GFP::tADH1*	This study
pRH3055	YIp *AED2-LUE2 pTDH3::lys1-W151Q-GFP::tADH1*	This study
pRH3069	YIp *AED2-LUE2 pTDH3::lys1-W151V-GFP::tADH1*	This study
pRH3105	YIp *AED2-LUE2 pTDH3::lys1-P194Q-GFP::tADH1*	This study
pRH3128	YIp *AED2-LUE2 pTDH3::ADE1-GFP::tADH1*	This study
pRH3135	YIp *AED2-LUE2 pTDH3::lys1-I245N-GFP::tADH1*	This study
pRH3139	YIp *AED2-LUE2 pTDH3::aro7-R33G-GFP::tADH1*	This study
pRH3142	YIp *AED2-LUE2 pTDH3::aro7-D147G-GFP::tADH1*	This study
pRH3148	YIp *AED2-LUE2 pTDH3::ade1-D37V-GFP::tADH1*	This study
pRH3150	YIp *AED2-LUE2 pTDH3::ade1-W64R-GFP::tADH1*	This study
pRH3152	YIp *AED2-LUE2 pTDH3::ade1-G54E-GFP::tADH1*	This study
pRH3153	YIp *AED2-LUE2 pTDH3::ade1-L102P-GFP::tADH1*	This study
pRH3154	YIp *AED2-LUE2 pTDH3::ade1-L32P-GFP::tADH1*	This study
pRH3155	YIp *AED2-LUE2 pTDH3::ade1-L32R-GFP::tADH1*	This study
pRH3164	YCp *LUE2 pTDH3::lys1-V26D-GFP::tADH1*	This study

Plasmid	Gene	Reference
pRH3165	YCp *LUE2 pTDH3::lys1-L29P-GFP::tADH1*	This study
pRH3168	YIp *AED2-LUE2 pTDH3::ade1-A195D-GFP::tADH1*	This study
pRH3175	YIp *AED2-LUE2 pTDH3::aro7-R33G-G141S-GFP::tADH1*	This study
pRH3178	YIp *AED2-LUE2 pTDH3::ade1-G54V-GFP::tADH1*	This study
pRH3180	YIp *AED2-LUE2 pTDH3::ade1-G54R-GFP::tADH1*	This study
pRH3196	YCp *LUE2 pTDH3::lys1-W151G-GFP::tADH1*	This study
pRH3197	YCp *LUE2 pTDH3::lys1-W151R-GFP::tADH1*	This study
pRH3198	YCp *LUE2 pTDH3::lys1-W353R-GFP::tADH1*	This study
pRH3214	YIp *AED2-LUE2 pTDH3::lys1-W151D-GFP::tADH1*	This study
pRH3215	YIp *AED2-LUE2 pTDH3::lys1-W151I-GFP::tADH1*	This study
pRH3216	YIp *AED2-LUE2 pTDH3::lys1-W151K-GFP::tADH1*	This study
pRH3217	YIp *AED2-LUE2 pTDH3::lys1-W151M-GFP::tADH1*	This study
pRH3218	YIp *AED2-LUE2 pTDH3::lys1-W151N-GFP::tADH1*	This study

Table 4.S2: Yeast strains used in this study

Strain	Genotype	Reference
RHY7447	BY4741	
RHY7448	RHY7447 *san1Δ::NatMX*	Heck et al., 2010
RHY7449	RHY7447 *ubr1Δ::NatMX*	Deletion collection
RHY7450	RHY7447 *san1Δ::NatMX ubr1Δ::NatMX*	Deletion collection
RHY10500	BY4741 *pdr5Δ::KanMX*	Deletion collection
RHY10507	BY4741 *ade1Δ::KanMX*	Deletion collection
RHY10528	BY4741 *lys1Δ::KanMX*	Deletion collection
RHY11213	RHY10528 pRH3196 (*YCp LUE2 pTDH3::lys1-W151G-GFP::tADH1*)	This study
RHY11263	RHY7449 pRH3042	This study
RHY11322	pdr5 lys1 pRH2946	This study
RHY11361	RHY7447 pRH3015 (*YIp AED2-LUE2 pTDH3::lys1-L29P-GFP::tADH1*)	This study
RHY11364	RHY7450 pRH3015	This study
RHY11366	RHY7447 pRH3016 (*YIp AED2-LUE2 pTDH3::lys1-V26D-GFP::tADH1*)	This study
RHY11369	RHY7450 pRH3016	This study
RHY11371	RHY7447 pRH3038 (*YIp AED2-LUE2 pTDH3::lys1-L146P-GFP::tADH1*)	This study
RHY11372	RHY7448 pRH3038	This study
RHY11373	RHY7449 pRH3038	This study
RHY11374	RHY7450 pRH3038	This study
RHY11377	RHY7447 pRH3002 (YIp AED2-LUE2 pTDH3::lys1-W353R-GFP::tADH1)	This study
RHY11378	RHY7448 pRH3002	This study
RHY11379	RHY7449 pRH3002	This study
RHY11380	RHY7450 pRH3002	This study
RHY11411	RHY10500 pRH3015	This study
RHY11415	RHY10500 pRH3016	This study
RHY11419	RHY7447 pRH3047 (*YIp AED2-LUE2 pTDH3::lys1-W151H-GFP::tADH1*)	This study
RHY11420	RHY7450 pRH3047	This study
RHY11421	RHY7447 pRH3046 (*YIp AED2-LUE2 pTDH3::lys1-W151L-GFP::tADH1*)	This study
RHY11422	RHY7450 pRH3046	This study
RHY11423	RHY7447 pRH3048 (*YIp AED2-LUE2 pTDH3::lys1-W151Y-GFP::tADH1*)	This study
RHY11424	RHY7450 pRH3048	This study

Strain	Genotype	Reference
RHY11425	RHY7447 pRH3042 (*YIp AED2-LUE2 pTDH3::lys1-W151E-GFP::tADH1*)	This study
RHY11426	RHY7450 pRH3042	This study
RHY11427	RHY7447 pRH3039 (*YIp AED2-LUE2 pTDH3::lys1-W151G-GFP::tADH1*)	This study
RHY11428	RHY7448 pRH3039	This study
RHY11429	RHY7449 pRH3039	This study
RHY11429	RHY7447 pRH3040 (*YIp AED2-LUE2 pTDH3::lys1-W151R-GFP::tADH1*)	This study
RHY11430	RHY7450 pRH3039	This study
RHY11430	RHY7448 pRH3040	This study
RHY11431	RHY7449 pRH3040	This study
RHY11431	RHY7447 pRH3043 (*YIp AED2-LUE2 pTDH3::lys1-W151S-GFP::tADH1*)	This study
RHY11432	RHY7450 pRH3040	This study
RHY11432	RHY7450 pRH3043	This study
RHY11433	RHY7447 pRH3053 (*YIp AED2-LUE2 pTDH3::lys1-W151A-GFP::tADH1*)	This study
RHY11434	RHY7450 pRH3053	This study
RHY11435	RHY7447 pRH3054 (*YIp AED2-LUE2 pTDH3::lys1-W151F-GFP::tADH1*)	This study
RHY11436	RHY7450 pRH3054	This study
RHY11437	RHY7447 pRH3055 (*YIp AED2-LUE2 pTDH3::lys1-W151Q-GFP::tADH1*)	This study
RHY11438	RHY7448 pRH3055	This study
RHY11488	RHY7447 pRH3069 (*YIp AED2-LUE2 pTDH3::lys1-W151V-GFP::tADH1*)	This study
RHY11489	RHY7450 pRH3069	This study
RHY11709	RHY10528 pRH3038	This study
RHY11711	RHY10528 pRH3105 (*YCp LUE2 pTDH3::lys1-P194Q-GFP::tADH1*)	This study
RHY11712	RHY10528 pRH3135 (*YCp LUE2 pTDH3::lys1-I245N-GFP::tADH1*)	This study
RHY11713	RHY10528 pRH3002	This study
RHY11717	pdr5 ade1 pRH2946	This study
RHY11790	pdr5 aro7 pRH2946	This study
RHY11848	RHY7447 pRH3135	This study
RHY11849	RHY7448 pRH3135	This study
RHY11850	RHY7449 pRH3135	This study
RHY11851	RHY7450 pRH3135	This study

Strain	Genotype	Reference
RHY11874	RHY7447 pRH3105	This study
RHY11875	RHY7448 pRH3105	This study
RHY11876	RHY7449 pRH3105	This study
RHY11877	RHY7450 pRH3105	This study
RHY11909	RHY7447 pRH3148 (YIp *AED2-LUE2 pTDH3::ade1-D37V-GFP::tADH1)*	This study
RHY11910	RHY7448 pRH3148	This study
RHY11964	RHY7447 pRH3150 (*YIp AED2-LUE2 pTDH3::ade1-W64R-GFP::tADH1*)	This study
RHY11965	RHY7448 pRH3150	This study
RHY11969	RHY7447 pRH3152 (*YIp AED2-LUE2 pTDH3::ade1-G54E-GFP::tADH1*)	This study
RHY11970	RHY7448 pRH3152	This study
RHY11995	RHY7447 pRH3153 (*YIp AED2-LUE2 pTDH3::ade1-L102P-GFP::tADH1*)	This study
RHY11996	RHY7448 pRH3153	This study
RHY12028	RHY10500 pRH3148	This study
RHY12037	RHY7447 pRH3154 (*YIp AED2-LUE2 pTDH3::ade1-L32P-GFP::tADH1*)	This study
RHY12038	RHY7448 pRH3154	This study
RHY12042	RHY7447 pRH3155 (*YIp AED2-LUE2 pTDH3::ade1-L32R-GFP::tADH1*)	This study
RHY12043	RHY7448 pRH3155	This study
RHY12049	RHY10507 pRH3148	This study
RHY12050	RHY10507 pRH3150	This study
RHY12051	RHY10507 pRH3152	This study
RHY12052	RHY10507 pRH3153	This study
RHY12053	RHY10507 pRH3154	This study
RHY12054	RHY10507 pRH3155	This study
RHY12055	RHY10507 pRH3168	This study
RHY12056	RHY10528 oRH3165 (*YCp LUE2 pTDH3::lys1-V26D-GFP::tADH1*)	This study
RHY12057	RHY10528 oRH3165 (*YCp LUE2 pTDH3::lys1-L29P-GFP::tADH1*)	This study
RHY12072	RHY7447 pRH3168 (*YIp AED2-LUE2 pTDH3::ade1-A195D-GFP::tADH1*)	This study
RHY12073	RHY7448 pRH3168	This study
RHY12083	RHY10500 pRH3154	This study
RHY12084	RHY10500 pRH3155	This study

Strain	Genotype	Reference
RHY12099	RHY7447 pRH3178 (*YIp AED2-LUE2 pTDH3::ade1-G54V-GFP::tADH1*)	This study
RHY12100	RHY7448 pRH3178	This study
RHY12103	RHY7447 pRH3180 (*YIp AED2-LUE2 pTDH3::ade1-G54R-GFP::tADH1*)	This study
RHY12104	RHY7448 pRH3180	This study
RHY12107	RHY10507 pRH3178	This study
RHY12108	RHY10507 pRH3180	This study
RHY12132	RHY10500 pRH3150	This study
RHY12133	RHY10500 pRH3152	This study
RHY12134	RHY10500 pRH3153	This study
RHY12135	RHY10500 pRH3168	This study
RHY12136	RHY10500 pRH3178	This study
RHY12137	RHY10500 pRH3180	This study
RHY12138	RHY10500 pRH3038	This study
RHY12139	RHY10500 pRH3039	This study
RHY12140	RHY10500 pRH3040	This study
RHY12141	RHY10500 pRH3105	This study
RHY12142	RHY10500 pRH3135	This study
RHY12143	RHY10500 pRH3002	This study
RHY12214	RHY10528 pRH3197 (*YCp LUE2 pTDH3::lys1-W151R-GFP::tADH1*)	This study
RHY12248	RHY7448 pRH3043	This study
RHY12249	RHY7448 pRH3069	This study
RHY12250	RHY7448 pRH3044 (YIp AED2-LUE2 pTDH3::lys1-W151T-GFP::tADH1)	This study
RHY12251	RHY7449 pRH3043	This study
RHY12252	RHY7449 pRH3069	This study
RHY12253	RHY7449 pRH3044	This study
RHY12254	RHY7447 pRH3216 (*YIp AED2-LUE2 pTDH3::lys1-W151K-GFP::tADH1*)	This study
RHY12255	RHY7448 pRH3216	This study
RHY12256	RHY7449 pRH3216	This study
RHY12257	RHY7450 pRH3216	This study
RHY12258	RHY7447 pRH3214 (*YIp AED2-LUE2 pTDH3::lys1-W151D-GFP::tADH1*)	This study
RHY12259	RHY7448 pRH3214	This study
RHY12260	RHY7449 pRH3214	This study
RHY12261	RHY7450 pRH3214	This study

Strain	Genotype	Reference
RHY12262	RHY7448 pRH3042	This study
RHY12264	RHY7449 pRH3055	This study
RHY12265	RHY7450 pRH3055	This study
RHY12266	RHY7448 pRH3053	This study
RHY12267	RHY7449 pRH3053	This study
RHY12268	RHY7447 pRH3041 (*YIp AED2-LUE2 pTDH3::lys1-W151P-GFP::tADH1*)	This study
RHY12269	RHY7448 pRH3041	This study
RHY12270	RHY7449 pRH3041	This study
RHY12271	RHY7450 pRH3041	This study
RHY12272	RHY7447 pRH3215 (*YIp AED2-LUE2 pTDH3::lys1-W151I-GFP::tADH1*)	This study
RHY12273	RHY7448 pRH3215	This study
RHY12274	RHY7449 pRH3215	This study
RHY12275	RHY7450 pRH3215	This study
RHY12276	RHY7447 pRH3045 (*YIp AED2-LUE2 pTDH3::lys1-W151C-GFP::tADH1*)	This study
RHY12277	RHY7448 pRH3045	This study
RHY12278	RHY7449 pRH3045	This study
RHY12279	RHY7450 pRH3045	This study
RHY12280	RHY7447 pRH3217 (*YIp AED2-LUE2 pTDH3::lys1-W151M-GFP::tADH1*)	This study
RHY12281	RHY7448 pRH3217	This study
RHY12282	RHY7449 pRH3217	This study
RHY12283	RHY7450 pRH3217	This study
RHY12284	RHY7447 pRH3218 (*YIp AED2-LUE2 pTDH3::lys1-W151N-GFP::tADH1*)	This study
RHY12285	RHY7448 pRH3218	This study
RHY12286	RHY7449 pRH3218	This study
RHY12287	RHY7450 pRH3218	This study
RHY12292	RHY7447 pRH3044	This study
RHY12293	RHY7450 pRH3044	This study

References

Abildgaard, A. B., Stein, A., Nielsen, S. V., Schultz-Knudsen, K., Papaleo, E., Shrikhande, A., … Hartmann-Petersen, R. (2019). Computational and cellular studies reveal structural destabilization and degradation of mlh1 variants in lynch syndrome. ELife, 8.

Al-Saryi, N. A., Al-Hejjaj, M. Y., Van Roermund, C. W. T., Hulmes, G. E., Ekal, L., Payton, C., … Hettema, E. H. (2017). Two NAD-linked redox shuttles maintain the peroxisomal redox balance in Saccharomyces cerevisiae. Scientific Reports, 7(1), 11868.

Auton, M., & Bolen, D. W. (2015). Predicting the energetics of osmolyte-induced protein folding/unfolding. Proceedings of the National Academy of Sciences of the United States of America, 102(42), 15065–15068.

Bengtson, M. H., & Joazeiro, C. A. P. (2010). Role of a ribosome-associated E3 ubiquitin ligase in protein quality control. Nature, 467(7314), 470–473.

Biederer, T., Volkwein, C., & Sommer, T. (1996). Degradation of subunits of the Sec61p complex, an integral component of the ER membrane, by the ubiquitin-proteasome pathway. The EMBO Journal, 15(9), 2069–2076.

Burk, D. L., Hwang, J., Kwok, E., Marrone, L., Goodfellow, V., Dmitrienko, G. I., & Berghuis, A. M. (2007). Structural Studies of the Final Enzyme in the α-Aminoadipate Pathway-Saccharopine Dehydrogenase from Saccharomyces cerevisiae. Journal of Molecular Biology, 373(3), 745–754.

Chua, N. K., Howe, V., Jatana, N., Thukral, L., & Brown, A. J. (2017). A conserved degron containing an amphipathic helix regulates the cholesterol-mediated turnover of human squalene monooxygenase, a rate-limiting enzyme in cholesterol synthesis. Journal of Biological Chemistry, 292(49), 19959–19973.

Cronin, S. R., & Hampton, R. Y. (1999). Measuring protein degradation with green fluorescent protein. Methods in Enzymology, 302(1993), 58–73.

Dikic, I. (2017). Proteasomal and Autophagic Degradation Systems. Annual Review of Biochemistry, 86(1), 193–224.

Farzin Khosrow-Khavar, Fang, N. N., Ng, A. H. M., Winget, J. M., Comyn, S. A., & Mayor, T. (2012). The yeast ubr1 ubiquitin ligase participates in a prominent pathway that targets cytosolic thermosensitive mutants for degradation. G3: Genes, Genomes, Genetics, 2(5), 619–628.

Flagg, M. P., Kao, A., & Hampton, R. Y. (2019). Integrating after CEN Excision (ICE) Plasmids: Combining the ease of yeast recombination cloning with the stability of genomic integration. Yeast, 36(10), 593–605.

Foresti, O., Rodriguez-Vaello, V., Funaya, C., & Carvalho, P. (2014). Quality control of inner nuclear membrane proteins by the Asi complex. Science, 346(6210), 751–755.

Foresti, O., Ruggiano, A., Hannibal-Bach, H. K., Ejsing, C. S., & Carvalho, P. (2013). Sterol homeostasis requires regulated degradation of squalene monooxygenase by the ubiquitin ligase Doa10/Teb4. ELife, 2013(2), 1–17.

Fredrickson, E. K., Gallagher, P. S., Candadai, S. V. C., & Gardner, R. G. (2013). Substrate recognition in nuclear protein quality control degradation is governed by exposed hydrophobicity that correlates with aggregation and insolubility. Journal of Biological Chemistry, 288(9), 6130–6139.

Fredrickson, E. K., Rosenbaum, J. C., Locke, M. N., Milac, T. I., & Gardner, R. G. (2011). Exposed hydrophobicity is a key determinant of nuclear quality control degradation. Molecular Biology of the Cell, 22(13), 2384–2395.

Gardner, R. G., Nelson, Z. W., & Gottschling, D. E. (2005). Degradation-mediated protein quality control in the nucleus. Cell, 120(6), 803–815.

Garofalo, R., Wohlgemuth, I., Pearson, M., Lenz, C., Urlaub, H., & Rodnina, M. V. (2019). Broad range of missense error frequencies in cellular proteins. Nucleic Acids Research, 47(6), 2932–2945.

Garza, R. M., Tran, P. N., & Hampton, R. Y. (2009). Geranylgeranyl pyrophosphate is a potent regulator of HRD-dependent 3-hydroxy-3-methylglutaryl-CoA reductase degradation in yeast. Journal of Biological Chemistry, 284(51), 35368–35380.

Geffen, Y., Appleboim, A., Gardner, R. G., Friedman, N., Sadeh, R., & Ravid, T. (2016). Mapping the Landscape of a Eukaryotic Degronome. Molecular Cell, 63(6), 1055–1065.

Generoso, S. F., Giustiniano, M., La Regina, G., Bottone, S., Passacantilli, S., Di Maro, S., … Stornaiuolo, M. (2015). Pharmacological folding chaperones act as allosteric ligands of Frizzled4. Nature Chemical Biology, 11(4), 280–286.

Gilon, T., Chomsky, O., & Kulka, R. G. (2000). Degradation Signals Recognized by the Ubc6p-Ubc7p Ubiquitin-Conjugating Enzyme Pair. Molecular and Cellular Biology, 20(19), 7214–7219.

Guerois, R., Nielsen, J. E., & Serrano, L. (2002). Predicting changes in the stability of proteins and protein complexes: A study of more than 1000 mutations. Journal of Molecular Biology, 320(2), 369–387.

Guerriero, C. J., & Brodsky, J. L. (2012). The delicate balance between secreted protein folding and endoplasmic reticulum-associated degradation in human physiology. Physiological Reviews, 92(2), 537–576.

Hampton, R. Y., Gardner, R. G., & Rine, J. (1996). Role of 26S proteasome and HRD genes in the degradation of 3-hydroxy-3-methylglutaryl-CoA reductase, an integral endoplasmic reticulum membrane protein. Molecular Biology of the Cell, 7(12), 2029–2044.

Hawthorne, D. C., & Mortimer, R. K. (1960). Chromosome Mapping in Saccharomyces: Centromere-Linked Genes. Genetics, 45(8), 1085–1085110.

Heck, J. W., Cheung, S. K., & Hampton, R. Y. (2010). Cytoplasmic protein quality control degradation mediated by parallel actions of the E3 ubiquitin ligases Ubr1 and San1. Proceedings of the National Academy of Sciences, 107(3), 1106–1111.

Huh, W. K., Falvo, J. V., Gerke, L. C., Carroll, A. S., Howson, R. W., Weissman, J. S., & O'Shea, E. K. (2003). Global analysis of protein localization in budding yeast. Nature, 425(6959), 686–691.

Ito, H., Fukuda, Y., Murata, K., & Kimura, A. (1983). Transformation of intact yeast cells treated with alkali cations. *Journal Bacteriol*, 153(1), 163–168.

Jayaraj, G. G., Hipp, M. S., & Ulrich Hartl, F. (2020). Functional modules of the proteostasis network. Cold Spring Harbor Perspectives in Biology, 12(1).

Johnson, P. R., Swanson, R., Rakhilina, L., & Hochstrasser, M. (1998). Degradation signal masking by heterodimerization of MATα2 and MATa1 blocks their mutual destruction by the ubiquitin-proteasome pathway. Cell, 94(2), 217–227.

Khmelinskii, A., Blaszczak, E., Pantazopoulou, M., Fischer, B., Omnus, D. J., Dez, G. Le, … Knop, M. (2014). Protein quality control at the inner nuclear membrane. Nature, 516(7531), 410–413.

Klaips, C. L., Jayaraj, G. G., & Hartl, F. U. (2018). Pathways of cellular proteostasis in aging and disease. Journal of Cell Biology, 217(1), 51–63.

Leidenheimer, N. J., & Ryder, K. G. (2014). Pharmacological chaperoning: A primer on mechanism and pharmacology. Pharmacological Research.

Levdikov, V. M., Barynin, V. V., Grebenko, A. I., Melik-Adamyan, W. R., Lamzin, V. S., & Wilson, K. S. (1998). The structure of SAICAR synthase: An enzyme in the de novo pathway of purine nucleotide biosynthesis. Structure, 6(3), 363–376.

Matreyek, K. A., Starita, L. M., Stephany, J. J., Martin, B., Chiasson, M. A., Gray, V. E., … Fowler, D. M. (2018). Multiplex assessment of protein variant abundance by massively parallel sequencing. Nature Genetics, 50(6), 874–882.

Maurer, M. J., Spear, E. D., Yu, A. T., Lee, E. J., Shahzad, S., & Michaelis, S. (2016). Degradation signals for ubiquitin-proteasome dependent cytosolic protein quality control (CytoQC) in yeast. G3: Genes, Genomes, Genetics, 6(7), 1853–1866.

Monk, B. C., Tomasiak, T. M., Keniya, M. V., Huschmann, F. U., Tyndall, J. D. A., O'Connell, J. D., … Stroud, R. M. (2014). Architecture of a single membrane spanning cytochrome P450 suggests constraints that orient the catalytic domain relative to a bilayer. Proceedings of the National Academy of Sciences of the United States of America, 111(10), 3865–3870.

Mordret, E., Dahan, O., Asraf, O., Rak, R., Yehonadav, A., Barnabas, G. D., … Pilpel, Y. (2019). Systematic Detection of Amino Acid Substitutions in Proteomes Reveals Mechanistic Basis of Ribosome Errors and Selection for Translation Fidelity. Molecular Cell, 75(3), 427-441.e5.

Muhlrad, D., Hunter, R., & Parker, R. (1992). A rapid method for localized mutagenesis of yeast genes. Yeast, 8(2), 79–82.

Murray, B. P., & Correia, M. A. (2001). Ubiquitin-dependent 26S proteasomal pathway: A role in the degradation of native human liver CYP3A4 expressed in Saccharomyces cerevisiae? Archives of Biochemistry and Biophysics, 393(1), 106–116.

Nielsen, S. V., Stein, A., Dinitzen, A. B., Papaleo, E., Tatham, M. H., Poulsen, E. G., … Hartmann-Petersen, R. (2017). Predicting the impact of Lynch syndrome-causing missense mutations from structural calculations. PLoS Genetics, 13(4), 1–26.

Pedemonte, N., Bertozzi, F., Caci, E., Sorana, F., Fruscia, P. Di, Tomati, V., … Galietta, L. J. V. (2020). Discovery of a picomolar potency pharmacological corrector of the mutant CFTR chloride channel. Science Advances, 6(8), 1–14.

Ravid, T., Kreft, S. G., & Hochstrasser, M. (2006). Membrane and soluble substrates of the Doa10 ubiquitin ligase are degraded by distinct pathways. EMBO Journal, 25(3), 533–543.

Redler, R. L., Das, J., Diaz, J. R., & Dokholyan, N. V. (2016). Protein Destabilization as a Common Factor in Diverse Inherited Disorders. Journal of Molecular Evolution, 82(1), 11–16.

Roman, H. (1956) A system selective for mutations affecting the synthesis of adenine in yeast. Compt. Rend. Trav. Lab. Carlsberg, Ser. physiol. 26, 299-314.

Rosenbaum, J. C., Fredrickson, E. K., Oeser, M. L., Garrett-Engele, C. M., Locke, M. N., Richardson, L. A., … Gardner, R. G. (2011). Disorder targets misorder in nuclear quality control degradation: A disordered ubiquitin ligase directly recognizes its misfolded substrates. Molecular Cell, 41(1), 93–106.

Rowe SM, Verkman AS. (2013) Cystic fibrosis transmembrane regulator correctors and potentiators. Cold Spring Harb Perspect Med. 1;3(7):a009761.

Jones EE, Broquist HP. (1965) Saccharopine, An Intermediate of The Aminoadipic Acid Pathway of Lysine Biosynthesis. II. Studies in Saccharomyces Cereviseae. J Biol Chem. 240, 2531-6.

Schnappauf, G., Krappmann, S., & Braus, G. H. (1998). Tyrosine and tryptophan act through the same binding site at the dimer interface of yeast chorismate mutase. Journal of Biological Chemistry, 273(27), 17012–17017.

Shearer, A. G., & Hampton, R. Y. (2004). Structural control of endoplasmic reticulum-associated degradation. Effect of chemical chaperones on 3-hydroxy-3-methylglutaryl-CoA reductase. Journal of Biological Chemistry, 279(1), 188–196.

Shearer, A. G., & Hampton, R. Y. (2005). Lipid-mediated, reversible misfolding of a sterol-sensing domain protein. EMBO Journal, 24(1), 149–159. https://doi.org/10.1038/sj.emboj.7600498

Stein, A., Fowler, D. M., Hartmann-Petersen, R., & Lindorff-Larsen, K. (2019). Biophysical and Mechanistic Models for Disease-Causing Protein Variants. Trends in Biochemical Sciences, 44(7), 575–588.

Sträter, N., Håkansson, K., Schnappauf, G., Braus, G., & Lipscomb, W. N. (1996). Crystal structure of the T state of allosteric yeast chorismate mutase and comparison with the R State. Proceedings of the National Academy of Sciences of the United States of America, 93(8), 3330–3334.

Swanson, R., Locher, M., & Hochstrasser, M. (2001). A conserved ubiquitin ligase of the nuclear envelope/endoplasmic reticulum that functions in both ER-associated and Mat α2 repressor degradation. Genes & Development, 2(20), 2660–2674.

Takahashi, M., Shimodaira, H., Andreutti-Zaugg, C., Iggo, R., Kolodner, R. D., & Ishioka, C. (2007). Functional analysis of human MLH1 variants using yeast and in vitro mismatch repair assays. Cancer Research, 67(10), 4595–4604.

Tang, Y., Hicks, J. B., & Hilvert, D. (1991). In vivo catalysis of a metabolically essential reaction by an antibody. Proceedings of the National Academy of Sciences of the United States of America, 88(19), 8784–8786.

Tapper, A. R., McKinney, S. L., Nashmi, R., Schwarz, J., Deshpande, P., Labarca, C., … Lester, H. A. (2004). Nicotine activation of α4* receptors: Sufficient for reward, tolerance, and sensitization. Science.

Van Goor, F., Hadida, S., Grootenhuis, P. D. J., Burton, B., Cao, D., Neuberger, T., … Negulescu, P. (2009). Rescue of CF airway epithelial cell function in vitro by a CFTR potentiator, VX-770. Proceedings of the National Academy of Sciences of the United States of America, 106(44), 18825–18830.

Van Goor, F., Hadida, S., Grootenhuis, P. D. J., Burton, B., Stack, J. H., Straley, K. S., … Negulescu, P. A. (2011). Correction of the F508del-CFTR protein processing defect in vitro by the investigational drug VX-809. Proceedings of the National Academy of Sciences of the United States of America, 108(46), 18843–18848.

Wangeline, M. A., & Hampton, R. Y. (2018). "Mallostery"—ligand-dependent protein misfolding enables physiological regulation by ERAD. Journal of Biological Chemistry, 293(38), 14937–14950.

Wangeline, M. A., Vashistha, N., & Hampton, R. Y. (2017). Proteostatic Tactics in the Strategy of Sterol Regulation. Annual Review of Cell and Developmental Biology, 33(1), 467–489.

Wilhovsky, S., Gardner, R., & Hampton, R. (2000). HRD gene dependence of endoplasmic reticulum-associated degradation. Molecular Biology of the Cell, 11(5), 1697–1708.

Wong, T. S., Roccatano, D., Zacharias, M., & Schwaneberg, U. (2006). A statistical analysis of random mutagenesis methods used for directed protein evolution. Journal of Molecular Biology, 355(4), 858–871.

Xue, Y., Lipscomb, W. N., Graf, R., Schnappauf, G., & Braus, G. (1994). The crystal structure of allosteric chorismate mutase at 2.2-Å resolution. Proceedings of the National Academy of Sciences of the United States of America, 91(23), 10814–10818.

Yue, P., Li, Z., & Moult, J. (2005). Loss of protein structure stability as a major causative factor in monogenic disease. Journal of Molecular Biology, 353(2), 459–473.

Zelcer, N., Sharpe, L. J., Loregger, A., Kristiana, I., Cook, E. C. L., Phan, L., … Brown, A. J. (2014). The E3 Ubiquitin Ligase MARCH6 Degrades Squalene Monooxygenase and Affects 3-Hydroxy-3-Methyl-Glutaryl Coenzyme A Reductase and the Cholesterol Synthesis Pathway. Molecular and Cellular Biology, 34(7), 1262–1270.

Zhao, Y., MacGurn, J. A., Liu, M., & Emr, S. (2013). The ART-Rsp5 ubiquitin ligase network comprises a plasma membrane quality control system that protects yeast cells from proteotoxic stress. ELife, 2013(2), 1–18.

Zheng, N., & Shabek, N. (2017). Ubiquitin Ligases: Structure, Function, and Regulation. Annual Review of Biochemistry, 86(1), 129–157.

CHAPTER V

Conclusions and Outlook

In the somewhat disparate studies above, it is clear that *Saccharomyces cerevisiae* remain a workhorse for investigating protein quality control (PQC). Chapter II demonstrates cost-effective and straightforward methods for cloning and screening with yeast, and in our personal experience, these techniques are readily used by undergraduate researchers, many of whom are featured in the author list of chapter IV. Chapter III demonstrates the ability to use yeast for in-depth, *in vivo* analysis of novel PQC pathways, and it shows the ways that novel modes of proteotoxicity can be elucidated and leveraged to better understand proteostasis as a whole. In a sense, chapter IV combines these themes but focuses more closely on misfolded proteins, perhaps the least well-understood aspect of PQC. In those studies, we were able to harness yeast genetics and cell biology to study structural biology.

Listed below are possible future directions for these studies. Undoubtedly, PQC will continue to be of central importance to translational research for many years to come, especially given the retinue of diseases that involve or are caused by deficiencies of the ubiquitin-proteasome system (Klaips, C. L., et al., 2018). There are also a number of exciting avenues ahead that bridge the gaps between structural biology, computational biology, and cell biology. These include basic research into biologically relevant misfolding and the underpinnings of the broad specificity of PQC E3 ligases; how, exactly, such ligases can recognize misfolding—including multiple misfolded variants of even one domain—without also constitutively degrading normal proteins remains a central mystery of the field.

Inner-nuclear-membrane-associated degradation and proteotoxicity

Much of chapter III is devoted to showing that the rhomboid pseudoprotease Dfm1 is not involved in the retrotranslocation of inner-nuclear-membrane-associated degradation (INMAD). Indeed, we carefully examined most known INM substrates and found no Dfm1 involvement in INMAD—this despite the central role of Dfm1 in the degradation of all transmembrane ER proteins studied to date and despite the seemingly canonical mechanisms of INMAD retrotranslocation that we were able to demonstrate: ubiqutination by the Asi-complex, extraction of the full-length substrate, and, ultimately, retrotranslocation into a soluble subcellular environment (presumably the nucleoplasm). There are few known candidates for the factor that acts in the stead of Dfm1. One possibility is Ubx1, which was shown to be required for the degradation of Asi1 (Pantazopoulou, M., 2016). Otherwise, putative retrotranslocons such as Doa10, Hrd1, and Asi2 have been systematically ruled out as the factor responsible for dislodging Sec61-2-GFP from the INM (Foresti, O., et al., 2014).

As mentioned in chapter III, the lethality associated with Sec61-2-GFP overexpression could provide a means to discovering a novel, INM retrotranslocon. This could be achieved by crossing Sec61-2-GFP in a *hrd1Δ* null to the deletion collection (Tong, A. H. Y. et al., 2001). Readouts for such a screen could include lethality by Gal induction, lethality by the counterselection scheme laid out in chapter III, GFP fluorescence, or some combination of these (Jaeger PA, Ornelas L, et al., 2018).

Another mode of inquiry revolves around the nature of transmembrane-protein toxicity. Our lab has been fortunate enough to discover two instances of such stress in recent years. The first and better defined revolves around Dfm1: simply put, ERAD-M and ERAD-C substrates are highly toxic in the absence of Dfm1 (Neal et al., 2018; Neal et al., 2020). Pressing questions include the mechanisms by which substrates are toxic and how Dfm1 ordinarily mediates that toxicity. Sec61-

2-GFP toxicity requires the additional loss of ASI-mediate INMAD to achieve full toxicity and is therefore somewhat distinct. Nonetheless, the INM and ER membrane, like the cytosol and the nucleoplasm, are clearly interconnected and constitute a proteostatic network. It will be fascinating to see the degree to which INM-ER-membrane proteostasis is connected with more canonical modes of ER stress. Recent work shows that Ire1 has an ability to detect perturbations of the lipid bilayer (Halbleib, K., et al., 2017; Ho, N., et al., 2020). Perhaps misfolded transmembrane proteins are detected by this mechanism. If so, it will be critical to elucidate the ways that this mode of UPR induction is similar to and distinct from the better understood ER luminal pathways.

Minimally Misfolded Proteins and Structure Misfunction Analysis

The studies in chapter IV could be complimented by several additional lines of inquiry, some of which have already begun.

A first is to use computational methods to compare the predicted ΔΔG of a mutation and the UPS response to it. In preliminary data not shown herein, Andy Kao and I have found that the half-lives of our Ade1 and Lys1 mutants correlated poorly with ΔΔG predicted by several pieces of software, including but not limited to FoldX (Guerois, R. et al., 2002). On the other hand, it seems that this software is more predicative when mutations at a single residue are analyzed. While FoldX makes some notable errors, including ranking W151H (a stable substitution) as highly destabilizing, it generally produces a much better correlation with kinetics in this case. Perhaps this points to a difference between predicting the kind of degron involved versus the degree to which it is unveiled. For instance, the degron unveiled by Lys1-V26D, -L29P, and -I36D seems to elicit far faster kinetics than the one unveiled by Lys1-W151P despite the fact that FoldX predicts similar ΔΔGs for each susbtitution. The software is simply incapable of predicting the degree to which the unveiled degron will elicit degradation. On the other hand, the iso-positional mutations at Lys1-W151 could favor the exposure of a single degron to a greater and greater extent as substitutions become more and more

destabilizing, leading to a better correlation. Thus, the software can predict the degree of misfoldedness but not the kind of degron.

It is also tempting, though perhaps ill advised, to pursue cis analysis of mutants isolated by structure misfunction analysis. We have done this to some extent with a fourth protein, Gnd1. The Gnd1 tertiary structure is organized into three sequential domains, the third of which acts to form a homodimer (He, W., et al., 2007). A *gnd1Δ* null strain is sensitive to hydrogen peroxide (Juhnke H., et al., 1996), and Gnd1-GFP fully rescues this phenotype (not shown). The first domain of Gnd1 is stable when expressed in the absence of the second and third domains, and we have determined, to some extent, the PQC pathways involved in the degradation of full-length mutants and domain-I-only mutants. A nonfunctional mutant is recognized and degraded by distinct pathways in the full-length and domain-I-only forms, suggesting a more global mode of unfolding. A functional-but-misfolded mutant produces relatively similar substrates in both contexts. While it is uncertain whether these observations will be formalized or brought to publication, they once again point to distinct local and global modes of misfolding. It is important to speculate, however, that "local" misfolding need not be local to the destabilizing mutation. If it is possible to increase the kinetics of certain enzymes by mutating residues distant from the active site (Brinkmann-Chen, S., et al., 2013), it is certainly possible for mutations to cause distant misfolding events.

There are also several questions to pursue with regard to Aro7. In the course of her investigations, Breanna Lam also pursued saturation mutagenesis at Aro7-R33. Some mutations were very sensitive to trp whereas others were completely insensitive. This will be an interesting collection to explore in the future. There is also an open question in these studies as to whether increased steady state levels reflect the local or allosteric effects of trp binding. It is tempting to suggest the latter since tyr has no stabilizing effects despite its almost identical mode of binding, but we have not developed a positive control for tyr entry into cells. Luckily, Aro7 is incredibly well studied, and an

orthogonal approach is possible. Namely, there is a defined mutant of Aro7 that is locked in the activated state (Schmidheini, T., et al., 1989). By combining this mutant with R33G, we can test the role of the allosteric transition induced by Trp.

Finally, our analysis of Lys1 mutants unveiled a pathway distinct from San1- and Ubr1-mediated cytosolic quality control. These mutants also seem to be ignored by Doa10, and even seem to continue to be degraded in a *doa10Δltn1Δsan1Δubr1Δ* background (data not shown). This raises the possibility of identifying a novel quality control pathway. In an attempt to identify such a pathway, Darren Lam will introduce Lys1-V26D-GFP into a collection of UPS-related knockouts. It is possible that these mutants are subject to a highly combinatoric PQC response and that individual deletions will not have discernable effects on kinetics. Still, there is a two-fold increase in Lys1-V26D-GFP steady-state levels upon MG132 treatment (data not show), so the dynamic range of the screen may be sufficiently large to uncover partial stabilization. The wild-type Lys1-GFP and the mutants recognized by San1 and Ubr1 also present excellent controls.

References

Brinkmann-Chen, S., Flock, T., Cahn, J. K. B., Snow, C. D., Brustad, E. M., McIntosh, J. A., … Arnold, F. H. (2013). General approach to reversing ketol-acid reductoisomerase cofactor dependence from NADPH to NADH. Proceedings of the National Academy of Sciences of the United States of America, 110(27), 10946–10951.

Foresti, O., Rodriguez-Vaello, V., Funaya, C., & Carvalho, P. (2014). Quality control of inner nuclear membrane proteins by the Asi complex. Science, 346(6210), 751–755.

Guerois, R., Nielsen, J. E., & Serrano, L. (2002). Predicting changes in the stability of proteins and protein complexes: A study of more than 1000 mutations. Journal of Molecular Biology, 320(2), 369–387.

Halbleib, K., Pesek, K., Covino, R., Hofbauer, H. F., Wunnicke, D., Hänelt, I., … Ernst, R. (2017). Activation of the Unfolded Protein Response by Lipid Bilayer Stress. Molecular Cell, 67(4), 673-684.e8.

He, W., Wang, Y., Liu, W., & Zhou, C. Z. (2007). Crystal structure of Saccharomyces cerevisiae 6-phosphogluconate dehydrogenase Gnd1. BMC Structural Biology, 7, 1–9.

Ho N, Yap WS, Xu J, Wu H, Koh JH, Goh WWB, George B, Chong SC, Taubert S, Thibault G. Stress sensor Ire1 deploys a divergent transcriptional program in response to lipid bilayer stress. J Cell Biol. 2020 Jul 6;219(7):e201909165.

Jaeger PA, Ornelas L, McElfresh C, Wong LR, Hampton RY, Ideker T. (2018) Systematic Gene-to-Phenotype Arrays: A High-Throughput Technique for Molecular Phenotyping. Mol Cell. 18;69(2):321-333.e3.

Juhnke H, Krems B, Kötter P, Entian KD. (1996) Mutants that show increased sensitivity to hydrogen peroxide reveal an important role for the pentose phosphate pathway in protection of yeast against oxidative stress. Mol Gen Genet. 252(4):456-64.

Klaips, C. L., Jayaraj, G. G., & Hartl, F. U. (2018). Pathways of cellular proteostasis in aging and disease. Journal of Cell Biology, 217(1), 51–63.

Neal, S., Jaeger, P. A., Duttke, S. H., Benner, C. K., Glass, C., Ideker, T., & Hampton, R. (2018). The Dfm1 Derlin Is Required for ERAD Retrotranslocation of Integral Membrane Proteins. Molecular Cell, 69(2), 306-320.e4.

Neal, S., Syau, D., Nejatfard, A., Nadeau, S., & Hampton, R. Y. (2020). HRD complex self-remodeling enables a novel route of membrane protein retrotranslocation. IScience, 23(9), 101493.

Pantazopoulou, M., Boban, M., Foisner, R., & Ljungdahl, P. O. (2016). Cdc48 and Ubx1 participate in a pathway associated with the inner nuclear membrane that governs Asi1 degradation. Journal of Cell Science, 129(20), 3770–3780.

Schmidheini, T., Sperisen, P., Paravicini, G., Hütter, R., & Braus, G. (1989). A single point mutation results in a constitutively activated and feedback-resistant chorismate mutase of Saccharomyces cerevisiae. Journal of Bacteriology, 171(3), 1245–1253.

Tong, A. H. Y., Evangelista, M., Parsons, A. B., Xu, H., Bader, G. D., Pagé, N., … Boone, C. (2001). Systematic genetic analysis with ordered arrays of yeast deletion mutants. Science, 294(5550), 2364–2368.